Fundamental Studies of Mouse Amacrine Cells

Gregory S. Newkirk

A dissertation
Submitted in partial fulfillment of the
Requirements for the degree of

Doctor of Philosophy

University of Washington
2013

Reading Committee:
Peter Detwiler, Chair
Marc Binder
Rachel Wong

Program Authorized to Offer Degree:
Neurobiology & Behavior

University of Washington

Abstract

Fundamental Studies of Mouse Amacrine Cells

Gregory S. Newkirk

Chair of the Supervisory Committee:

Peter B. Detwiler

Physiology & Biophysics

Vision begins in the retina where information about the salient features of an image projected on a mosaic of rod and cone photoreceptors is extracted and digitally encoded in neural impulses that are conducted by the axons of the optic nerve to the brain where the message is decoded and interpreted as a visual perception. In spite of the enormity of all that has been learned over the thousands of years that vision has been philosophically contemplated, behaviorally evaluated and experimentally interrogated, the cellular mechanisms that underlie retina function are still not known. An essential step in understanding how any complex machine works is to have a parts list and to understand what each part does. In the case of the

amacrine cell family, of its 20 to 30 different subtypes only three have been have been functionally characterized. My research has sought to further our understanding of this diverse and largely unexplored class of retinal cell types by examining the mechanisms that give rise to light-evoked signals in two types of amacrine cells in the mouse retina. One of these is the dopaminergic amacrine cell (DAC), the other is an un-named amacrine cell type that to my knowledge has not been previously identified or examined using electrical recording and will henceforth be referred to as the small bistratified amacrine cell (SBAC).

I have succeeded in doing this by utilizing a BAC-transgenic mouse line (GENSAT d2dr-GFP) in which the promoter for dopamine receptor 2 (DR2) drives selective expression of GFP in two populations of amacrine cells (DACs and SBACs) that can be distinguished from each other on the basis of soma size as discussed below. The fluorescently labeled cells were visualized and targeted for whole cell recording using multi-photon laser scanning fluorescence microscopy. The functional properties of the two GFP labeled amacrine cell types were characterized in separate studies described below.

TABLE OF CONTENTS

INTRODUCTION

To fully understand how an automobile engine is able to propel a person down the road at a high rate of speed, it is imperative to understand the function of each part of the car; from the pistons to the driveshaft. Without a basic knowledge of each piece, it would be difficult to explain to another person how the engine converts a chemical reaction into a controllable means of transport and entirely impossible to build an automobile engine on your own. The same problem exists in biological systems: a detailed understand of the parts is necessary to understand the mechanism and effects of their actions. In the retina, a basic understanding exists, but I do not yet fully understand the responsibilities and interactions of a large number of cell types. In this thesis, I will attempt to increase our knowledge of the retina by describing the fundamental properties and actions of two different types of amacrine cells that have yet to be studied.

The retina is a true marvel of biological engineering. It is able to faithfully detect the few photons that are visible from starlight to millions of photons detected from bright sunshine to give us information about our surroundings. The ability to collect and process the visual world over a 12-fold range of light intensities makes the retina the champion of all sensory systems. The ability to perform this task with only two basic types of photoreceptors makes the task all the more impressive.

At first glance, the retina appears to be relatively simple. It is organized into sections containing somas of different cell types that are separated by layers of processes that make synaptic contacts between the cells. The three cell body layers are: the Outer Nuclear Layer (ONL), the Inner Nuclear Layer (INL), and the Ganglion Cell Layer (GCL). The ONL consists

of cell bodies of both photoreceptor types with their inner and outer segments in the Photoreceptor Layer. The INL consists of cell bodies of bipolar, horizontal, and amacrine cells, while the GCL contains both ganglion cell and displaced amacrine cell bodies. Between these cell layers are two layers where synaptic connections occur that are named the Outer Plexiform Layer (OPL) and the Inner Plexiform Layer (IPL). Bipolar cells, as their name suggests, are the only cells that have processes that extend into both plexiform layers making synaptic connections with photoreceptors in the OPL and with ganglion cells in the IPL. Bipolar cells are the intermediary for connecting the photoreceptors to ganglion cells and these three cell types together make up the vertical pathway, which is responsible for relaying signals to the brain. Each cell in the vertical pathway uses glutamate as their neurotransmitter. Horizontal and amacrine cell types form the horizontal pathway and modulate the connections via inhibitory neurotransmission in the vertical pathway with synapses in the OPL and IPL, respectively. Interactions between these five cell types allow the retina to detect light and process visual images. The simple retina becomes more complex as I take a closer look at the organization and function of the retina.

Two types of photoreceptors capture light and turn photons into an electrical signal through a process called phototransduction. Rod photoreceptors are sensitive to single photons and are designed to work in dim light (scotopic vision), while cones are less sensitive but able to function in bright light (photopic vision) without saturating. In the absence of photons, photoreceptors are steadily releasing neurotransmitter due to an influx of Na^+ ions through open cyclic nucleotide gated channels, which depolarizes the cell. When photopigment molecules detect photons in the outer segments of the photoreceptors, a counterintuitive mechanism initiates a signaling cascade that results in a decrease in the release of glutamate neurotransmitter. Photoreceptors release glutamate onto two basic types of cells: horizontal

cells and bipolar cells. Horizontal cells inhibit neighboring photoreceptors through GABA when stimulated by glutamate and are inhibited in the presence of light. Cone photoreceptors also release glutamate onto two different types of bipolar cell: the ON bipolar cell and OFF bipolar cell that are named for their preferred excitation light condition. ON bipolar cells have metabotropic glutamate receptors, which actually cause the ON bipolar cell to hyperpolarize in the presence of glutamate. Because there is less glutamate released when a photoreceptor detects light, this relieves the tonic inhibition that the ON bipolar cell receives in the dark, effectively inverting the signal from the photoreceptor and exciting the ON bipolar cell. OFF bipolar cells have AMPA receptors that are excited in the absence of light and conserve the photoreceptor signal. Rod photoreceptors have a specific type of bipolar named the Rod Bipolar Cell, but lack a comparable OFF bipolar cell. Therefore, due to the type of glutamate receptor present on the bipolar cell, the retina is able to form separate pathways for the absence and presence of light. The ON and OFF bipolar cell determine the type of response for all downstream neurons, and all other cell types in the retina are categorized as being either ON or OFF based on bipolar cell innervation.

ON and OFF bipolar cells are distinctly stratified in the IPL based on their type, with the OFF bipolar cell axon terminals in the outermost portion of the IPL and the ON bipolar cell terminals in the innermost portion. It is possible that cells that have processes in both layers of the IPL can receive signals from both ON and OFF bipolar cells. Therefore, the retina maintains some morphological order in the IPL despite the increasing complexity of the neuronal signal.

As our understanding of the retina increases, so does the complexity of this neural circuit. For many years, recordings have focused on both the photoreceptors and ganglion cells

as they are the most accessible for electrophysiological recording. This data has provided a wealth of information on how the retina detects light and processes visual images.

In between the photoreceptors and ganglion cells, a large amount of convergence and processing takes place. A 1:1 ratio of photoreceptors to downstream neurons would provide the highest visual acuity, but these signals would be difficult to detect from noise in the system. Therefore, spatial resolution is sacrificed for increasing sensitization at low light levels. Each bipolar cell receives information from about 15 rods, while ganglion cells get up to 250 inputs from upstream neurons to provide the roughly 16-20 different types of output channels that are encoded in the form of action potentials sent from the estimated 20 types of ganglion cells through the optic nerve to visual cortex (Masland, 2012). These modalities include information about shapes, color, motion, and other outputs that we are just beginning to understand. The key to understanding these outputs is likely held in the number and variety of different cell types in the retina, of which there is little information.

Photoreceptors are the most abundant cell type in the retina with an estimated number near 6.5 million in the mouse, the majority (97%) being of the rod type (Jeon, et al, 1998). The small numbers of cone photoreceptors are further divided into two types that have photosensitive opsin molecules with different spectral absorptions that give rise to color vision. Horizontal cells are the least abundant cell type in the mouse retina, having no diversity among the population (Peichl and González-Soriano, 1994; Jeon, et al., 1998). There is a single type of rod specific bipolar cell, but in the mouse there appears to be a proposed catalog of 11 different types of cone bipolar cell that are morphologically and functionally distinct (Wässle, et al., 2009). The 12 different encodings of light output computed by the bipolar cells are modulated by an unknown number of amacrine cells. There is no complete catalog of amacrine cells type in the mouse retina, but estimates made from studies in other animals puts the

number at 25-30 (Wässle & Boycott, 1991; Strettoi and Masland, 1996; MacNeil and Masland, 1998). These amacrine cells can be divided into two general types: narrow and wide-field amacrine cells. Narrow-field amacrine cells have a dendritic field that is typically <150 μm in diameter and generally provide glycinergic inhibition to its synaptic. Currently there is no complete study of the diversity of narrow-field amacrine cells, but at least eight different types have been described in the rat (Menger et al., 1998). Their small dendritic fields eliminate the need for action potentials to propagate signals, although a complete study is lacking. Wide-field amacrine cells have larger dendritic trees (>200 μm diameter) and provide GABAergic inhibition to their synaptic targets. In addition to GABA, some wide-field amacrine cells are known to release other neuromodulators such as dopamine or acetylcholine. Many wide-field amacrine cells are known to possess axon-like processes and produce action potentials to propagate signals to long-range targets (Davenport et al., 2007; Zhang et al., 2007). In the mouse retina, eleven different types of wide-field amacrine cells have been reported, but authors admit that this is likely an underestimation as wide-field amacrine cells, due to their large dendritic fields, need fewer cells to cover the retina (Masland, 2012). Similarly, the exact number of ganglion cells in the mouse retina is currently not known, but estimates range from 11 to 22 based on techniques and classification methods (Kong et al., 2005; Völgyi, et al., 2009). However, it should be noted that there appears to be approximately a 2:1 amacrine cells to ganglion cell diversity and the absolute number of amacrine cells in the mouse retina is nearly an order of magnitude higher compared to ganglion cells (Jeon et al., 1998). Despite being the most morphologically diverse retinal cell type, amacrine cells are poorly understudied compared to other cells in the retina.

There are three main problems causing the gap in amacrine cell knowledge. As described above, the absolute number and diversity of these cells provides a daunting task to

learn about a specific population of these neurons. This is compounded by the majority of amacrine cells lacking a morphological distinction to ease the difficulty of targeting for recording. Second, their location in the INL makes them relatively inaccessible for electrophysiological recordings. It is not coincidental that the most well studied cells of the retina, the photoreceptors and ganglion cells, reside at the periphery of either edge of the tissue. Last, and most importantly, is the obscurity of their functionality. Amacrine cells can make synapses either onto bipolar cell terminals, ganglion cells, other amacrine cells, or any combination of the three. The most well studied amacrine cells have unique characteristics that have allowed us to overcome these difficulties.

Of the 25-30 types of amacrine cells, only three cells have been studied in any great detail. They include: the AII amacrine cell, the A17 amacrine cell, and the Starburst amacrine cell. The AII amacrine cell is the most abundant and well-studied amacrine cell due to its role in processing rod bipolar cell input. In fact, the chief method of passing rod-driven signals requires this narrow-field amacrine cell to transfer the signal from the rod bipolar cell to the ganglion cells. It is electrically coupled to ON ganglion cells and uses glycine to inhibit OFF ganglion cells when stimulated. The A17 amacrine is a wide-field amacrine cell that makes reciprocal synapses with rod bipolar cells, presumably to amplify dim light signals across large areas of the retina. Starburst amacrine cells are known to use acetylcholine and GABA as neurotransmitters and have important roles in direction selectivity. The morphology, synaptic wiring, and function of the AII, A17, and Starburst amacrine cells have been described in detail, but there is little known about the approximately two dozen other amacrine cells in the retina.

To increase our knowledge of amacrine cells in the mouse retina, I will make recordings from unstudied cells in the INL of the mouse retina. Amacrine cells are divided into

to two distinct groups based on the expanse of their dendrites, narrow and wide field, and represent an equal proportion of the amacrine cell types. However, narrow-field amacrine cells have greater absolute numbers. This underlies the specific challenges for targeting both types of cell. In narrow-field cells, smaller cell bodies increase the targeting difficulty, while wide field cells have a reduced number of targetable cells. In this thesis, I will study both a bistratified narrow-field amacrine cell and the wide-field Dopaminergic Amacrine Cell (DAC); both have yet to be described in the intact mouse retina.

The release of neuromodulators is an interesting function of some amacrine cell types. A PubMed search of the terms "retina" and "dopamine" returns >1600 articles associated with the function of dopamine in the retina, but little is known about the physiology of the dopamine releasing cell beyond what can be gleaned from the results of experimentation with its neurotransmitter. They can, however, be labeled and specifically targeted for electrical recording using transgenic methods in which the promoter for tyrosine hydroxylase, the rate-limiting enzyme for dopamine biosynthesis, directs the selective expression of a reporter, either alkaline phosphatase (Gustincich et al., 1997) or fluorescent protein (Zhang et al., 2004). The ability to immunolabel tyrosine hydroxylase has allowed for a morphological description of DACs as well as their synaptic inputs and outputs. In the retina DAC somas sit along the border of the INL and IPL, and give rise to 4-5 primary dendrites with a 600 μm dendritic field that stratifies entirely in the outermost (OFF) portion of the IPL. DACs also have 2-3 axon-like processes that extend from either the cell body or primary dendrites and extend for many millimeters in the retina, combining with the dendrites to create a large web of processes that release dopamine in a paracrine-like fashion throughout the retina (Contini and Raviola, 2003). Although DAC processes are present only in the OFF sublayer of the IPL, they receive direct ON bipolar input through synaptic ribbon synapses on bipolar cell axons, breaking the well-

established stratification “rules” of the IPL discussed above (Hoshi et al., 2009; Dumitrescu et al., 2009). Studies of synaptic outputs suggest that DACs may make GABAergic synapses with AII amacrine cells, as their dendrites contact the base of the soma of AII amacrine cells in a formation resembling a “necklace". Immunolabeling and electron microscopy demonstrate the colocalization of $GABA_A$ receptors and GABA synaptic machinery between the two cells, suggesting that in addition to the effects of dopamine throughout the retina, the cell may have direct modulating effects on the switch from scotopic to photopic vision through traditional inhibitory synapses (Contini and Raviola, 2003).

DACs are the major source of the dopamine transporter (DAT), meaning that if dopamine escapes reuptake at the INL/IPL border, it is free to diffuse to all parts of the retina (Bjelke et al., 1996; Cheng et al., 2006). Evidence suggests that dopamine plays a key role in numerous cellular functions that accompany the switch from rod-mediated (scotopic) to cone-mediated (photopic) vision throughout the retina. It is known that dopamine concentration is higher during the day compared to night (Melamed et al.,1984; Wirz-Justice et al., 1984; Nir et al., 2000*a*). Dopamine has a critical effect on gap junction coupling of horizontal, bipolar, and amacrine cell types (reviewed in Bloomfield and Völgyi, 2009). Dopamine, acting through metabotropic D1 receptors in these various cell types, reduces the amount of gap junction coupling in the network and effectively increasing spatial resolution by reducing the receptive field sizes of the cells. These results mimic the effect of light on gap junction coupling. During the day, photoreceptors receive large amounts of light that increases the signal to noise ratio in the cells, which reduces the need for convergence of signals thereby increasing spatial resolution. D1 and D2 receptors are located on all cell types in the retina with various other effects on ion channel conductance and photoreceptor disk shedding and melatonin production,

all seemingly associated with changes between scotopic and photopic vision (reviewed in Witkovsky, 2004).

DACs are sparsely populated in the retina, at a density of 20-30 per mm^2, with ~450 in each mouse retina (Gustincich et al., 1997; Marshak, 2001). This makes them difficult to target compared to other well studied amacrine cells in the retina, which have characteristics that improve targeting for recordings. The AII amacrine cell's location in the innermost portion of the INL and well-described shape makes it easy to target in retinal slices. In addition there are a greater number of AII cells per retina than DACs. The A17 cell also has a distinct morphological shape and is known to accumulate serotonin. The Starburst Amacrine cell is displaced in the Ganglion Cell Layer and has a characteristic shape in the presence of a fluorescent counterstain. To improve the ability to target a population of cells lacking in distinct morphological characteristics, an additional tool must be utilized to obtain an adequate experimental sample.

Transgenic animals have provided a solution to targeting problems. Modifications to genetic material, by inserting coding for fluorescent protein, allows for precise labeling in a specific subset of cells. For example, subsets of retinal ganglion cells driven to express YFP under direction of the Thy1 promoter provide a reliable cell-specific reporter that can be effectively used for targeting (Feng et al., 2000). However, there are limitations and difficulties associated with the use of fluorescent markers for electrophysiological targeting. In standard fluorescence microscopy, the use of labeled cells requires light in the visible spectrum. A photon in the visible spectrum excites a fluorophore, which increases the energy level of an electron in the fluorophore. When the electron returns from the higher energy state back to the ground state loss of the energy causes emission of a photon, known as fluorescence. Exposure to visible wavelength light can saturate rod photoreceptors and change the adaptation

state of the retina, which is known to have effects on the input and outputs of cell responses (Dunn et al., 2007). Excessive light can induce bleaching of photopigment in the photoreceptors, particularly if the retinal tissue is isolated from the Retinal Pigment Epithelium. This impairs the photoreceptor's ability to reproduce photosensitive molecules necessary for light responses. Two-photon laser-scanning fluorescence microscopy provides a less detrimental method for using fluorescence to target labeled cells. Two-photon laser-scanning fluorescence microscopy utilizes two nearly simultaneous lower energy photons to excite a fluorophore to the same energy level in standard fluorescence. Instead of the visible spectrum, the wavelength of the lower energy photons are in the infrared spectrum and do not greatly stimulate photoreceptors. Using this method allows the retina to remain in a dark-adapted state and prevents photobleaching of pigment compared to standard fluorescent techniques.

The second cell type that I intend to discuss is a completely novel type of amacrine cell. The cell is a narrow-field amacrine cell with a dendritic field of less than 150 µm, which suggests that it releases glycine when stimulated. It appears to have a band of dendrites in the OFF layer, and to be diffusely stratified in the ON layer. Due to the bistratification and smaller soma size, I have preliminarily named it the Small Bistratifed Amacrine Cell (SBAC). Unfortunately, there is little morphological information about the types of narrow-field amacrine cells in the mouse and I am unable to find a comparable amacrine cell type in other animals (MacNeil and Masland, 1998). Compared to the DAC, there are no previous studies about the SBAC making it an exciting and interesting cell to study, but unfortunately there is no background information on its possible role in the retina. However, just as with the DAC, I will describe the baseline activity, light responses, and synaptic circuitry for this novel amacrine cell type.

Using two-photon laser-scanning fluorescence microscopy to target sparsely labeled amacrine cells, I plan to demonstrate the first extensive whole-cell recording study of DACs and SBACs in the intact retina. I will utilize a transgenic mouse from the GENSAT Brain Atlas Project at Rockefeller University, where enhanced Green Fluorescent Protein (eGFP) expression is driven by a BAC transgene inserted into the promoter region of the D2 dopamine receptor. In the retina, this animal has two distinct populations of cells labeled in the INL that I can discriminate based on soma size. The first cell, with a larger soma diameter (14-17 μm), shows colocalization with tyrosine hydroxylase immunolabeling demonstrating that it is a DAC. I will also target the SBAC for recordings, which has a much greater density, but smaller soma size (7-8 μm) compared to DACs. Using this animal, I hope to add to the fundamental studies of the retina by fully describing the baseline activity, synaptic circuitry, and general physiological properties of both amacrine cell types. This data will begin to help fill in the gaps present in the current literature involving amacrine cells in the retina.

METHODS

All experiments were conducted in accordance with institutional and national guidelines for animal care using procedures and protocols that were reviewed and approved by the Institutional Animal Care and Use Committee at the University of Washington. We used P21-P50 day old Gensat BAC transgenic mice (RP23-161H15) crossed into in C57/B6 background. In this line, green fluorescent protein (GFP) transgene was inserted immediately after the ATG start codon of the dopamine receptor 2 promoter. Animals were housed in University of Washington approved facilities on a 12-hour light/dark cycle with *ad libitum* access to food and water.

Tissue Preparation

Experiments began during the animal subjective day, approximately 5 hours into their daily light cycle. After 2 to 3 hours of dark adaptation, mice were killed by cervical dislocation and eyes were removed in the dark using infrared illumination with image converters, placed in Carbogenated (95% O_2 and 5% CO_2) Ames' medium (Sigma, St. Louis, MO) at room temperature and hemisected. The posterior half of the eyecup was cut into 3 to 5 smaller pieces. Retina was isolated from each of the pieces as needed and adhered photoreceptor side down to a translucent Anodisc filter (Whatman, Florham Park, NJ) by wicking away excess solution and transferred to a recording chamber fixed to the stage of a custom-built two-photon laser scanning fluorescence microscope. The mounted retina was perfused with warmed (30 –34°C) Carbogenated Ames' medium at a rate of 5-7 ml/min and viewed with a CCD camera using infrared illumination.

Cell Identification

In the *Drd2-GFP* BAC transgenic mouse line, GFP expression was visualized in whole mount retina using two-photon microscopy (Denk et al., 1990; Denk and Detwiler, 1999; Euler et al., 2009). The light source for two fluorescent excitation was a pumped laser (Mira, Coherent) that delivered ~ 100 femtosecond laser pulses of 930nm light at 100 MHz with estimated average power at the retina of 4 - 8 mW. Fluorescence emission was collected by a 40X 1.0NA water-immersion objective (Nikon). Custom band pass (BP) filters (Chroma Technology) directed green (535 BP50nm) and red (622 BP36nm) fluorescence to two independent photomultiplier tubes (Hamamatsu). The green channel was used to visualize GFP-positive cells in the inner nuclear layer (INL), and the red channel was used to visualize the recording pipette filled with an intracellular recording solution containing 100 μM Alexa-594 (Invitrogen).

Retinal photoreceptors are not blind to the pulses of long wavelength (930 nm) light used to excite fluorescence by two-photon absorption in laser scanning microscopy (Euler et al., 2009). The light sensitivity of alpha RGCs was used to assess the effect of laser exposure on retinal function. All recordings were done in the presence of 2 Rh*/rod/s background illumination. After a 2- 3 minute period of laser scanning that mimicked the conditions used to target DACs using GFP fluorescence, the threshold intensity (500 ms step of 440 nm light) for a just detectible change in extracellularly recorded spike activity (loose cell attached patch) was increased by about 1 -1 .5 log unit for 20 to 40 s before returning to a control step sensitivity of ~ 1 Rh*/rod/step. At the onset of laser scanning, with the focal plane in the inner plexiform layer (IPL), alpha RGCs were initially sensitive to the excitation light and fired spikes in synchrony with the rate of image scanning as the laser spot swept across the receptive field of the cell. With continued scanning, the retina adapted to the stimulus and the laser-

evoked spike activity disappeared. Spike response to test flashes as well as laser exposure returned with the recovery of light sensitivity following the termination of laser scanning. These observations indicate that the two-photon imaging methods we have used to target DACs for whole cell recording did not have a persistent effect on retinal function as appraised by light sensitivity.

Electrophysiology

GFP labeled cells in the INL were accessed on a diagonal trajectory from a micro-dissected hole in the internal limiting membrane, 50-75 μm from the targeted cell (Margolis and Detwiler, 2007). Patch clamp recordings were obtained using 3-5 MΩ electrodes and signals were amplified using an Axopatch 200B amplifier (Axon Instruments). For current clamp recordings, the standard internal solution contained (in mM): K-gluconate 122, Na-HEPES 10, KCl 6, K-EGTA 6, Mg-ATP 3, Tris-GTP 0.2 and brought to pH 7.4 with NaOH. The internal solution used for voltage-clamp recordings contained (in mM): Cesium Methyl Sulfonate 105, TEA-Cl 10, K-EGTA 10, QX-314 2, Mg-ATP 5, Tris-GTP 0.5, brought to pH 7.3 with ~ 35mM CsOH. Voltages were corrected for a -10 mV liquid junction potential that was determined experimentally (Neher, 1992). Series resistances (R_S), as measured from the average response to trains of - 5 mV steps, were 10 to 20 mΩ and holding potentials were corrected offline by subtracting the product of leakage current and R_S from the applied voltage. Voltage and current signals were filtered at 2 kHz and digitized at a sampling interval of 0.1 ms via an ITC-16 interface (Instratech) using custom software written in Igor Pro (WaveMetrics) by Fred Rieke (University of Washington, Seattle, WA).

Receptor antagonists

To block synaptic transmission, neurotransmitter receptor antagonists were added to the extracellular solution. These included (in μM): 10 CGP 55845 ((2S)-3-[[(1S)-1-(3,4-Dichlorophenyl-)ethyl]amino-2-hydroxypropyl](phenylmethyl)phosphinic acid) 40 Gabazine (SR-95531), 50-75 L-APB (L- (+) -2-Amino-4-phosphonobutyric acid), 20-40 NBQX (2,3-dihydroxy-6-nitro-7-sulfamoyl-benzo[f]quinoxaline-2,3-dione), 50 TPMPA ((1,2,5,6-Tetrahydropyridin-4-yl) methylphosphinic acid hydrate), 1 Strychnine. Chemicals were purchased from Sigma or Tocris (Ellisville, MO).

Light Stimuli

An optical bench (Baylor and Hodgkin, 1973) with a quartz-halogen light source was used with a substage condenser to deliver focused visual stimuli to the photoreceptor layer of the retina. Unless otherwise noted, stimuli were 500 ms steps of 720 μm diameter (full-field) circular spots of 440 nm light centered on the receptive field of the cell with an unattenuated intensity of 2.1×10^6 photons $\square m^{-2}$ s^{-1}, which corresponds to 9×10^5 Rh*/rod/0.5 s step using an effective collecting area of 0.85 $\square m^2$ for mouse rods (Lyubarsky et al., 2004). All experiments were done in the presence of a background light intensity equivalent to 2 Rh*/rod/s to provide a defined and reproducible baseline level of illumination and consistent light-adaptational state.

Immunohistochemistry

Retinas were isolated in cold oxygenated mouse artificial cerebrospinal fluid (mACSF, pH 7.4) containing (in mM): 119 NaCl, 2.5 KCl, 2.5 $CaCl_2$, 1.3 $MgCl_2$, 1 NaH_2PO_4, 11 glucose, and 20 HEPES, and mounted retinal ganglion cell side up on black membrane filters (Millipore, HABP013). The retina and filter paper were then immersed for 20 minutes in 4%

paraformaldehyde in 0.1M phosphate buffered saline (PBS), rinsed with PBS, pre-incubated in PBS with 5% donkey serum and 0.5% triton overnight, and then incubated for 3 nights with primary antibodies. For vibratome sections, 60 μm slices were made post-fixation. Antibodies used were directed against TH (mouse monoclonal, 1:500, Chemicon), GFP (rabbit polyclonal, 1:1000, Chemicon), $GABA_A$ receptor □3 subunit (guinea pig polyclonal, 1:3000, kindly provided by J.M. Fritschy), $GABA_A$ receptor □1 subunit (guinea pig polyclonal, 1:5000, kindly provided by J.M. Fritschy), $GABA_C$ receptor □□subunit (rabbit polyclonal, 1:500, kindly provided by R. Enz), Glycine receptor □2 subunit (goat polyclonal, 1:300, Santa Cruz), and VIAAT (rabbit polyclonal, 1:1000, Synaptic Systems). Secondary antibodies utilized were either anti-isotypic Alexa Fluor conjugates (1:1000, Invitrogen) or DyLight conjugates (Jackson ImmunoResearch). Secondary antibody incubation was carried out in PBS overnight, and the retinas were subsequently mounted in Vectashield (Vector labs).

For DAC fills, 5 mM neurobiotin was used and retinas were post-fixed for 20 mins and processed thereafter for receptor labeling. To amplify the neurobiotin signal, streptavidin conjugated to Alexa Fluor 568 (1:200, Invitrogen) was included with the secondary antibody.

Image Analysis

Images were acquired on an Olympus FV1000 laser scanning confocal microscope, using a 1.35NA 60X oil objective. Raw image stacks were processed using MetaMorph (Universal Imaging) and Amira (Mercury Computer Systems) software. For volume estimation, the neurobiotin signal was used to mask in 3D, the DAC dendrites or axon using the 'label field' function in Amira. Alternatively, the TH signal was used to mask the DAC soma in 3D. Thereafter, the DAC mask was multiplied to the receptor channel to isolate the receptor signal exclusively within the mask. A constant threshold, chosen subjectively to exclude background

(average fluorescence intensity of non-clustered pixels), was then applied to the receptor-labeled channel to isolate receptors within the mask. The volume of the pixels above this threshold was expressed as a percentage of the total volume occupied by the pixels within the mask. To determine whether or not immunolabeled receptor clusters represent inhibitory synaptic sites, we quantified the extent to which $GABA_A\alpha3$ receptor clusters (most abundant on DAC processes) were apposed to inhibitory presynaptic terminals. To do so, we performed triple immunostaining for the receptors (α3), vesicular inhibitory amino acid transporter (VIAAT) and TH positive process in retinal slices. Receptor puncta within the TH mask were isolated, the VIAAT signal thresholded, and apposition of both signals was judged by eye upon rotation of the image volumes in 3D. Each GABA receptor cluster was considered to be apposed to a VIAAT positive terminal if the two signals showed overlap of pixels (>1 pixel overlap) at all angles of the 3D rotation.

DOPAMINERGIC AMACRINE CELLS

Dopamine (DA) is a modulatory neurotransmitter that is present in the peripheral and central nervous system of all vertebrates. In the retina, it is synthesized and released from a subset of amacrine interneurons called dopaminergic amacrine cells (DACs) and plays a key role in numerous events that accompany the switch from rod (dim light) to cone (bright light) mediated vision as night turns to day (Witkovsky, 2004). In spite of their importance in orchestrating the diurnal changes in the performance of the visual system, *in situ* functional studies of DACs have been hindered by the fact that they are sparsely distributed, 20 - 30 per mm^2, ~450/ mouse retina (Gustincich et al., 1997) and are indistinguishable amongst the myriad of other similar-looking neurons in the intact retina. They can, however, be labeled and specifically targeted for electrical recording using transgenic methods in which the promoter for tyrosine hydroxylase, the rate-limiting enzyme for dopamine biosynthesis, directs the selective expression of a reporter, either alkaline phosphatase (Gustincich et al., 1997) or fluorescent protein (Zhang et al., 2004).

Such methods have been used most commonly to identify DACs isolated from enzymatically dissociated retina for studies of their biophysical properties and repertoire of neurotransmitter receptors using pharmacology and immunohistochemistry (Gustincich et al., 1997; Feigenspan et al., 1998; Gustincich et al., 1999; Feigenspan et al., 2000; Steffen et al., 2003; Xiao et al., 2004). This approach has also been used to fluorescently tag DACs in whole mount retina for recording purposes (Zhang et al., 2007; Zhang et al., 2008). These studies were based, however, on extracellular recorded spike activity and used only intensely saturating light stimuli. For these reasons they provide an incomplete description of the cellular

physiology of DACs and the stimulus dependence of their light responses. In this study, we use whole cell current- and voltage-clamp recording to present an in-depth study of the functional properties of DACs in the intact retina and the synaptic inputs that give rise to their responses to a full range of light intensities.

Amacrine cells were targeted for whole cell recording using two-photon laser scanning fluorescence microscopy in a BAC transgenic mouse line in which the promoter for dopamine receptor 2 *(Drd2)* drove expression of GFP. In this line, two distinct populations of amacrine cells express GFP. One population comprised exclusively DACs, which could be identified on the basis of characteristic morphological features and co-localization with tyrosine hydroxylase (TH) labeling. The DAC population was morphologically homogeneous but physiologically diverse. DACs exhibited spontaneous activity with a stable spike pattern that ranged from nearly silent, to rhythmic firing at a steady rate, to firing in periodic bursts. These differences were accompanied by cell-to-cell differences in membrane properties. All of the DACs in the recorded sample generated light responses that depended on stimulus strength. At light onset threshold stimuli evoked glycinergic inhibition whereas stronger stimuli evoked a net excitatory response that was followed by a GABAergic inhibitory response at light offset. Furthermore, the postsynaptic receptor composition of these inhibitory inputs and their distribution across the DAC were identified by immunolabeling.

Results

Cell identification and targeted recording

In the *Drd2-GFP* transgenic mouse line, the promoter sequence for dopamine receptor 2 drives selective GFP expression in two separate populations of retinal amacrine cells that can be distinguished on the basis of soma size and density (Fig. 1A). The smaller cells, with soma diameters of 7 - 9 μm, were distributed numerously in the inner quarter of the inner nuclear layer (INL). They had dendrites that branched out first as a narrow band extending laterally along the outer boundary of the inner plexiform layer (IPL) and then diffusely in the middle third of the IPL. These cells are the subject of an ongoing investigation and will not be discussed further. The second population of *Drd2-GFP* amacrine cells had large (13 - 18 μm in diameter) spherical somas that were distributed sparsely along the inner boundary of the INL. In all regions (dorsal, ventral, temporal and nasal) of the *Drd2-GFP* Gensat retina, cells that were immunolabeled with TH antibodies also expressed GFP (n=76 cells, n=4 retinas; Fig. 1A, B). Images of neurobiotin filled cells (Fig. 1C) showed somas with 2 to 3 mono-stratified primary dendrites that spread out tangentially in the outer most (S1) strata of the IPL over an area roughly 600 μm diameter. The dendrites gave rise to two different kinds of secondary extensions. One was a small number (1 to 3) of axon-like processes that were beaded with varicosities and coursed laterally for long distances (1 -2 mm) across the retina (Fig. 1D). The primary dendrites also gave rise to a number of faint interplexiform processes that projected vertically into the outer plexiform layer (OPL) (Fig.1E). There were no apparent differences in the gross morphology of DACs targeted for intracellular dye-filling at randomly selected retinal eccentricities.

On the basis of these anatomical features (Versaux-Botteri et al., 1984; Dacey, 1990; Kolb et al., 1991; Gustincich et al., 1997), along with the fact that these cells (unlike the GFP positive cells with small somas) colocalized with tyrosine hydroxylase (TH) labeling (Fig. 1), the large soma *Drd2-GFP* cells were classified as interplexiform dopaminergic amacrine cells

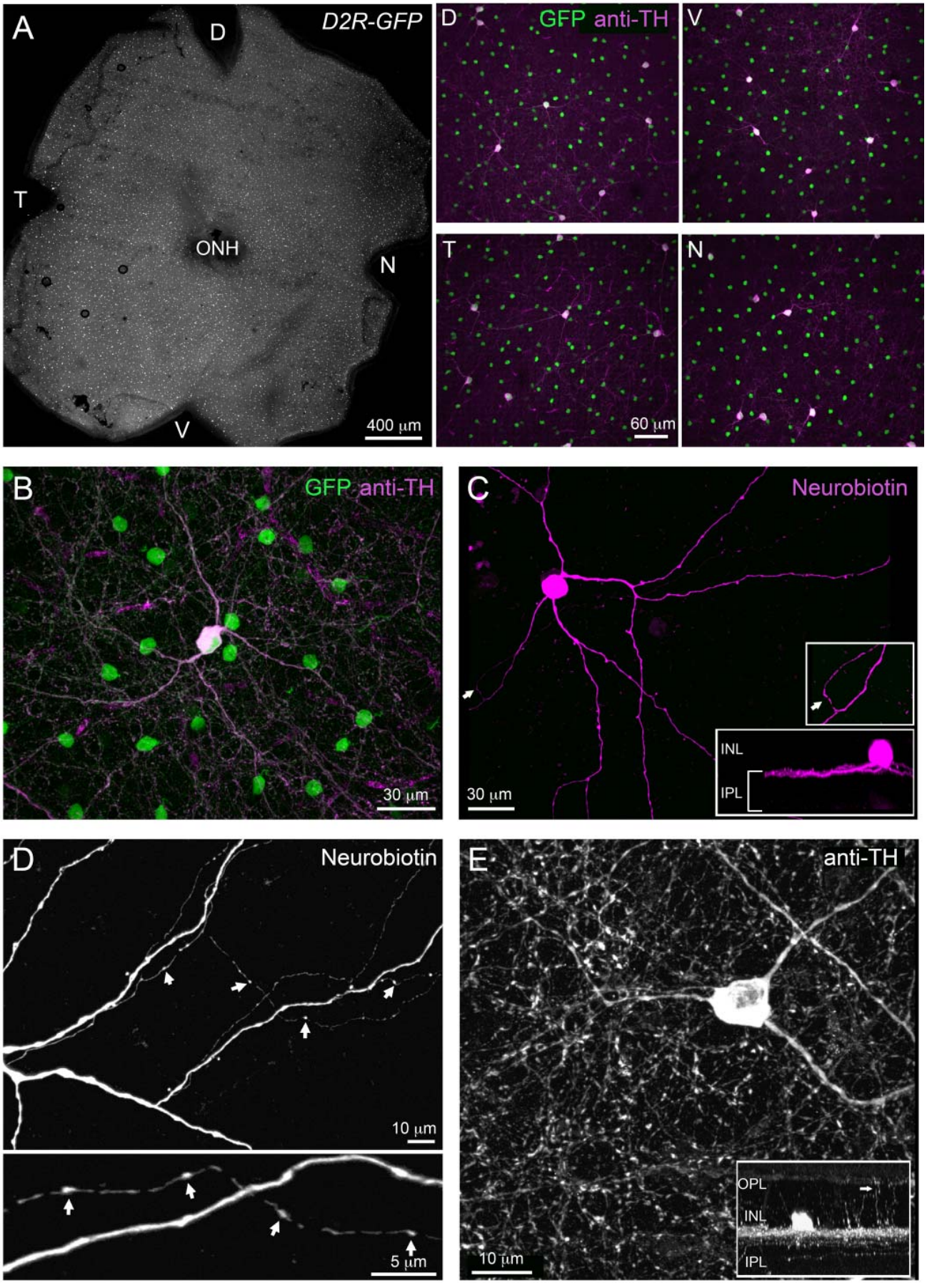
A
D2R-GFP
D
T
ONH
N
V
400 μm
D
GFP anti-TH
V
T
N
60 μm
B
GFP anti-TH
30 μm
C
Neurobiotin
INL
IPL
30 μm
D
Neurobiotin
10 μm
5 μm
E
anti-TH
OPL
INL
IPL
10 μm

Figure 1. Morphology of dopaminergic amacrine cells in *Drd2-GFP* transgenic. (A) Distribution of GFP expressing cells across a *Drd2-GFP* retina. Higher magnification of four representative regions immunolabeled for tyrosine hydroxylase (TH) in different parts of the *Drd2-GFP* retina (D, dorsal; V, ventral; T, temporal and N, nasal. ONH, optic nerve head). All GFP expressing cells with large somata are TH positive. (B) Higher magnification view showing a large TH positive, GFP expressing cell. (C) Morphology of a large GFP positive cell as revealed by intracellular filling with neurobiotin. Its cell body lies in the inner nuclear layer (INL) and processes stratify in the outermost part of the inner plexiform layer (IPL; inset 1). An axonal process is highlighted by arrows and shown at higher magnification in inset panel 2. (D) A neurobiotin filled DAC with varicosities along its axonal process (arrows). (E) TH immunolabeling in retinal whole-mounts shows a fraction of dopaminergic amacrine processes (arrow in inset panel) reaching the outer plexiform layer (OPL).

(DACs); also referred to as type 1 catecholamine cells. Our observations suggest that in the transgenic mouse used in our study, fluorescent protein expression in cells with large somata represent a single population of dopaminergic neurons based on their morphology.

Resting properties of DACs

In whole cell current clamp recordings, DACs had resting potentials in the vicinity of -30 to - 65 mV (mean 54 ± 1.04 mV, n = 81) and generated action potentials spontaneously (in such cells resting potential was defined as the baseline voltage at spike threshold). The pattern of spontaneous spike activity was not the same in all cells (Fig. 2). In a set of experiments on 59 DACs, in which the analysis focused on spontaneous activity in darkness, only five (8%) were quiet cells that generated spikes infrequently (< 0.1 Hz) at irregular intervals (Fig. 2A1). In all other cells in this sample spontaneous spike discharge occurred more frequently, at either a steady rate of ~ 2 to 8 Hz (in 25% of the cells) (Fig. 2B1) or in bursts (in 62% of the cells) that were intermingled with a more regular rate of ongoing spike activity (Fig. 2C1). In 5% (3/59) of the recorded cells discrete high-frequency bursts of action potentials were generated at regular (~ 1 to 5 s) intervals on an otherwise quiet background of spike activity (Fig. 2D). The cell-to-cell variation in the pattern of spontaneous spike activity was not associated with observable differences in DAC gross morphology or cellular health, as judged by the stability of resting membrane potential and the presence of action potentials. There were no significant differences in the resting potentials of cells that exhibited the different categories of activity, with mean values that ranged from -52 to - 48 mV in quiet and periodic bursting DACs, respectively. The characteristics of the spontaneous activity in a particular cell did not change over the course of a typical whole cell recording lasting 30 to 45 mins. In cells having a

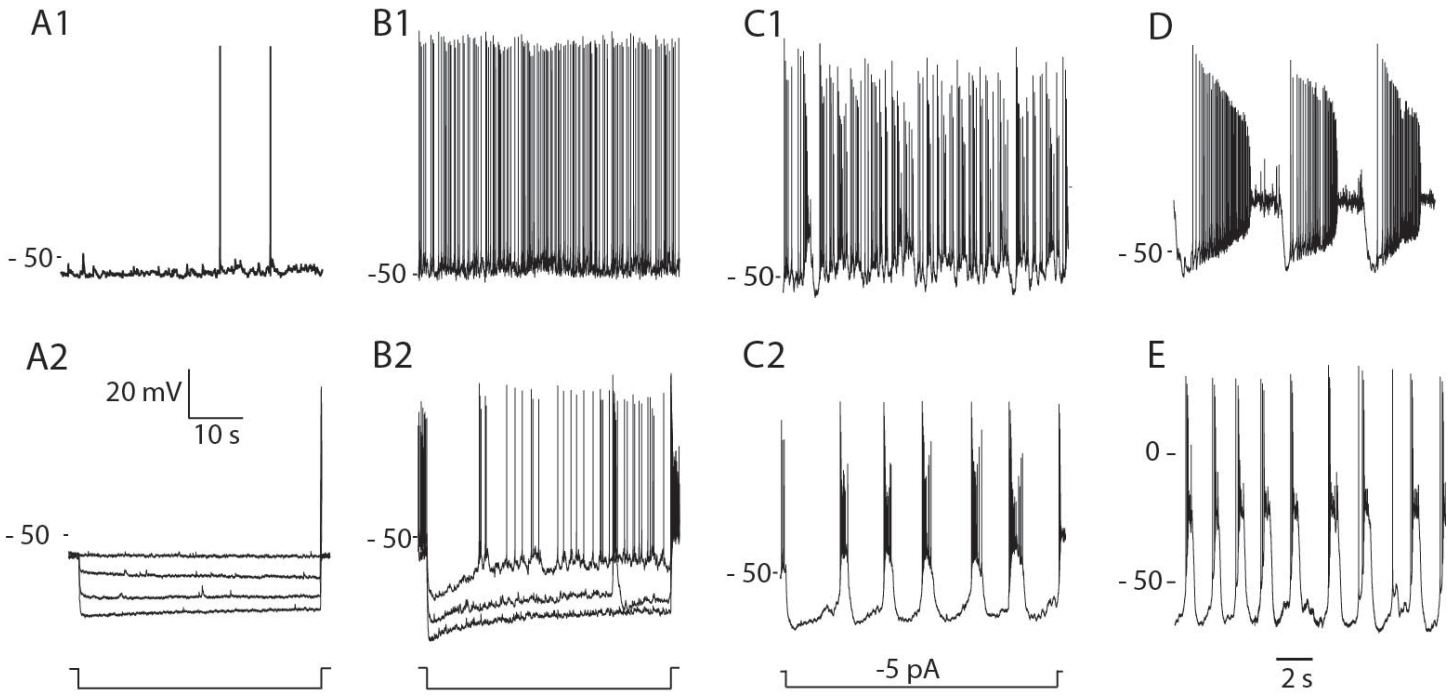

Figure 2. Cellular properties of DACs. Resting spontaneous spike activities in four different cells provide examples of DACs that are nearly silent (A1), continuously active (B1), steady discharge with intermixed bursts of spikes (C1) or periodic bursts (D). Resting membrane potentials (mV) are indicated by labels left of each trace. The voltage responses evoked by constant current steps in the same cells are shown by traces in A2, B2, and C2. Negative current steps in A2 and B2 were 20, 30 and 40 pA. Periodic burst firing persists in the presence of a mixture of excitatory and inhibitory synaptic blockers (in μM): APB (50), AP5 (50), CNQX (50), picrotoxin (50), and strychnine (1). Labels to the left of each recording identify the resting potential (mV) relative to the voltage trace using the provided voltage scale.

mixture of single spikes and bursts of activity, hyperpolarizing current injection accentuated the bursting component of the activity and revealed an underlying "pacemaker-like" periodicity (Fig. 2 C1, C2).

Bursting spike activity and the unmasking effect of hyperpolarization persisted in the presence of a combination of excitatory and inhibitory synaptic blockers (Fig. 2E), consistent with generation by an intrinsic mechanism. In quiet cells that displayed little to no spontaneous activity the voltage response to a hyperpolarizing step of current was flat and showed no evidence of relaxing from an initial peak hyperpolarization (Fig. 2A2). In contrast, the hyperpolarizing step response in cells with regular and/or bursts of spike activity exhibited a prominent sag as voltage relaxed from an initial negative peak back towards a less negative steady state potential with a time constant of 1 - 2 s (Fig. 2B2). This suggests a hyperpolarization activated inward current (I_H) may play a role in the biophysical mechanism that gives rise to the periodic bursts of action potentials, similar to what has been reported for several other types of neurons exhibiting bursting behavior (Alonso and Llinas, 1989; McCormick and Pape, 1990a; Yung et al., 1991; Mercuri et al., 1995).

Light response properties of DACs

Over the course of this study, we have recorded from more than 300 DACs and have yet to find one that did not respond to light. This result differs sharply from earlier reports where a large fraction (40%) of DACs did not respond to light (Zhang et al., 2007; Zhang et al., 2008).

The minimally detectable full field (720 μm diameter) scotopic stimulus evoked a hyperpolarizing potential change and a transient suppression of spontaneous spike activity at the onset of steps of 440 nm light with intensities that ranged from 9 to 70 Rh*/rod across cells

(Fig. 3A, B). In many but not all cases, the recovery from the hyperpolarizing response evoked by dim light included a brief increase in spike activity caused by a delayed excitatory after potential (Fig. 5A). This is a feature of responses evoked at the end of hyperpolarizing voltage steps in neurons that express I_H (Robinson & Siegelbaum, 2003).

With increasing step intensity, the DAC light response grew to become dominated by excitatory input at light onset and a strong hyperpolarizing response at light offset (Fig. 3A,C). The ON and OFF components of the DAC response to a bright stimuli are apparent in a raster plot as an initial burst of spikes followed by an inhibition of spike activity at light offset (Fig. 3C). Small diameter (35 μm) spots of bright light evoked similar light responses when centered on the soma as when displaced from it by up to 300 μm (data not shown), suggesting that DACs do not receive antagonistic synaptic input from a surround that extends over that area.

In a minority of cells, the strongest stimuli recruited an additional excitatory input that overcame the inhibitory OFF response and extended the step response well beyond the duration of the stimulus (Fig 3D). The prolongation of the response grew with further increase in light intensity, resulting in responses to the brightest light that typically lasted 15 to 20 s; 7 to 10-fold longer than the responses evoked by the same stimulus in the majority of DACs. Long lasting responses such as these have been reported previously in extracellular recordings of DACs and attributed to there being a subset of DACs that receive excitatory synaptic input from intrinsically photosensitive retinal ganglion cells (ipRGCs) (Zhang et al., 2008). Recordings from these types of cells were infrequent (~ 12% of recorded DACs) and since they obscured the inhibitory response evoked at light offset our experiments concentrated on GFP labeled DACs that did not exhibit any evidence of ipRGC input.

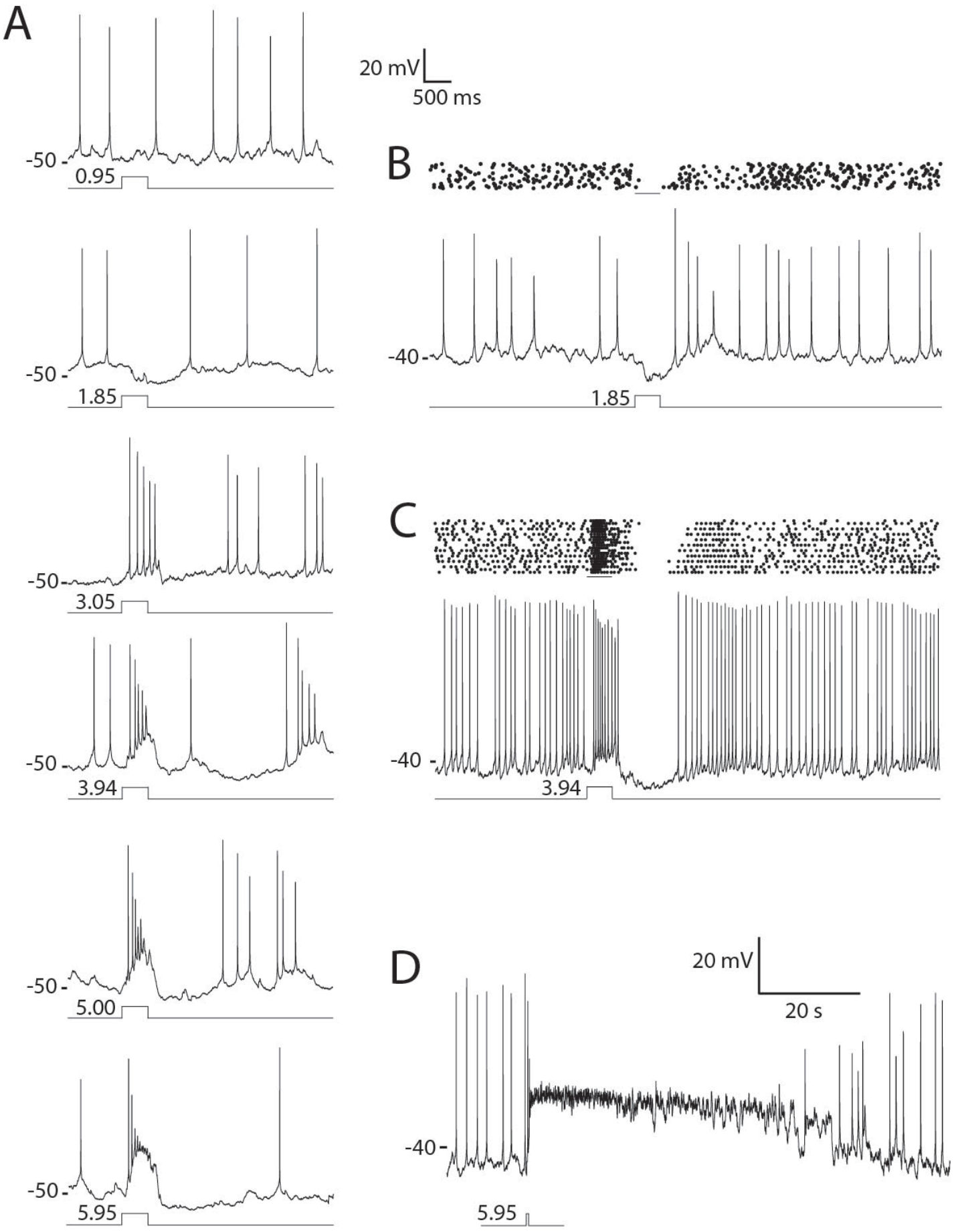
A
20 mV
500 ms
-50
0.95
-50
1.85
-50
3.05
-50
3.94
-50
5.00
-50
5.95
B
-40
1.85
C
-40
3.94
D
20 mV
20 s
-40
5.95

Figure 3. DAC light response properties. (A) DAC light response evoked by 500 ms steps of full field (700 μm diameter spot) 440 nm light of indicated intensities ($\log_{10}$ Rh*/rod/step). (B & C) Spike rasters and example trace showing responses to light steps in different cells. (D) An example of DAC that exhibited a prolonged response to a bright full field step of 440 nm light ($9x10^5$ Rh*/rod/0.5s). Labels to the left of each recording indicate the resting potentials in mV relative to the voltage trace using the voltage scales provided.

As the amplitude of the depolarizing ON response grew with increasing light intensity, spike threshold was exceeded and action potentials were triggered that declined in amplitude over the course of the excitatory response (Fig. 3A). With further increase in stimulus strength the frequency of the evoked spike discharge increased whereas the accompanying decline in spike amplitude accelerated resulting in the failure of action potential generation (Fig. 3A). The rapid inactivation of spike production by depolarization block is a characteristic feature of DAC electrophysiology as well as an established attribute of midbrain dopaminergic neurons (Bunney and Grace, 1978; Grace and Bunney, 1986). It limits the response evoked by intense stimuli to an initial transient burst of spikes at the onset of a strongly depolarizing synaptic potential (Fig 3A,D).

Depolarization block shapes the response to steady illumination in a similar manner (Fig 4A). Action potentials evoked at the onset of a step of bright light decline rapidly in amplitude to the point of spike failure after a short-lived burst of activity. The absence of spike activity persists until the underlying depolarizing potential decays for sufficient relief of inactivation for the generation of spikes that first appear as miniature (~ 5 mV peak amplitude) spikes and grow to full amplitude (~ 90 mV) at an irregular firing rate. Depolarization block also plays a role in shaping the responses evoked by a train of repetitive flashes of light (Fig 4B). Stimuli that flicker ON and OFF at a low rate (1 - 3 Hz) evoke a brief burst of spikes at the onset of the periods of light exposure that are quickly silenced by depolarization block. Under these conditions the hyperpolarizing (inhibitory) OFF response accelerates the recovery from depolarization block and serves to remove spike inactivation in time for the next flash in the stimulus train.

Light-evoked synaptic currents

The underlying excitatory and inhibitory synaptic currents that gave rise to the DAC light response were revealed by recording stimulus-activated currents in voltage-clamped cells held at either -60 or 0 mV, i.e. respectively at potentials where net current flow through inhibitory or excitatory transmitter gated ion channels would be expected to be eliminated (Fig. 5). Dim light evoked a net outward current when the cell was held at 0 mV, consistent with the DAC threshold light response being a hyperpolarizing voltage change in current clamp recordings. In cells held at -60 mV, stimuli in the same intensity range had no effect on the recorded current whereas stronger stimuli evoked an inward current response that grew in amplitude and duration with further increase in intensity. In cells held at 0 mv, the amplitude of the outward current evoked by dim stimuli remained constant until the stimuli reached the intensity level that had first evoked an inward current response when the cell was held at - 60 mV. From that point on, the outward response declined with increasing light intensity to become a net inward current response when stimulated with the brightest light (Fig. 5). These changes in the amplitude and polarity of the response suggest that the responses to all but the weakest stimuli are the sum of inhibitory and excitatory inputs with relative strengths that change with light intensity. This may arise as a consequence of voltage-clamp error due to the well-established inability to control dendritic voltage by clamping somatic voltage (Armstrong and Gilly, 1992; Williams and Mitchell, 2008); a particularly acute problem in cells, such as DACs, with extensive dendritic arbors. Under these conditions setting the somatic voltage at the expected reversal potential for excitatory synaptic current would not uniformly nullify the current throughout the dendritic tree. This would allow the contribution of inward currents from excitatory dendritic inputs to the net stimulus-activated current recorded in the soma to increase with stimulus intensity. This can also account for the fact that the hyperpolarizing potential change that is associated with the offset of steps of bright light in current clamp

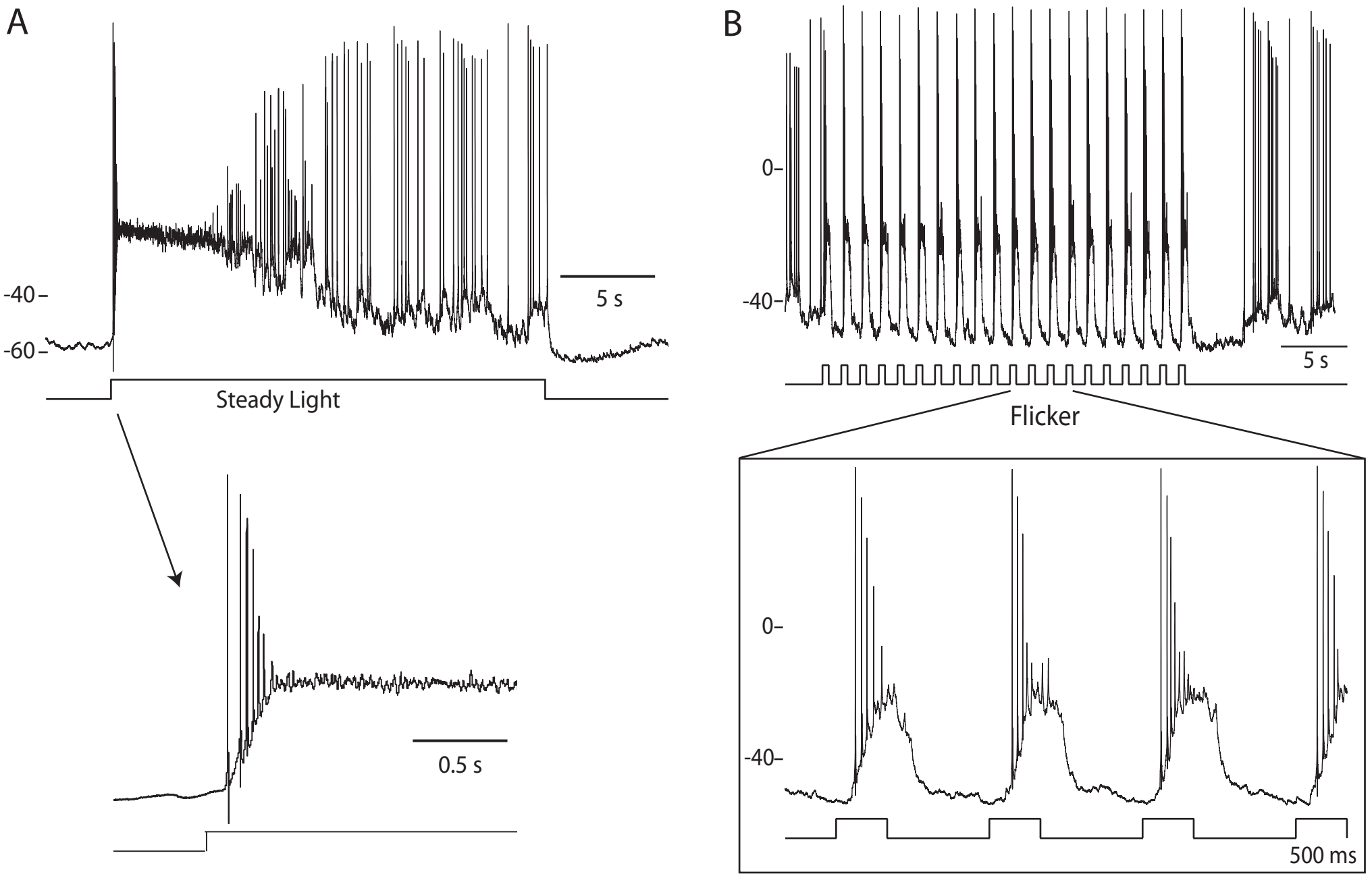
A
-40
-60
5 s
Steady Light
0.5 s
B
0
-40
5 s
Flicker
0
-40
500 ms

Figure 4. DAC responses and steady and flickering light. (A) 20 s step of light evoked a transient burst of spikes at light onset that gave way to irregular lower frequency spike discharge as the cell adapted to the steady light (n=4). The termination of action potential discharge at the leading edge of the response by depolarization spike block is shown on an expanded time base in the insert (arrow). The traces (B) show the entrainment of DAC spike responses to periodic 500 ms stimulus (3.94 $\log_{10}$ Rh*/rod/0.5s) that flickers ON and OFF at 0.7 Hz on two different time scales. Labels to the left of each recording indicate the resting potentials in mV relative to the voltage trace using the voltage scales provided.

recording is not apparent in voltage clamp as an outward current at V_{hold} = 0 mV. The presence of the inhibitory OFF response is however apparent as an outward current when the contamination by light-activated inward current has been eliminated by blocking excitatory input with L-APB (Fig. 7B, & 8C).

Taken together, there are three distinguishing components to the DAC light response: a dim step ON inhibition, a moderate to bright step ON excitation and an OFF inhibition. These intensity dependent features of the light response were observed in DACs that had a low rate of resting spike activity (quiet cells) as well as in DACs that spontaneously discharged spikes at either a steady rate or intermingled with bursts of activity. The intensity dependence of the light responses in the relatively small number (~ 5%) of DACs that fired spikes in discrete periodic bursts (Fig. 2D) could not be clearly demonstrated on the background of the pacemaker-like fluctuations in cell voltage that generated the periodic bursts of activity.

Synaptic origin of light response components

To investigate the synaptic inputs that underlie the DAC light responses we next examined the three light response components with the help of pharmacological agents.

Dim step ON inhibition: Bath application of 1 μM strychnine eliminated the hyperpolarizing voltage response as well as the outward current response evoked by dim light in current (V_{rest} @ I_{zero}) - and voltage –clamp (V_{hold} = 0 mV) recordings (Fig. 6; n=7 in current clamp, n=3 in voltage clamp recordings). The inhibitory input stimulated by low intensity steps persists in the presence of GABAzine (40 μM) and TPMPA (50 μM) and is blocked by either L-APB (50 μM) or NBQX (40 μM), indicating that DACs receive light driven glycinergic input from an amacrine cell type that is excited by ON rod bipolar cells. The glycinergic input to the DACs at light onset does not appear to be mediated by AII amacrine

cells, which are an established source of glycinergic inhibition under scotopic conditions (Bloomfield and Dacheux, 2001). This is because the inhibitory input evoked by bright light is blocked by NBQX (Fig. 6C,) showing that glycinergic input is not able to be driven by electrical coupling with ON cone bipolar cells, as would be the case if the amacrine in question were an AII (Xin and Bloomfield, 1999; Veruki and Hartveit, 2002; Pang et al., 2007).

Bright step ON excitation: Bath application of L-APB blocked the transient spike discharge triggered by the onset of a bright step of light in current clamp recordings (Fig. 7A1, 2; n=6) as well as an inward current response in voltage clamped cells at light onset (Fig. 7B1, 2; n= 4). That the DAC excitatory ON response is also blocked by NBQX alone (data not shown) indicates that it is mediated by glutamate release from ON bipolar cells acting on postsynaptic ionotropic glutamate receptors. This is in agreement with experiments showing that solitary DACs express AMPA receptors activated by either glutamate or kainate (Gustincich et al., 1997). It appears that the excitatory input to the DAC maybe driven by light activation of both cone and rod pathways. The switch of the DAC light response from net inhibition at light onset to net excitation occurs when the step intensity is sufficiently bright to excite cones, suggesting that DACs receive excitatory input from ON cone bipolar cells (CBCs). As the threshold response in cells held at 0 mV is an outward current that decreases with increasing stimulus intensity before reaching photopic (bright) light levels, suggests that scotopic (dim light) stimuli are too weak to directly excite cones, and instead give rise to stimulus-evoked currents that are the sum of rod mediated excitatory and inhibitory synaptic currents (Fig. 5).

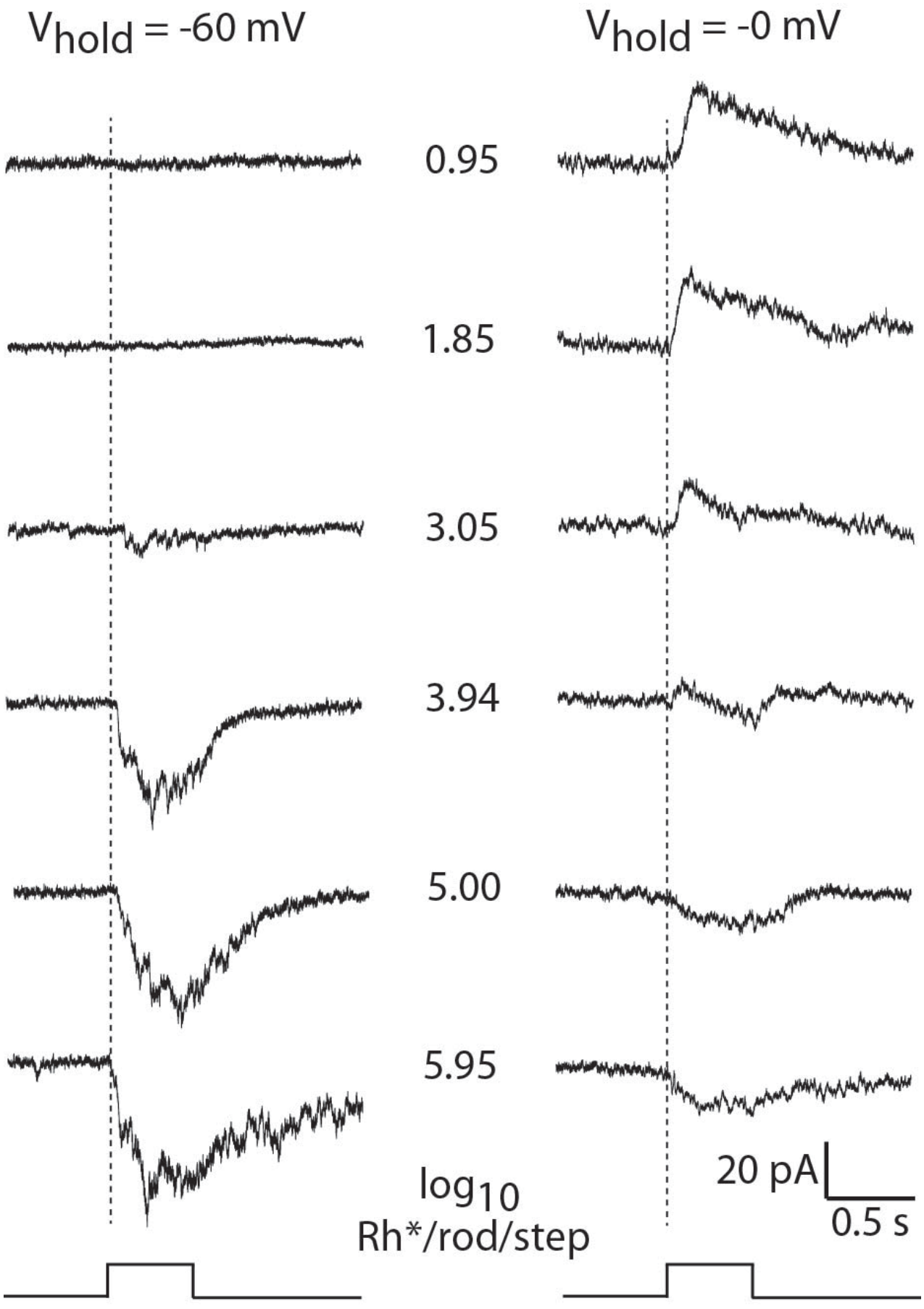
V_{hold} = -60 mV
V_{hold} = -0 mV
0.95
1.85
3.05
3.94
5.00
5.95
log_{10} Rh*/rod/step
20 pA
0.5 s

Figure 5. Light response intensity series in voltage clamp. Responses evoked by 500 ms steps of full field 440 nm light at the intensities (central column) expressed as $\log_{10}$ Rh*/rod/0.5s in a representative DAC held at a voltage close to the reversal potential for inhibitory synaptic input (- 60 mV; left column) and excitatory synaptic input (0 mV; right column) in Ames's solution.

Bright step OFF inhibition: In current clamp recordings, the inhibitory OFF response causes a transient suppression of spike activity at light offset and was not affected by bath application of strychnine or TPMPA (Fig. 8A; n=4 for strychnine, n=3 for TPMPA), ruling out mediation by glycinergic input or by GABAergic drive mediated by $GABA_C$ receptors. The duration of the depolarizing light response evoked by moderate to bright light was increased by more than two-fold (Figure 8B, B1; n=9) in the presence of GABAzine, a selective $GABA_A$ antagonist. This is consistent with the elimination of inhibitory synaptic input at light offset that would normally curtail the light response by opposing the excitatory ON response. GABAzine treatment was associated with the generation of a spontaneous voltage oscillation that trigger bursts of spikes that were followed by a silent period of suppressed spike activity. This made it difficult to use light-evoked spike activity to evaluate the effect of GABAzine on the inhibitory OFF response as in the experiments with strychnine and TPMPA (Fig. 8A). To circumvent this problem we tested the effect of GABAzine on the inhibitory OFF response in voltage clamp (Fig. 8C; n=3). In the presence of a high concentration (75 μM) of L- APB, a step of bright light evoked an inward current (V_{hold} = 0 mV) that developed slowly during the step and was followed by a larger and faster outward current at light offset (Fig. 8C). Both components of the response were eliminated by GABAzine, suggesting that the DAC receives tonic GABAergic input in darkness from an unidentified amacrine cell (AC) that is excited by OFF CBCs, as postulated previously (Critz and Marc, 1992; Gustincich et al., 1997, see however Zhang et al., 2007). Light, by inhibiting OFF bipolar cells, extinguishes the GABAergic input to the DAC causing a reduction of the outward current that appears as a slow activation of a net inward current during the step of light. At light offset the OFF pathway is disinhibited, which excites the GABAergic amacrine cell in the circuit causing, in turn, an outward current response at the termination of the stimulus (Fig 8C).

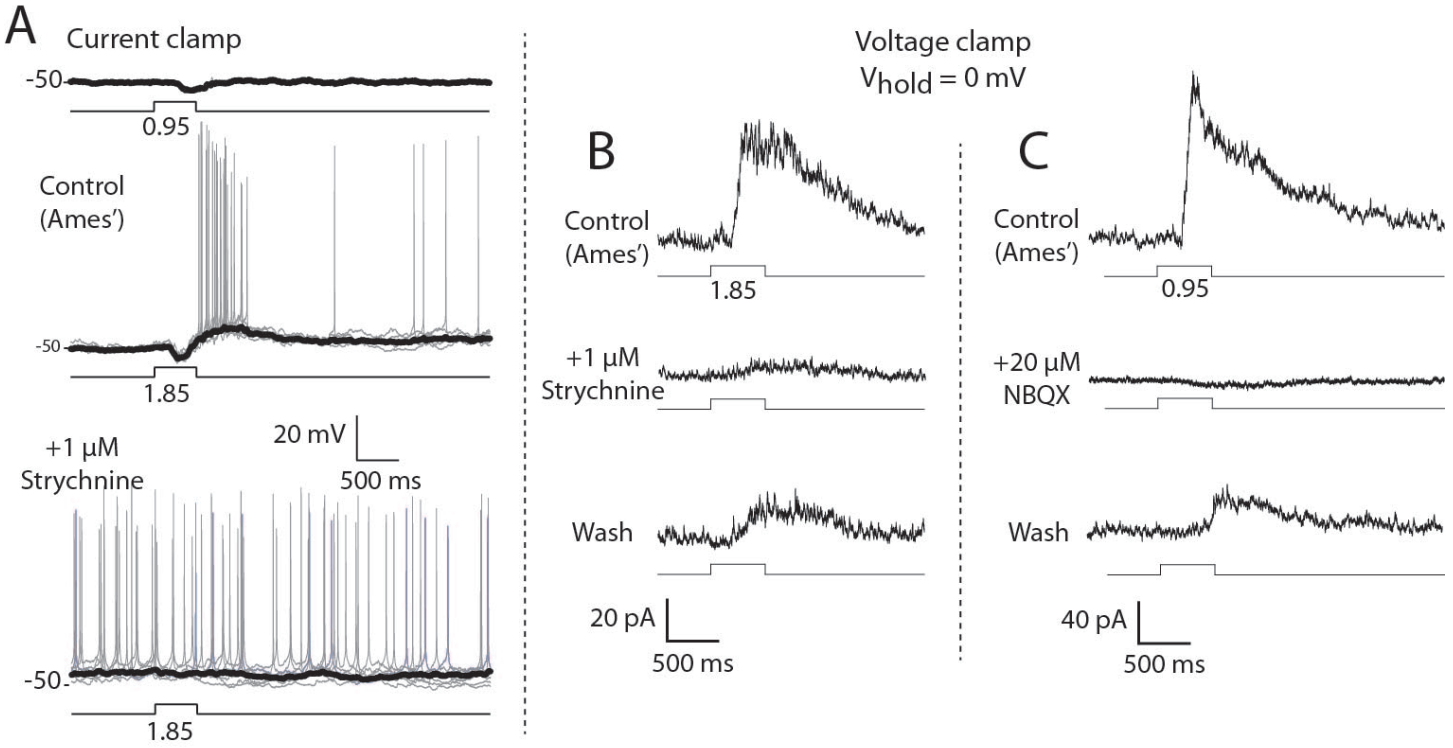

Figure 6. Inhibitory ON response evoked by a dim step of light is blocked by strychnine. (A) Current clamp recordings of responses in weak steps of light in absence and presence of 1 µM strychnine (n=7). Average response is shown in black and individual responses are displayed in gray. Labels to the left of each recording indicate the resting potentials in mV relative to the voltage trace using the voltage scale provided. (B) Voltage clamp recordings of outward current response at 0 mV holding potential evoked by dim steps in absence and presence of 1 µM strychnine. Stimulus intensities are reported as log10 Rh*/rod/0.5s for full field 440 nm light and associated with the traces showing the timing of the light step.

These results can be summarized by a synaptic wiring diagram in which the DAC receives excitatory and inhibitory input via the ON pathway and inhibition via the OFF pathway (Fig. 9). In the proposed circuit the threshold response to scotopic stimuli is generated by inhibitory input at light onset from an unidentified glycinergic amacrine cell that is activated by excitatory input from rod driven ON bipolar cells. Photopic stimuli evoke a net depolarizing ON response that is produced by direct excitatory input to the DAC from cone ON bipolar cells. The inhibitory OFF response that is a characteristic feature of the response to photopic stimuli includes GABAergic input to the DAC from an unidentified amacrine cell that is excited by OFF cone bipolar cells. This limb of the circuit provides tonic GABAergic inhibition to the DAC in the dark that is suppressed by light and re-excited at light offset. While the glycinergic and GABAergic amacrine cells in the proposed diagram are unidentified they are likely to have narrow and wide-field dendrites, respectively based on the type of neurotransmitter they release (Wassle et al., 1998).

Inhibitory receptor subtypes expressed on mouse DACs

Our pharmacological analysis suggests that distinct inhibitory inputs shape the DAC response to light onset and light offset (ON-glycinergic, OFF-GABAergic), and that different GABA receptor subtypes ($GABA_A$ and not $GABA_C$) are involved. To correlate the physiological observations with expression of GABA and glycine receptors on DACs, we performed immunolabeling using antibodies directed against specific GABA and glycine receptor subunits. In the IPL of the rodent retina individual $GABA_A$ and glycine receptor clusters contain specific □-subunits (□1-□3) (Koulen et al., 1996; Wassle et al., 1998; Wassle et al., 2009). TH-immunopositive DAC processes exhibited numerous clusters of □1-$GABA_A$ and □3-$GABA_A$ receptors, some □2-glycine receptor clusters but few, if any, $GABA_C$

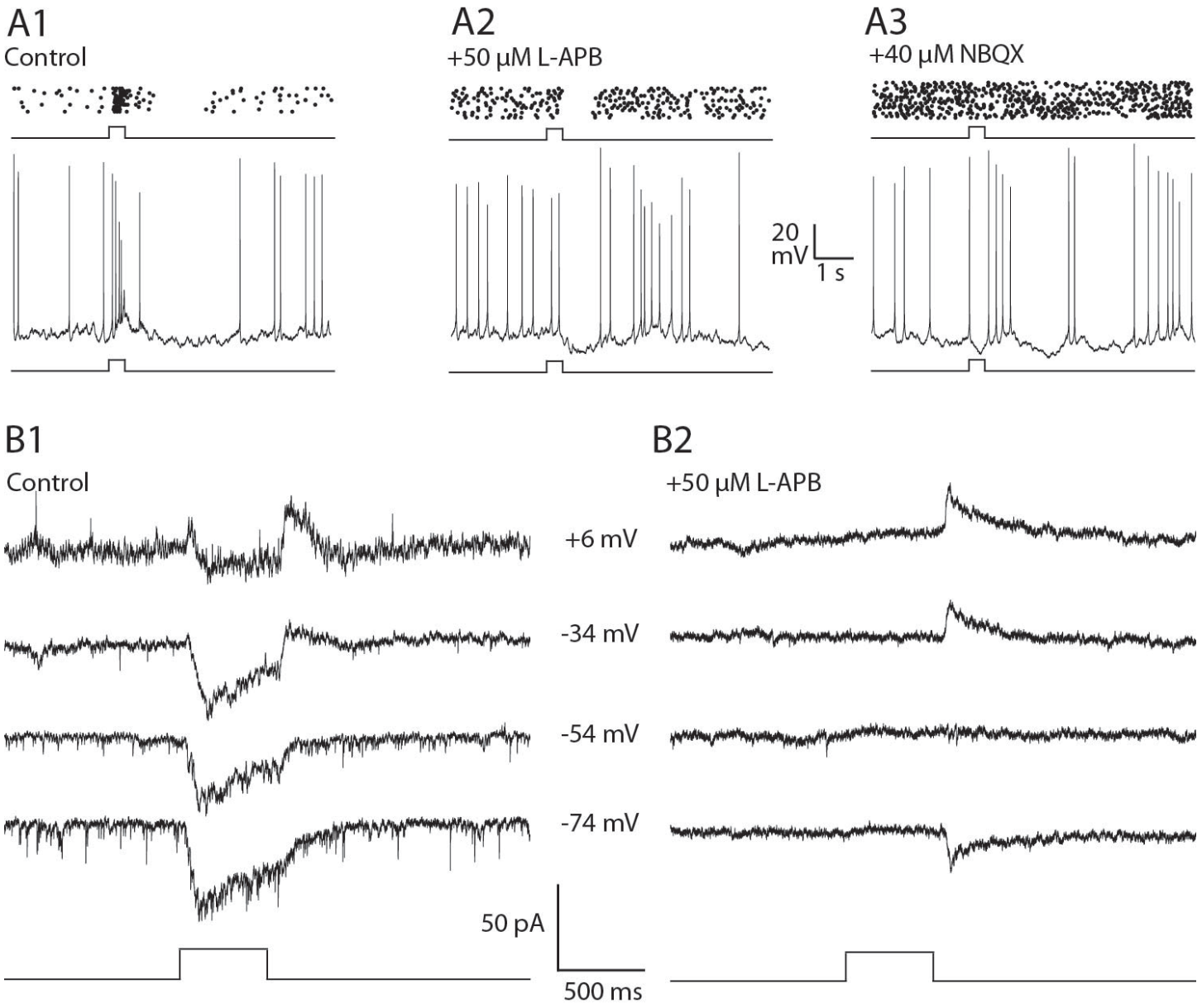

Figure 7. Synaptic origin of the excitatory ON response evoked by bright light. Spike raster plots and example single traces (below) show the response evoked by bright step of light in absence of glutamatergic reagents (A1) and in the presence of L-APB, a metabotropic glutamate receptor agonist that quenches the excitatory light response in ON bipolar cells alone (A2) and with the addition of NBQX (A3). The results show that the control response had an excitatory ON response that was eliminated by L-APB and an inhibitory OFF response that was blocked by the addition of NBQX (n=6). B1 and B2 show the currents evoked by bright light in voltage clamp recordings at the indicated holding potentials (midline labels) in the absence (control) and presence of L-APB (B2). The ON pathway antagonist eliminated the inward current evoked at light onset but not the outward current at light offset (n=4). Light stimuli: 500 ms full field steps of 440 nm light equivalent to 5.0 log10 Rh*/rod/0.5s.

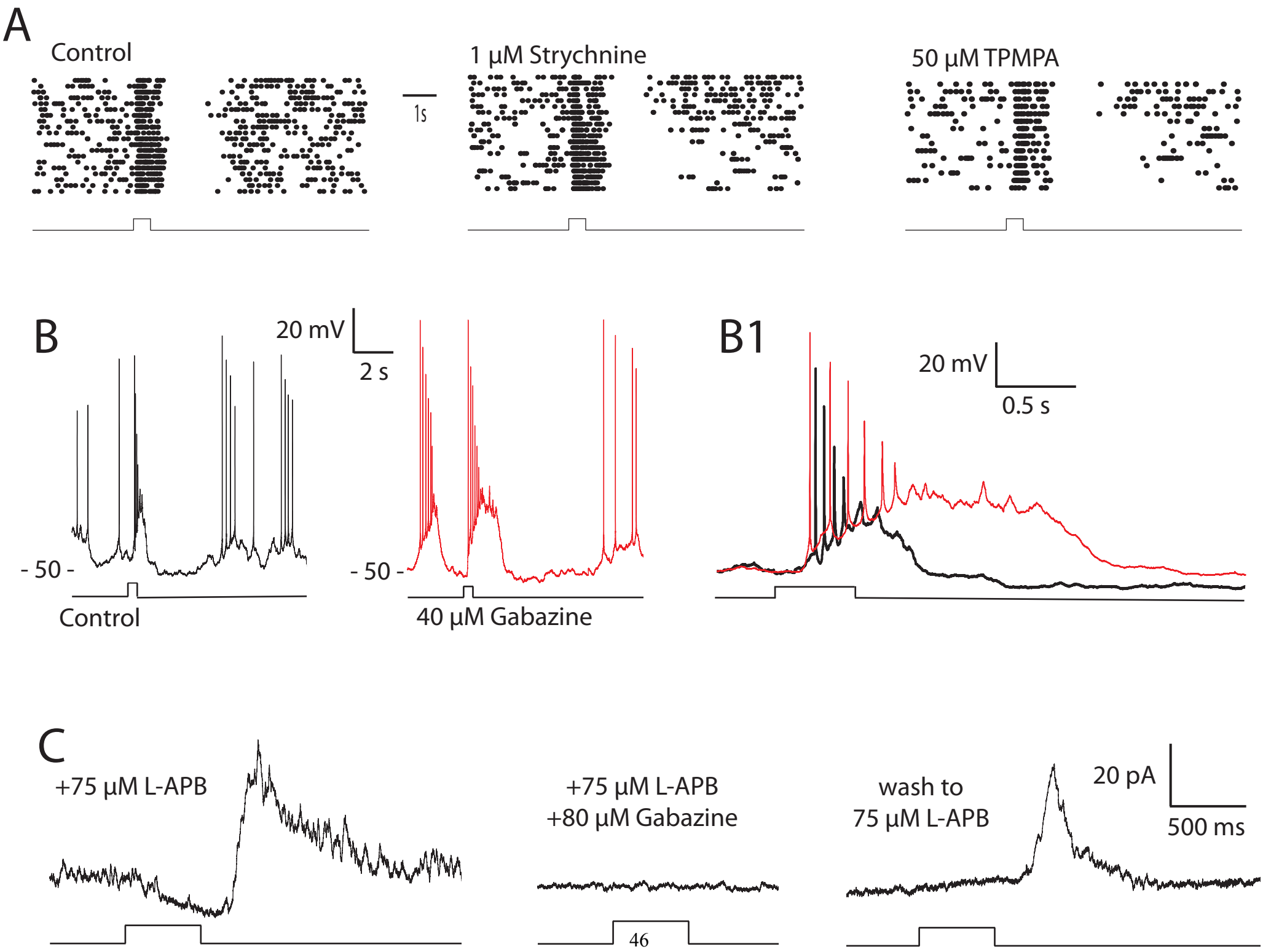
A
Control
1 µM Strychnine
50 µM TPMPA
1s
B
20 mV
2 s
- 50 -
Control
- 50 -
40 µM Gabazine
B1
20 mV
0.5 s
C
+75 µM L-APB
+75 µM L-APB
+80 µM Gabazine
wash to
75 µM L-APB
20 pA
500 ms

Figure 8. GABAergic inhibitory OFF response evoked by bright light. (A) Spike rasters showing the persistence of the inhibitory OFF response in the presence of strychnine (n=4), a glycine receptor antagonist, and TPMPA (n=3), a $GABA_C$ receptor antagonist. (B) Bath application of GABAzine (red trace) prolonged the depolarizing response to light, shown on an expanded time base (B1) that compares superimposed responses in absence (black) and presence (red) of GABAzine (n=9). Labels to the left of each recording indicate the resting potentials in mV relative to the voltage trace using the voltage scales provided. (C) In voltage clamp recordings (V_{hold} = 0 mV) in the presence of L-APB there was a slowly increasing negative (inward) current during the light step that was supplanted by a large positive (outward) current at light offset. Both components of the step response were eliminated by GABAzine and partially reversed upon washout (n=3). Light stimuli: 500 ms full field steps of 440 nm light equivalent to 3.94 (A, B) and 5.95 (C) $\log_{10}$ Rh*/rod/0.5s.

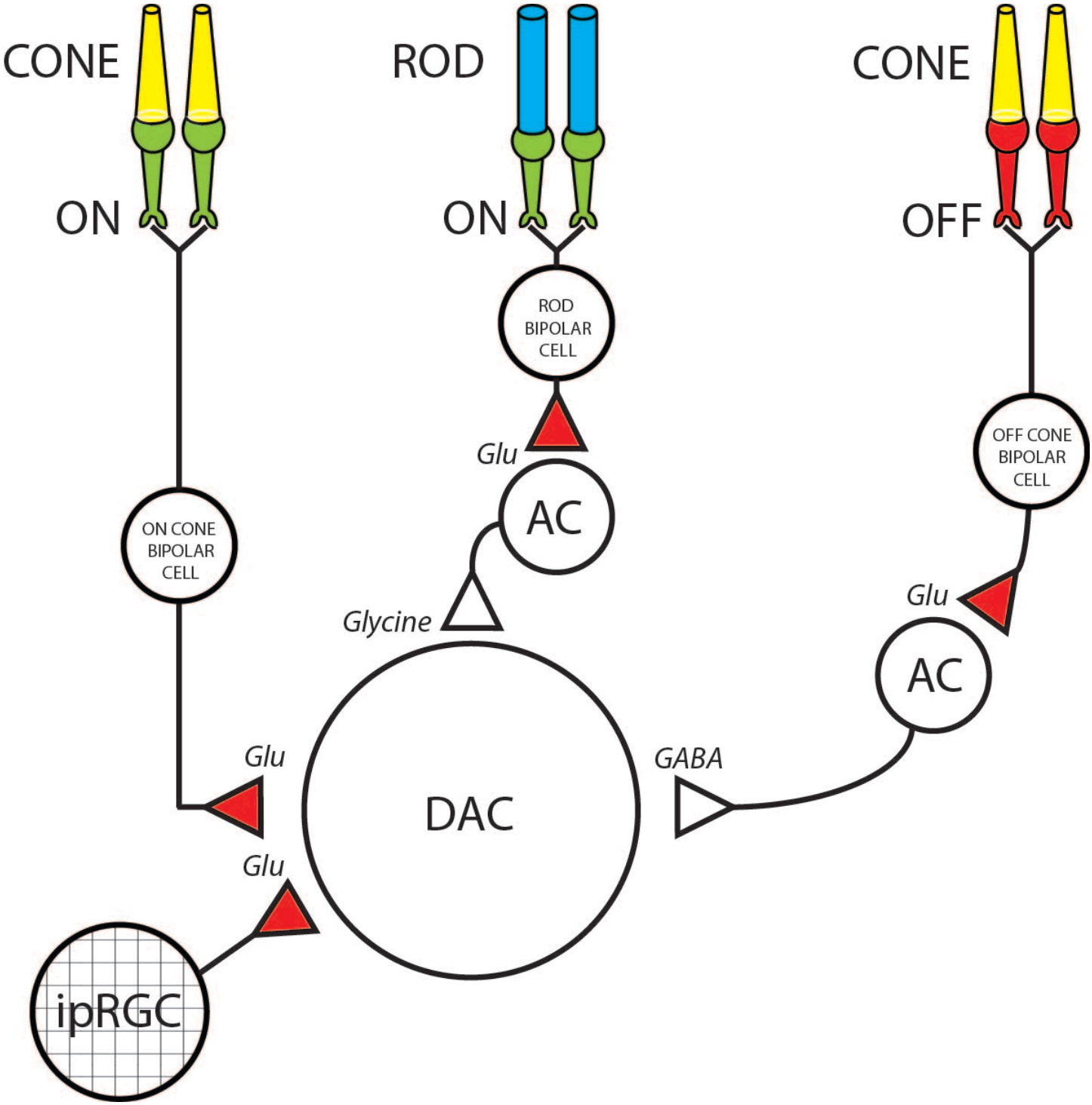

Figure 9. DAC synaptic wiring diagram. In the proposed schematic DACs receive excitatory glutamatergic input from ON cone bipolar cells as well as from ipRGCs in a subset (~ 15%) of DACs. In addition, DACs received inhibitory input from two sources. One is an unidentified glycinergic amacrine cell that is driven by excitatory input from rod bipolar cells and the other is an unidentified GABAergic amacrine cell that is driven by excitatory input from OFF cone bipolar cells. Red and green terminals represent ionotropic (AMPA / kainate) and metabotropic (mGluR) glutamatergic synapses, respectively.

receptors clusters. To quantify the relative expression levels of the various GABA and glycine receptor types, DACs in the *Drd2-GFP* whole mount retina were intracellularly filled with neurobiotin and afterward immunolabeled for $GABA_A$□3, $GABA_A$□1, GlyR□2, and $GABA_C$□□receptor subunits (Fig. 10A). Three-dimensional masks of the dendritic and axonal processes were generated to exclude receptor staining outside the DAC processes of interest (Fig. 10B, C) and estimate the percent volume occupied by a particular receptor type (Fig. 10E). This was then used to compare the relative abundance of each receptor type on DAC axonal and dendritic processes. $GABA_A$□3 receptors were the most abundant inhibitory receptor type expressed on both DAC dendrites and axonal processes (Fig. 10E), followed by $GABA_A$□1, and to a much lesser extent GlyR□2 receptor clusters. $GABA_C$ receptors were minimally expressed on both the axonal and dendritic compartments of the DAC.

Receptor expression on DAC soma was estimated in a similar way, but after generating a 3-D mask of TH immuno-positive somata (Fig 10D) rather than using neurobiotin filled cells in which the soma was stained strongly and generated a saturating fluorescence signal. $GABA_A$□1 and $GABA_A$□3 were equally abundant on the soma Fig. 10E) in contrast to DAC processes that express higher levels of receptors with □3 than □1 subunits. This suggests that the DAC uses different $GABA_A$ receptor subsets to process dendritic/axonal versus somatic inhibition. The soma, like the DAC dendrites and axons, exhibited very few receptor clusters that were $GABA_C$□ positive (Fig. 10E). These results are consistent with the persistence of the inhibitory OFF response in the presence of bath applied TPMPA, a selective $GABA_C$ receptor antagonist (Fig. 8).

Because of the dense labeling of receptors in the IPL, two strategies were used to evaluate the specificity of receptor labeling within DAC processes. First, DACs were filled with neurobiotin and the retina double-labeled with an antibody against the C-terminal-binding

protein 2 (CtBP2). We chose CtBP2 because it is densely expressed throughout the IPL. Also CtBP2 is localized at synaptic ribbons of excitatory glutamatergic presynaptic terminals in the retina (Schmitz et al., 2000; Soto et al., 2011) and thus should not be within DAC processes. Upon quantification, the % occupancy of CtBP2 puncta on DAC dendritic and axonal processes was found to be only 0.98 ± 0.17 % and 0.64 ± 0.15 % (N= 2 cells) of the available dendritic and axonal volume, respectively. This suggests that the probability of random association of receptor clusters with DAC processes is less than 1 in 100. Second, we determined the percentage of $GABA_A\square 3$ (most abundant receptor type on DACs) clusters on TH immuno-positive processes that were apposed to terminals labeled with antibodies directed against vesicle inhibitory amino acid transporter (VIAAT) (Sagne et al., 1997; Soto et al., 2011) (Fig. 11A). TH positive processes were masked to isolate $GABA_A\square 3$ receptor clusters specifically within the DAC neurite; we found that 87.9 ± 2.4% (N=152 $GABA_A\square 3$ puncta, 2 animals) of the $GABA_A\square 3$ clusters were apposed to VIAAT positive presynaptic terminals (Fig. 11B). Thus, we conclude that the vast majority of immunolabeled receptor puncta on DAC processes represent sites of inhibitory synaptic input.

Discussion

Functional diversity of DACs

DACs appear to be a morphologically homogeneous population of cells but exhibit cell-to-cell differences in their functional properties. These are apparent in the cell-to-cell variation of their spontaneous activity in darkness. The characteristics of their spike activity fell into four categories: quiet cells that generated spikes infrequently at random intervals, rhythmic cells that fired spikes at a maintained rate, and cells that generated bursts that were either mixed in with single spikes or occurred in discrete bursts at regular intervals (Fig. 2). The

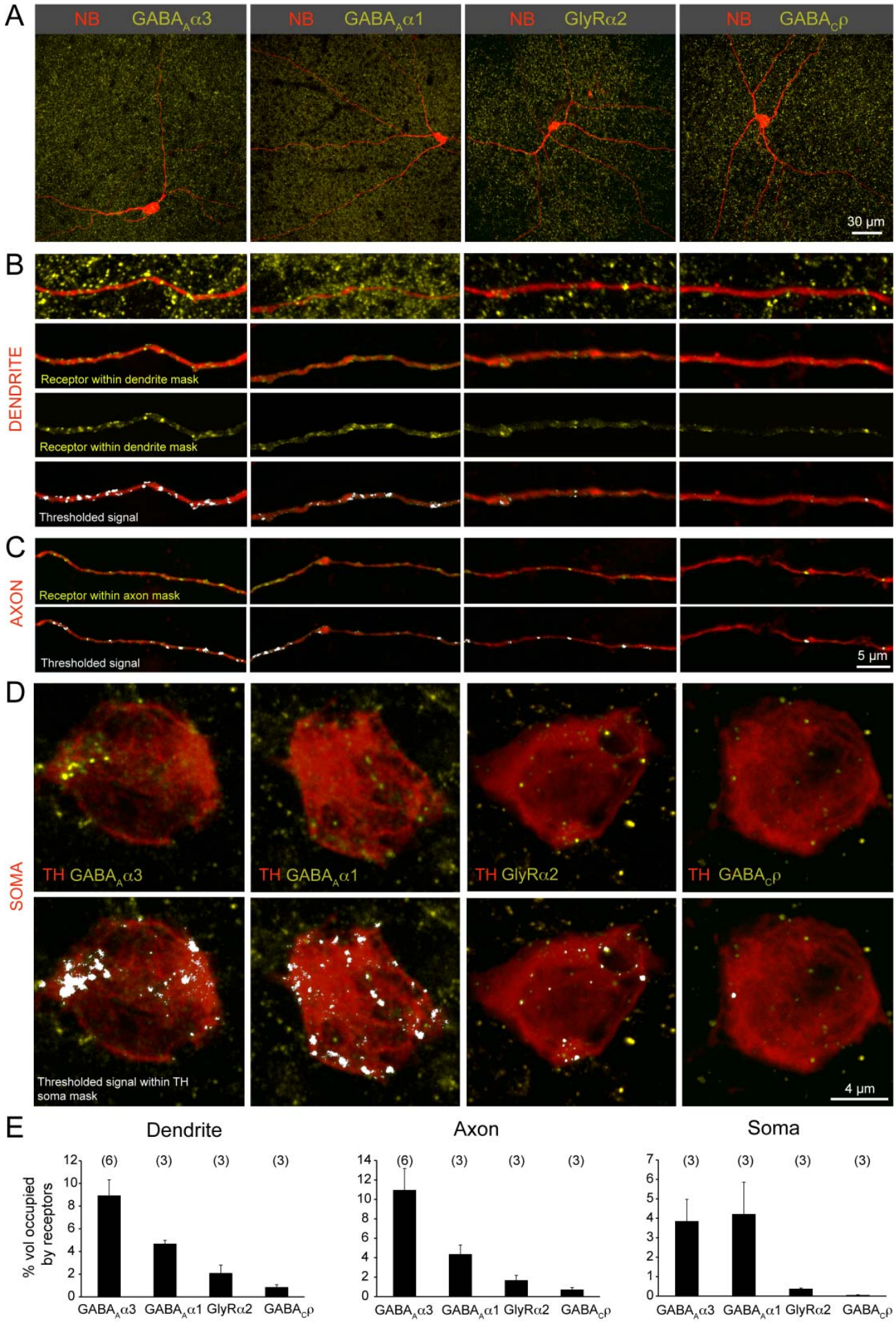
A
NB GABA$_A$α3
NB GABA$_A$α1
NB GlyRα2
NB GABA$_C$ρ
30 µm
B
DENDRITE
Receptor within dendrite mask
Receptor within dendrite mask
Thresholded signal
C
AXON
Receptor within axon mask
Thresholded signal
5 µm
D
SOMA
TH GABA$_A$α3
TH GABA$_A$α1
TH GlyRα2
TH GABA$_C$ρ
Thresholded signal within TH soma mask
4 µm
E
Dendrite
Axon
Soma
% vol occupied by receptors
(6) (3) (3) (3)
GABA$_A$α3 GABA$_A$α1 GlyRα2 GABA$_C$ρ

Figure 10. Inhibitory receptor density on DACs. (A) Neurobiotin fills (NB-568) of dopaminergic amacrine cells in the *Drd2-GFP* line co-labeled for specific inhibitory receptor subsets: $GABA_A$ receptors (α3 or α1 subunit), glycine receptor (α2 subunit) and $GABA_C$ receptors (ρ subunit). (B) Higher magnification of a stretch of dendrite and receptor labeling. Receptors localized within the volume of the dendrite are visualized by first creating a 3-D 'dendrite mask' of the NB-568 signal, and then digitally excluding signal from the receptor immunolabeling outside this mask. A threshold is imposed above which receptor signal intensities are quantified. (C) Receptor labeling within the axon mask. (D) Receptor labeling within the soma mask. Somata labeled here by anti-TH. (E) Quantification of the percentage of volume of the dendrite, axon or soma occupied by receptors containing different subunits.

existence of two categories of DAC bursting activity agrees with Zhang et al. (2007), as does the presence of a minority of DACs that are not spontaneously active. The presence of cells in the DAC population that exhibit the observed categories of spiking activity is also consistent with the range of cell-to-cell differences in spontaneous spike discharge exhibited by midbrain dopaminergic neurons (Grace and Bunney, 1984a, b). The differences in spike patterns ranging from infrequent discharge of single spikes to periodic bursts may participate in setting the basal tone of DA release; the only function that DACs and dopaminergic midbrain neurons have in common. A diversity in resting DA release across the DAC population might have the advantage of offering a richer selection of options for regulation than if all the cells had the same level and mode of DA release. In any case, the variability in spike activity appears to be a feature of DACs in the intact retina since solitary DACs isolated from enzymatically dissociated mouse retina generate spikes rhythmically at a steady rate (3 - 9 Hz) that is remarkably uniform from one cell to the next and devoid of periodic burst firing (Gustincich et al., 1997; Feigenspan et al., 1998; Steffen et al., 2003; Xiao et al., 2004).

The difference between quiet and active DACs is not due to differences in cell health, recording time or experimental conditions but it is associated with differences in their responses to hyperpolarizing current injection (Fig. 2). Active, but not quiet, DACs express a voltage-dependent cation conductance that is turned on by hyperpolarization. Since I_H is a known contributor to pacemaking and oscillatory spike discharge in a variety of cell types, including midbrain dopaminergic neurons (Alonso and Llinas, 1989; McCormick and Pape, 1990a; Yung et al., 1991; Mercuri et al., 1995), it reasonable to suggest that it plays a role in the mechanism that generates burst firing in active DACs. In this regard it is relevant to note that spontaneous spike activity in solitary DACs is silenced by a 5 to 10 mV hyperpolarizing step that does not exhibit a voltage sag (I_H), or unmask pacemaker activity as it does with

DACs in the intact retina (Gustincich et al., 1997; Feigenspan et al., 1998; Steffen et al., 2003; Xiao et al., 2004). The reason for the differences between the intrinsic properties of solitary DACs and DACs in the intact retina are not clear. It could be that the ion conductances that are the source of biophysical differences between solitary and intact DAC reside in the neurites that are shorn off in the dissociation process and constitute the bulk of surface area of the DAC. It is also possible that the retina milieu includes neuromodulators that are absent from the saline solution in which solitary cells are maintained.

The explanation for the cell-to-cell differences in membrane properties of *in-vivo* DACs is not known. It is possible that the DAC population is divided into physiologically discrete subtypes with fixed differences in their intrinsic properties. It is also possible that DACs exhibit physiological differences depending on the strength of neuromodulatory control and/or circadian regulation. Neuromodulators, such as dopamine, are known to influence the repertoire of ion channel expression in a variety of neuronal cell types and affect their pattern of spontaneous spike activity (Lacey et al., 1987; Pape and McCormick, 1989; McCormick and Pape, 1990b; Stefani et al., 1995). Furthermore, DACs contain clock genes (Dorenbos et al., 2007) and dopamine release oscillates in tune with the circadian cycle (Mangel and Dowling, 1987; Weiler et al., 1997; Ribelayga et al., 2004; Storch et al., 2007). Although our present observations do not discriminate between these possibilities, our findings do raise the need for future experiments to correlate the spontaneous spike patterns of DACs with their release of dopamine.

DAC light responses and distinct modulatory roles for GABA and glycine

The DAC light response depends on stimulus intensity. Onset of dim light evoked a hyperpolarizing response that was initiated by rods and mediated by inhibitory synaptic input

from an unidentified glycinergic amacrine cell (AC) that appears not to be an AII amacrine (Fig. 6C). At brighter light intensities the DAC ON response switched from being inhibitory to net excitatory. This was attributed to the recruitment of cones and direct excitatory input to DACs from ON cone bipolar cells (CBCs). While we have assumed that the glycinergic AC responsible for the inhibitory response evoked by dim light is excited by direct synaptic input from ON rod bipolar cells (Fig. 9), we cannot exclude the possibility that rod signals evoked by weak stimuli can electrically spread to cones via gap junctions. Such coupling would allow glycinergic ACs to be excited by ON CBCs. Since inhibition evoked by dim light is eliminated by strychnine without unmasking a residual depolarizing response, the ON CBCs that are excited by cones coupled to rods would have different properties than the ON CBCs providing direct excitatory input to DACs in response to bright light. The segregation of ON CBC signals evoked by rod to cone coupling from those evoked by light activated cones could be based on differences in the ON CBCs, such that weak signals in the cone stimulate ON CBCs that excite glycinergic AC whereas strong signals stimulate ON CBC that excite DACs directly.

The DAC OFF response is evoked by stimuli in the same intensity range as the stimuli associated with the switch in the ON response from being inhibitory to net excitatory at light levels that begin to activate cones as well as rods. The OFF response evoked by moderate to bright light is generated by strong inhibitory synaptic inputs from unidentified GABAergic ACs that are excited by cone driven OFF CBCs. The synaptic circuit inferred from the intensity dependence and pharmacology of the DAC light response (Fig 9) is consistent with immunohistochemistry showing the expression of $GABA_A\alpha1$, $GABA_A\alpha3$ and $GlyR\alpha2$ receptor clusters on DAC processes. The distinct receptor subtypes were not confined to specific cellular compartments; each receptor subtype was present on the soma, axon and

dendrites. This indicates that glycinergic inhibition evoked by dim light onset and GABAergic inhibition at bright light offset are not correlated with a differential distribution of GABA and glycine receptors. While DAC somata possess similar amounts of $GABA_A$□1 and □3 receptor clusters, $GABA_A$□3 receptors were relatively more abundant in the dendritic and axonal processes. That gating kinetics are slower and the agonist affinity higher in $GABA_A$ receptors with □3 than with □1 subunits (Gingrich et al., 1995) suggests that GABAergic regulation of DAC activity is complex and tuned by a variety of factors. The presence of inhibitory input on dendrites may modulate excitatory synaptic input whereas the inhibitory input on the axonal processes, which have not been described previously in retina, may serve to modulate the fidelity of spike mediated communication between the DAC soma and its wide field synaptic targets. The exclusive expression of glycine receptors with □2 receptors contrasts with previous observations in the primate retina showing that DACs preferentially express GlyR□3 receptors (Jusuf et al., 2005). The functional significance of the species difference in GlyR□-subunit expression in the same type of amacrine cell is not known.

The DAC is thus a novel example of a retinal neuron that receives inhibitory input at light onset and offset using different transmitters. The physiological consequences of this arrangement are not clear but it is reasonable to consider it in the context of DA release, which is the central DAC function. Our results show that DACs exhibit diverse intrinsic properties and receive a repertoire of synaptic contacts that regulate strength of excitatory input and axonal output. These cellular attributes of DAC physiology may act together to fine tune spike triggered DA release in a manner that would not be possible if the cell behaved as a simple on/off switch. Numerous studies based on quantitative chemical analysis of DA levels in retina superfusate have established that DA release is increased by light (Nichols et al., 1967; Kramer, 1971; Iuvone et al., 1978; Morgan and Kamp, 1980; Kamp and Morgan, 1981;

O'Connor et al., 1987; Ishita et al., 1988; Kirsch and Wagner, 1989), in which case rod mediated glycinergic inhibition may act to suppress spike activity and DA release in darkness. Previous studies have also demonstrated that DA release is increased more strongly by light that flickers ON and OFF at a low frequency (1 - 3 Hz) than by steady illumination (Dowling and Watling, 1981; Kirsch and Wagner, 1989; Kolbinger and Weiler, 1993; Weiler et al., 1997). Our results, along with evidence that DA release from isolated DACs is spike dependent (Puopolo et al, 2001), provide an explanation for the difference in the effectiveness of these two stimulus procedures. Light that flickers ON and OFF triggered strong bursts of spikes in phase with periods of light exposure (Fig. 4B), whereas steady light evoked an initial transient burst of spikes at light onset that was rapidly silenced by the depolarizing block and remained silent until the depolarizing excitatory response declined to a level that relieved spike block at which point spike generation resumed at an irregular rate not that different from the cell's rate in darkness (Fig. 4A); consistent with reports that DA release is not increased over its level in darkness by continuous light exposure (Godley and Wurtman, 1988; Kolbinger and Weiler, 1993; Weiler et al., 1997). The inhibitory OFF response participates in the response to flicker by hyperpolarizing the cell during periods of darkness thereby relieving depolarizing spike block in time for the generation of action potentials at the onset of the next period of light exposure.

The reason for the difference in the effectiveness of flicker and steady light in triggering DA release is not known, but seems likely to be the result of facilitated vesicular release that in other neuronal cell types is commonly associated with repetitive firing and increased intracellular Ca2+ due to summated influx (Fioravante and Regehr, 2011). This is in agreement with evidence that neuromodulator release is evoked more strongly by phasic than tonic spike generation (Dutton and Dyball, 1979; Gonon, 1988; Floresco et al., 2003). The

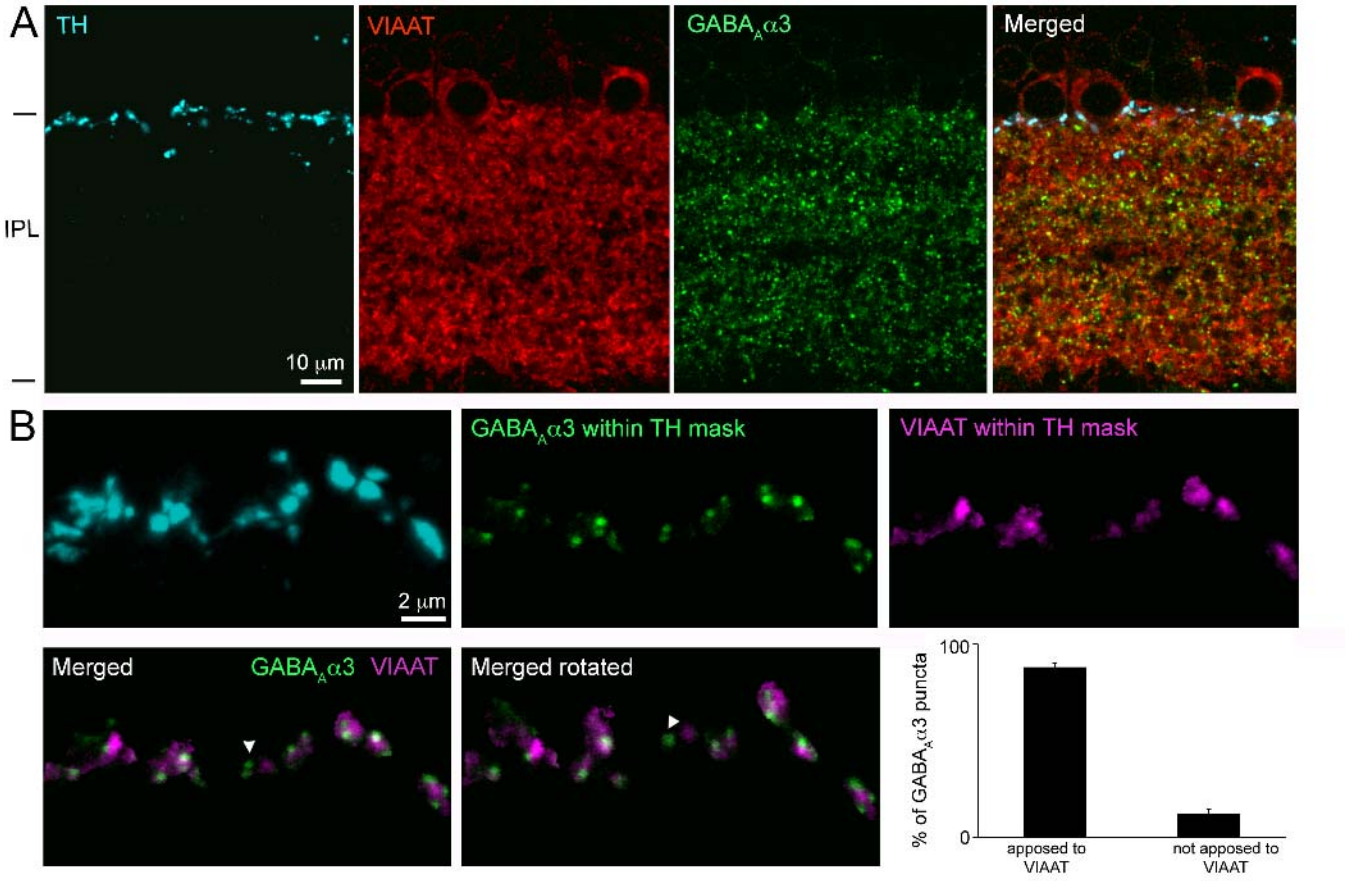

Figure 11. GABA receptor puncta on TH immuno-positive processes are apposed to inhibitory presynaptic terminals. (A) Dopaminergic amacrine processes labeled with TH in retinal slices, together with labeling for GABAAα3 receptors and the inhibitory presynaptic marker, VIAAT (IPL, inner plexiform layer). Maximum intensity projection of confocal image stack representing 0.9 μm thicknesses. (B) To quantify GABAAα3-VIAAT appositions, TH labeled processes were masked in thicker image stacks (4.8 μm). GABAAα3 and VIAAT signal within the masks were isolated to reveal appositions in 3D. The majority of GABAAα3 receptor puncta were apposed to VIAAT (exception, arrowhead, merged panel). Plots show quantification of the appositions identified by 3D rotation of the merged images.

inhibitory OFF response evoked by moderate to bright light rapidly terminates spike discharge after a period of light exposure and thus benefits the generation of responses characterized by transient increases in spike discharge. In the midbrain DA system tonic and phasic spike activity control different higher level behaviors (Floresco et al., 2003; Zweifel et al., 2008; Tsai et al., 2009) and have been modeled in terms of changes in the balance between DR1 and DR2 signaling pathways (Dreyer et al., 2010). It is possible that DA signaling in the retina is influenced in a similar manner and that a mixture of inhibitory inputs are important controlling factors in this process, a suggestion that remains to be explored.

Comparison with previous studies

The results presented here differ in several significant ways from the results presented in the only two previous papers on *in situ* DACs that were identified and targeted for single cell recording in intact retina using fluorescence protein expression in a transgenic mouse line (Zhang et al. 2007, 2008). The earlier studies reported that 40% of DACs do not respond to light and that the remaining light sensitive cells belonged to two distinct classes in which light onset evoked either a transient burst or a sustained train of spikes with no evidence of an OFF response in either. The ON-sustained response, which was recorded from 44% of the subpopulation of light sensitive DACs, was attributed to excitatory input from ipRGCs.

In contrast, over the course of our experiments we found that 100% of the recorded DACs responded to light and whether they generated a sustained or transient spike response depended on stimulus intensity (Fig. 3A). Sustained spike trains were evoked by weak stimuli whereas depolarization block limited the ON response evoked by bright light to an initial transient burst of spikes at response onset. This was also the case in a minority of DACs in our sample that generated exceptionally prolonged large depolarizing responses to strong stimuli,

which we considered to be the result of direct excitatory input from ipRGCs (Fig. 3D). In addition, our results show clear evidence of inhibitory ON and OFF responses, which contradicts previous reports that neither GABAergic nor glycinergic OFF-channel signals were involved in DAC light responses (Zhang et al. 2007, 2008).

Whereas both the earlier studies and our study were based on recording from DACs in different transgenic mouse lines, this seems unlikely to be an explanation for the difference in the results since in the *Drd2-GFP* Gensat line used here all amacrine cells that were label with antibodies to TH also express GFP. This would presumably encompass population of DACs that were targeted by using the TH promoter to drive red fluorescent protein expression in the studies by Zhang and colleagues. It seems more likely that discrepancies between our results and those of Zhang et al (2007, 2008) are related to important differences in methodology. In the earlier studies DACs were targeted using fluorescence excited by one-photon absorption of short wavelength light. Although no specific information is given about the intensity or illumination area of the excitation light it was presumed to have reduced the light sensitivity of the retina (Zhang et al. 2008). Changes in the adaptational state of the retina were avoided in the present study by exciting fluorescence using 2-photon absorption of infrared light (see methods). Furthermore the results of the earlier studies were based on extracellularly recorded spike activity evoked using only intense photopic stimuli that would saturate the photoresponses of both rods and cones. The use of saturating light exposure to evoke responses that can only be detected if they are super-threshold for action potential production provides a severely limited description of the light response properties and fails to fully characterize the dynamic range of DAC light sensitivity and the subthreshold synaptic inputs that give rise to the intensity dependent properties of the DAC light response.

In the Zhang studies, a reduction in the light sensitivity from the use of short wavelength light to excite fluorescence for cell targeting and from repeated exposure of the retina to steps of saturating light could account for the presence of cells that do not generate a strong enough response to evoke spikes and thus are classified as non-responsive (null) DACs. In any case, the absence of light-evoked spike activity in a retinal neuron is not sufficient evidence to conclude that it does not respond to light. Light-adaptational changes in the retina might also serve to reduce the amplitude of the depolarizing response evoked by excitatory input to a level that is not sufficient to cause a depolarizing spike block accounting for the presence of a sub-population of DACs in which the response to saturating light is a sustained spike train rather than a transient burst as seen in our recording.

In view of the fundamental differences in the experimental methods used in this and the earlier studies it is not surprising that there is limited agreement in the results. The main points of accordance include cell-to-cell variation in the pattern of spontaneous spike activity (with disagreement about the extent of the differences) and the elimination of the transient excitatory ON response by L-APB.

In summary our experiments on *in situ* DACs characterize the intensity dependence of the synaptic inputs that give rise to their response to light. The onset of dim stimuli evoked an inhibitory response that with increasing light intensity become a net depolarizing response that is truncated at light offset by GABAergic inhibition via the OFF pathway. The interplay between light intensity and the strength and timing of multiple excitatory and inhibitory inputs determine the DAC response to light and the role it plays in modulating retina function through the release of dopamine.

SMALL BISTRATIFIED AMACRINE CELLS

Studies suggest that there is anywhere from 20-30 different types of amacrine cells in the mammalian retina (Masland 1988; Wässle & Boycott, 1991). Of these cells, only four cells have been studied in any detail. The AII amacrine cell is the most well studied of all amacrine cell, followed by the Starburst amacrine cell, A17 amacrine cell, and the less well studied Dopaminergic amacrine cell. Of these cells, the AII, Starburst, and A17 have been well characterized due to the relative ease of obtaining recordings based on morphology, location in the retina, etc. Dopaminergic amacrine cells are less numerous and much more difficult to find in the retina, but information about their behavior has been indirectly studied due to the importance of dopamine, the main neuromodulator in the retina. That leaves upwards of two dozen amacrine cells in the mammalian retina that have not been characterized due to difficulty of obtaining recordings and unclear function in modulating the signals that are passed from bipolar to ganglion cells.

The advancement in transgenic animals with fluorescent labeling in the retina has allowed for targeting of unknown cell types in the whole mount retina. I have obtained the GENSAT d2dr-GFP mouse line that labels two populations of cells in the retina. These two populations can be discriminated using soma size, where cells with larger diameter somas (14-16 µm) are more sparsely distributed and have shown to colocalize with tyrosine hydroxylase immunolabeling, making them Dopaminergic Amacrine Cells. Cells with smaller somas (7-8 µm) are more abundant and do not show tyrosine hydroxylase immunoreactivity.

The small cell appears to be diffusely bistratified with a narrow dendritic field. I have named this cell the small bistratified cell (SBAC). Although this cell is labeled due to expression

of GFP inserted into the D2DR promoter region, I have not studied the effects of dopamine on this cell type. I have focused on the light responses of this cell throughout a range of stimulus intensities, where the cell appears to have a complex inhibitory response to the on and offset of light.

Results

Anatomy

The GENSAT d2dr-GFP mouse labels SBACs in the mouse inner nuclear layer (INL). The distribution of the SBAC in the INL of the mouse retina is much greater compared to the DAC. I estimate an approximate density of 500 SBACs/mm^2 compared to approximately 25 DACs/mm^2. There appears to be no discernible difference in population density in the dorsal, ventral, temporal, or nasal regions of the retina (See DAC figure 1). SBACs are evenly spread across the retina, with no fluorescent cell somas contacting their closest neighbors and no areas of increased density in the magnified images.

The average soma diameter of a SBAC is 7-8 µm compared to 14-17 µm for DACs, the other fluorescent cell labeled in the GENSAT d2dr-GFP mouse line. The cell body generally sits in the middle of the INL compared to the border of the INL and the Inner Plexiform Layer (IPL) of the DAC. I visualized the morphology of SBACs by intracellular filling with 100 µM Alexa 594 dextran dye during whole cell recordings. Filled cells were then visualized on a confocal microscope that allowed us to see the extent and stratification of their dendritic field. The SBAC belongs to the narrow field class of amacrine cells as their dendritic field extended for 70-80 µm in multiple layers of the retina. The primary dendrite of the SBACs travels through the outermost portion of the IPL before stratifying radially in the OFF layer (sublamina 2) in a 70-80

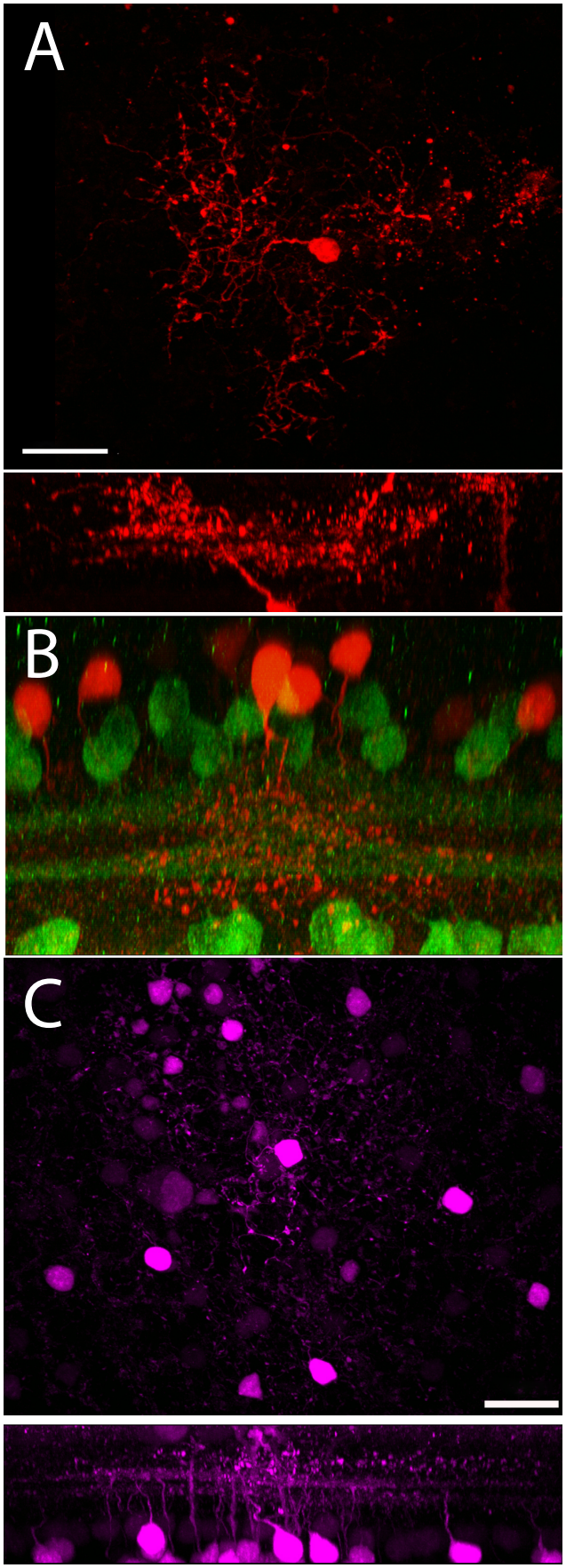

Figure 12. Morphology of small bistratified amacrine cells (SBAC) in Drd2-GFP transgenic. (A) Morphology of an SBAC as revealed by intracellular filling with Alexa 594 dextran (10,000 MW). Its cell body lies in the middle of inner nuclear layer (INL) and processes stratify in the middle and innermost portions of the inner plexiform layer (IPL; below). (B) A SBAC filled with neurobiotin (red) and ChAT immunolabeling (green) in retinal wholemounts shows the distribution of dendrites compared to the 2nd and 4th sublaminal layers of the IPL. (C) Morphology of the coupling of SBACs as revealed by intracellular filling with neurobiotin. One intracellular filled SBAC fills the nearest 10 neighbor SBACs. Scale bars 20 μm.

μm diameter (Figure 12A). There is a noticeable break in the stratification between the OFF and ON layers of the IPL before the SBAC has a second 70-80 μm diameter stratification in the ON layer (sublamina 4). The stratification in the ON layer continues as the dendrites diffusely stratify in the innermost portion of the IPL (sublamina 5), where their dendrites appear to have lobular appendages that extend for the entire 70-80 μm diameter to the extent of their other dendritic layers. The layers of the IPL can be more closely examined using immunolabeling for Choline Acetyltransferase (ChAT), which labels starburst amacrine cell dendrites that evenly divide the IPL into 5 equal layers due to the presence of their dendrites in layer 2 and layer 4 of the IPL (Figure 12B).

Coupling

As with DACs, I first attempted to fill the cytosol of SBACs with neurobiotin to amplify the tracer signal after tissue fixation. Imaging of the processed retina revealed that neurobiotin had filled more than the targeted cell alone. Neurobiotin is a molecule small enough to pass through gap junctions, suggesting that SBACs are in an electrically coupled network with other SBACs. When filling one SBAC with neurobiotin the tracer spreads to upwards of 10 other SBACs (Figure 12C). It appears neighboring cells share the same dendritic stratification as the targeted cell, but it is not known if the SBAC is electrically coupled to any other type of amacrine or bipolar cell.

Recordings

Whole cell current-clamp recordings were made from SBACs by targeting cells for recording in the same manner as previously described for DACs (See Methods). While SBACs

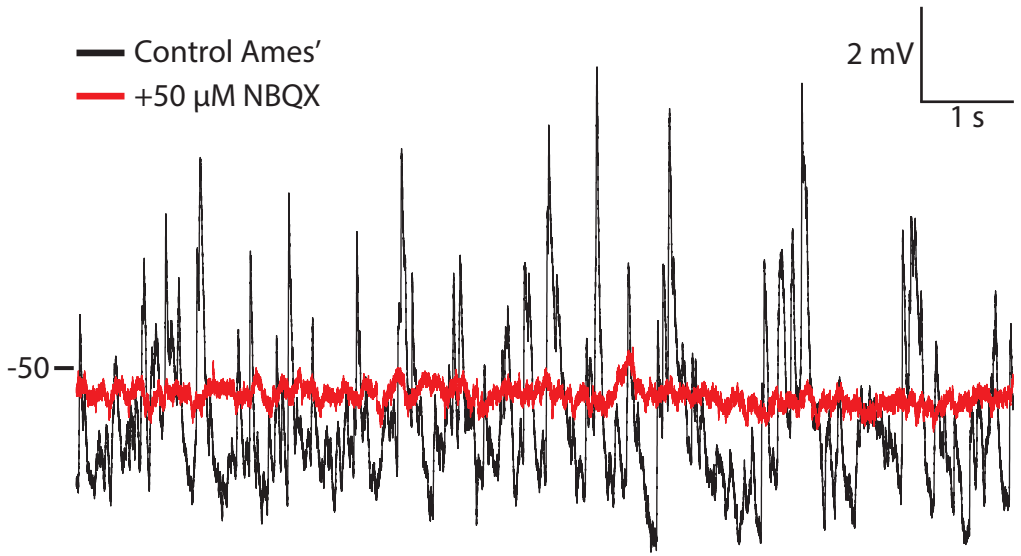

Figure 13. Baseline membrane activity of SBACs. The resting membrane potential for SBACs in control Ames' medium (black) and in the presence of 50 µM NBQX (red). The presence of the AMPA receptor blocker eliminates the baseline membrane fluctuations, but has no effect on the resting potential.

are more numerous in the retina, the smaller soma size increases the difficulty of obtaining quality recordings. To compound the difficulty, SBAC somas are found in the middle of the INL compared to the innermost portion of the INL for DACs, forcing the electrode to penetrate further into the INL to obtain recordings. In spite of these additional difficulties, I was able to obtain numerous recordings from light sensitive SBACs in the whole mount intact retina.

SBACs are non-spiking cells that have an average resting potential of -50.5 mV (Std. Dev.= 4.2; n=32). At a baseline light background of 2 Rh*/rod/s, SBACs are relatively quiet, but occasionally have depolarizing miniature potentials that cause small ~3 mV spikes in the baseline resting potential (Figure 13). The excitatory potentials are eliminated with the addition of 50 µm NBQX to the perfusion, but the AMPA antagonist does not appear to have an effect on the resting potential of the SBACs (Figure 13). That SBAC resting potentials become entirely quiescent with the addition of an AMPA receptor antagonist suggests that these cells receive some tonic excitatory input without light stimulation that does not set the baseline resting potential of the cell. The effects of AMPA receptor antagonists on the SBAC light response will be further discussed in *Pharmacology*.

Light Response Properties of SBACs

I have recorded from 32 SBACs, all which have shown the same general characteristic light response to similar light stimuli. The minimally detectable "threshold response" of every SBAC when presented with a 440 nm, 720 µm diameter spot of light was a 5 mV hyperpolarization (Figure 14). There were subtle differences in each cell, but the hyperpolarization threshold appeared to be at 4 Rh*/rod/step, suggesting that rod inputs are driving the cell to hyperpolarize. As light intensity increased from rod light levels, the

hyperpolarization maintained the same amplitude, but the onset and kinetics of the response increased. Following our brightest steps of light (100,000 Rh*/r/s), I discovered that it required up to 10 minutes of rest from bright light stimulation to recover the threshold response of SBACs. I tested this by measuring the threshold response, then delivering a 2 second high intensity stimulus (data not shown). I then probed the SBAC rod recovery by delivering threshold light until the response was recovered to initial levels. This effect is due to saturation of the rod photoreceptors with the high intensity light, providing more evidence that our lowest light stimuli are only activating rod photoreceptors.

At the offset of light, the cell again hyperpolarizes, but more strongly this time (5-10 mV) suggesting that the cell again receives rod inputs that are driving the cell to hyperpolarize following light stimulation (Figure 14). Initially, cells were stimulated with 500 ms steps of light, but when it was determined that SBACs had ON-OFF responses to dim light, I increased the duration of the light stimulus to 2 seconds to be more easily able to differentiate between the ON and OFF components of the responses. Following this, I determined the threshold response resulted in a transient hyperpolarization to light that did not continue to the end of the stimulus, while the duration of the OFF hyperpolarization was not affected by the duration of the light stimulation (Figure 14). Increasing the stimulus duration also revealed a small light evoked depolarization that followed the initial ON hyperpolarization. The amplitude of this response varied in every cell, but at the threshold response, was never more than 5 mV.

As the intensity of the stimulus increased from 9 to 100,000 Rh*/rod/s, SBACs continued to hyperpolarize at both light on and offset. However, at 1,000 Rh*/rod/s the hyperpolarization amplitudes of the ON and OFF responses increased to nearly double the size of the threshold response. As the light intensity increases to over 10,000 Rh*/rod/s, a fast 5-30 mV

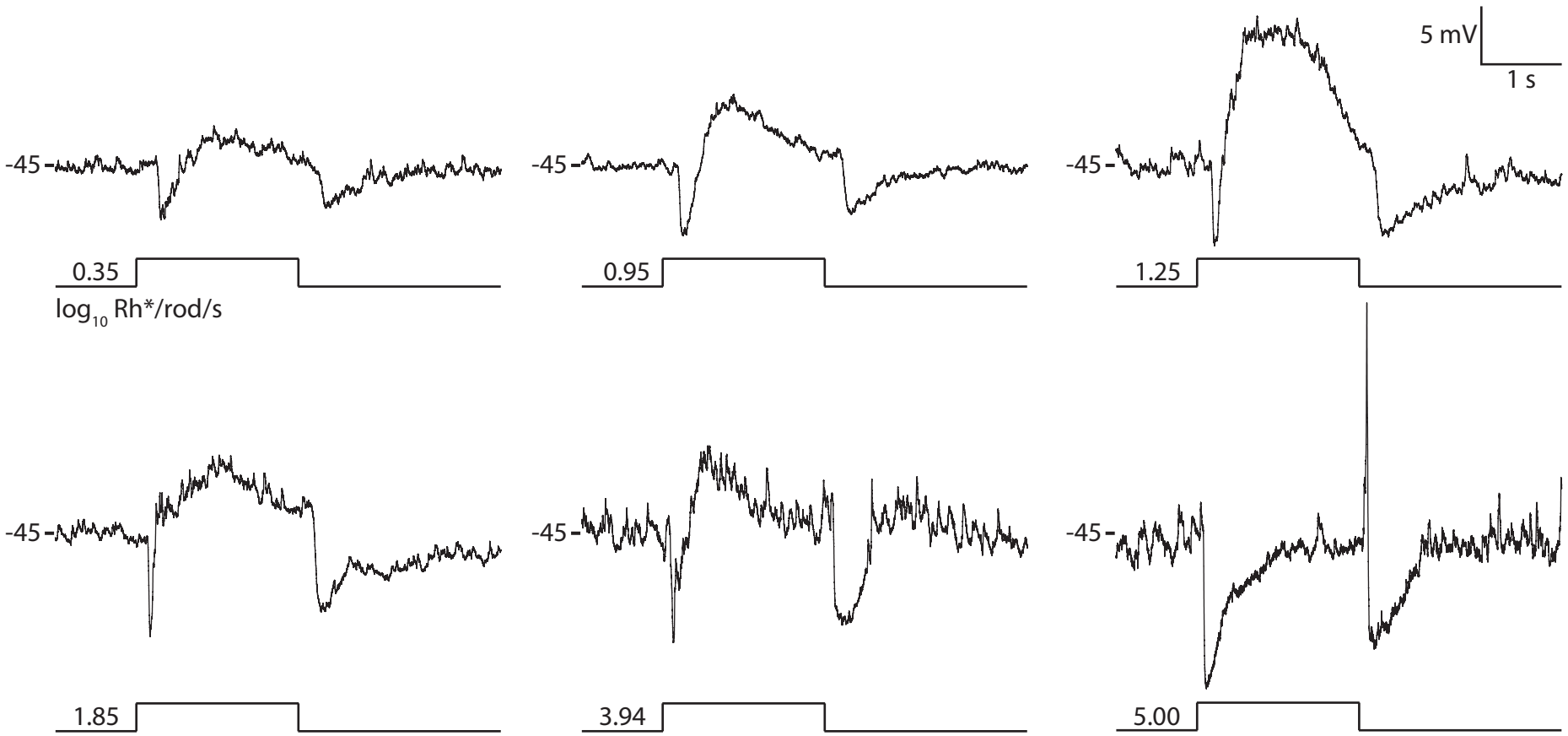

Figure 14. SBAC light response intensity series. SBAC light response evoked by 2 second steps of full field (700 µm diameter spot) 440 nm light of indicated intensities (log10 Rh*/rod/s).

depolarization spike is visible immediately following the offset of light (Figure 14). The spikelet-like depolarization is immediately followed by the hyperpolarizing after potential that was seen in dimmer light stimuli. The amplitude of the spikelet appears to be dependent on light intensity, but does not overshoot 0 mV like an action potential, but typically reaches a peak at -20 mV. A similar, but smaller depolarization (3-5 mV) during low and medium intensity light stimulations (500 to 1000 Rh*/rod/s) is visible following the initial ON hyperpolarization during light stimulation, but it is not clear if these depolarizations are due to a rebound effect of the initial hyperpolarization.

As the intensity of the stimulus increases to the maximum levels used in our study (100,000 Rh*/rod/s), a 2 s stimulus gave an initial hyperpolarization that was similar to medium to bright stimuli (500 to 10,000 Rh*/rod/s). Following the light stimulation, the cell again gives a fast depolarization followed by the standard hyperpolarization that was described earlier. It appears that SBACs get simultaneous inhibitory and excitatory input at both light ON and OFFset that may be present at all light levels, but only becomes more apparent as the light intensity increases to stimulate both rods and cones. It is possible that these excitatory inputs are present at dim light levels, but are overpowered by stronger inhibitory inputs.

Light stimuli were tested over a 6 log units of intensity level and the peak voltage changes for each of the three components of the light response were plotted (Figure 15) showing the small response range of SBACs regardless of stimulus intensity.

Dim Light Pharmacology

The threshold light response consists of three separate inputs: an ON hyperpolarization, a delayed ON depolarization, and an OFF hyperpolarization. I attempted to dissect the circuitry

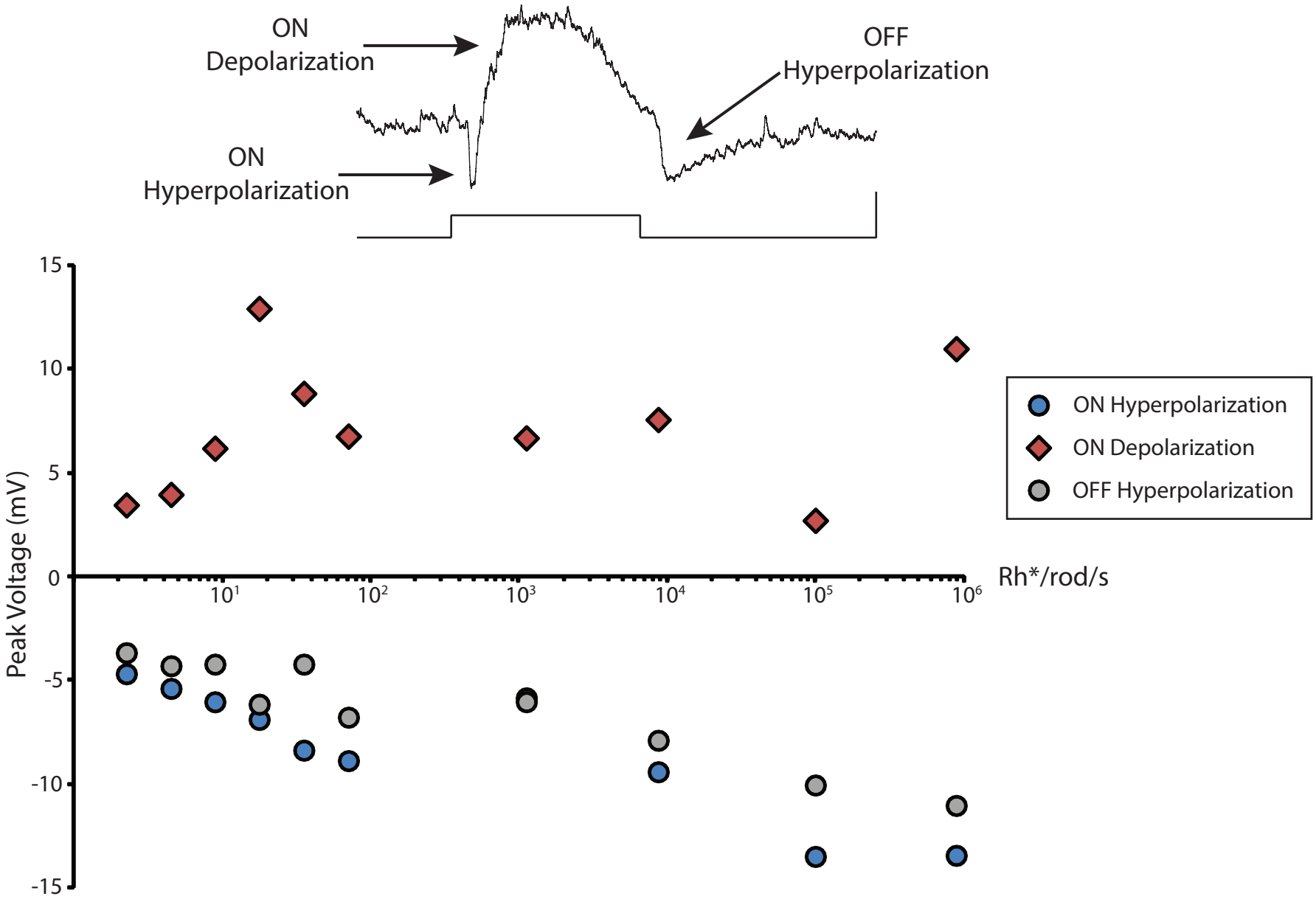

Figure 15. SBAC light evoked response properties. Peak voltage of the three basic components of the SBAC light evoked response over a range of stimulus intensities. (Above) An SBAC light response at 1.25 log10 Rh*/rod/s demonstrating the three components of the response. The components are plotted via a semi-log axis of stimulus intensity.

underlying the threshold light responses in SBACs using standard neurotransmitter blockers as described in DACs. Here, I present the findings of these experiments and attempt to derive a circuit diagram from these studies.

L-APB

As I reported earlier, the typical SBAC threshold response results in a hyperpolarization during and immediately following light presentation and a slower depolarization during the light stimulus. I tested if any of these signals were coming through the ON pathway with the use of L-APB. L-APB is an agonist for metabotropic glutamate receptors, which effectively blocks the transmission of signals through both rod and cone ON pathways due to the presence of these receptors on rod and ON cone bipolar cells.

When presented with a 2 second 9 Rh*/rod/s step of 440 nm light, the addition of L-APB eliminated the ON hyperpolarization in the SBAC. (Figure 16A). The hyperpolarization at dim light onset was eliminated in every cell (n=3) suggesting that the input originates in a rod bipolar cell. L-APB did not eliminate the small depolarization at the onset of threshold light levels. The amplitude of the depolarization increased with stimulus intensity when presented up to 1000 Rh*/rod/s. The depolarizations presented as bursts of activity that were maximal at the beginning of light stimulation and decreased as the stimulation continued for the duration of the 2 second light. L-APB did not significantly change the SBAC baseline membrane potential.

The OFF hyperpolarization was present in the ON bipolar cell blocker with no apparent differences between control conditions, suggesting that the OFF response comes through the OFF pathway.

NBQX

While L-APB specifically blocks the ON pathway, AMPA receptors are involved in both ON and OFF pathways in the retina. I attempted to eliminate synaptic inputs using NBQX; a selective AMPA/Kainate receptor antagonist (n=5). The effects of NBQX were immediately noticeable before presenting a light stimulus. While the baseline membrane potential was unchanged, NBQX completely eliminated the excitatory potential noise present in control conditions without affecting the baseline membrane potential.

The ON and OFF hyperpolarizations were absent at the lowest light levels presented in NBQX (9 Rh*/rod/s; Figure 16B). As predicted, the delayed ON depolarization was also eliminated due to AMPA receptors within the SBAC retinal circuitry. When the stimulus was increased by nearly an order of magnitude (70 Rh*/rod/s) both hyperpolarizations were present and increased in amplitude with increasing light intensity. The threshold for cones has been reported to be around 100 Rh*/cone/s (Naarendorp, et al., 2010) suggesting that at these slightly brighter light levels, SBACs may be beginning to receive cone-originating input. This provides more assurance that our dim-light stimulus was only stimulating rod photoreceptors.

AP-5

AP-5 is an antagonist that inhibits the glutamate binding site of NMDA channels. In an attempt to understand the presence of synaptic inputs in the absence of excitatory transmission, I performed experiments looking at the effects of NMDA receptors on SBAC light responses. Although I only used a single cell (n=1), it is apparent that the addition of AP-5 had no visible effects on the ON and OFF hyperpolarizations seen for the threshold light response in the SBAC (Figure 16C). The SBAC membrane potential was unchanged in the presence of AP-5.

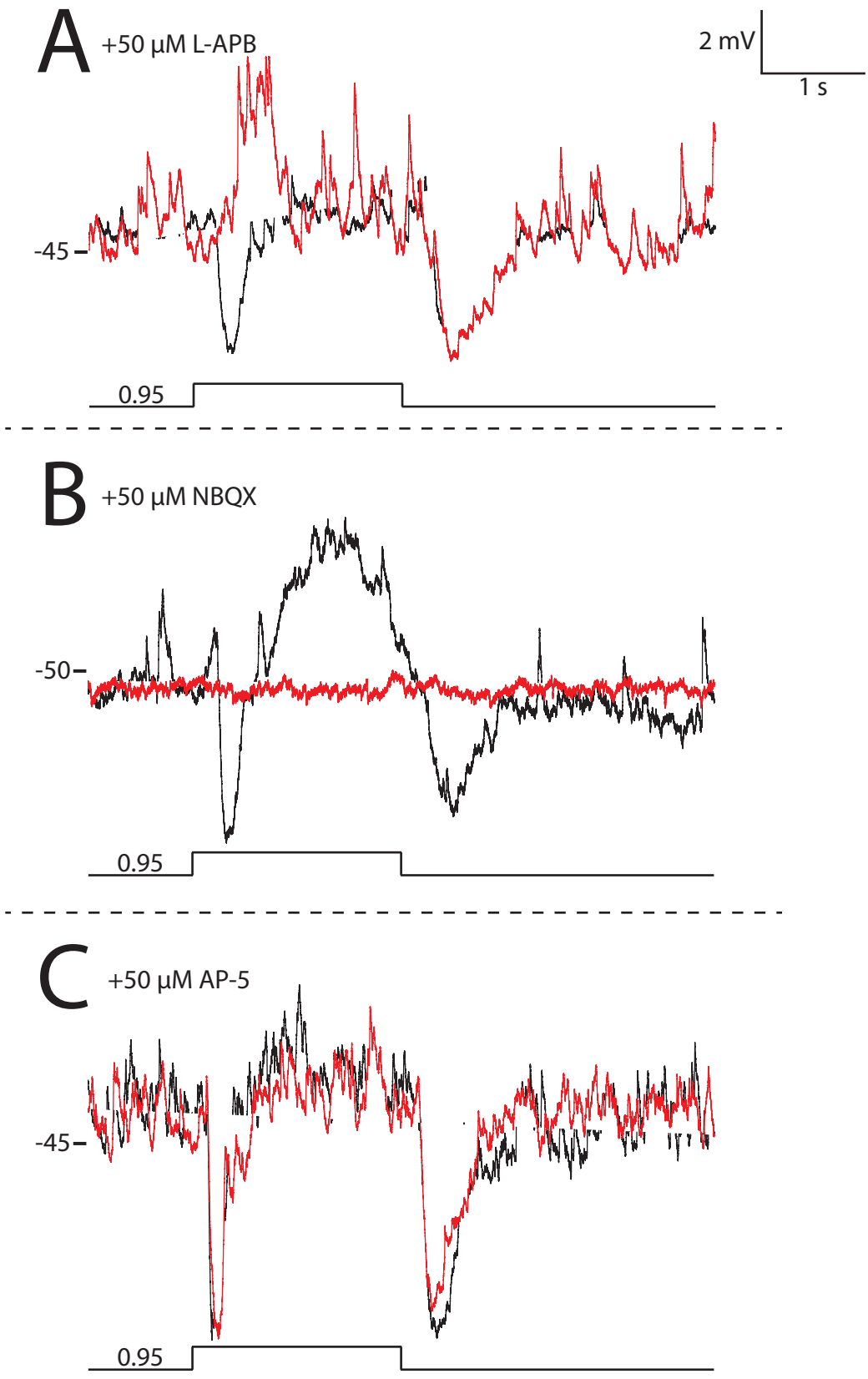

Figure 16. SBAC threshold light responses in control (black) and excitatory blockers (red). (A) Current traces showing the elimination of the ON hyperpolarization in the presence of L-APB. (B) NBQX eliminates all components of the threshold light response. (C) AP-5 does not appear to have an effect on the SBAC threshold light response. Stimuli of 2 second full field steps of 440 nm light with indicated intensities (log10 Rh*/rod/s).

Gabazine

Having tested the effects of excitatory synaptic blockers on SBACs, I attempted to isolate the excitatory inputs through the use of inhibitory blockers to eliminate the ON and OFF hyperpolarizations. In the presence of the $GABA_A$ antagonist Gabazine, the ON hyperpolarization produced during light stimulation was completely eliminated and replaced with a 15-20 mV depolarization that returned to the baseline potential after 1.5 seconds (Figure 17). At the cessation of the light stimulus the cell appeared to maintain the OFF hyperpolarization but the response was delayed by 500 ms compared to control conditions. This may be due to the cessation of the depolarization during light stimulation. In the presence of Gabazine the ON hyperpolarization was eliminated and uncovered stronger ON excitatory inputs demonstrating that the hyperpolarization at light onset is from a GABA-ergic amacrine cell, while the origin of the OFF hyperpolarization has yet to be determined. Gabazine depolarized the membrane potential 5-10 mV from control conditions suggesting that SBACs receive tonic GABAergic input in control conditions.

Strychnine and TPMPA

I tested two standard inhibitory antagonists on SBACs. The glycine receptor antagonist strychnine (2 μM) did not appear to have an effect on any threshold response component on the SBAC or the baseline membrane potential (Figure 17B).

TPMPA is an antagonist of $GABA_c$ receptors, which I previously described in the IPL of the mouse retina on DACs (Newkirk et al., 2013). While I did not apply TPMPA individually, I show that in the presence in Gabazine it does not appear to have an effect on any of the three main components of the threshold response compared to Gabazine alone (Figure 17C). The

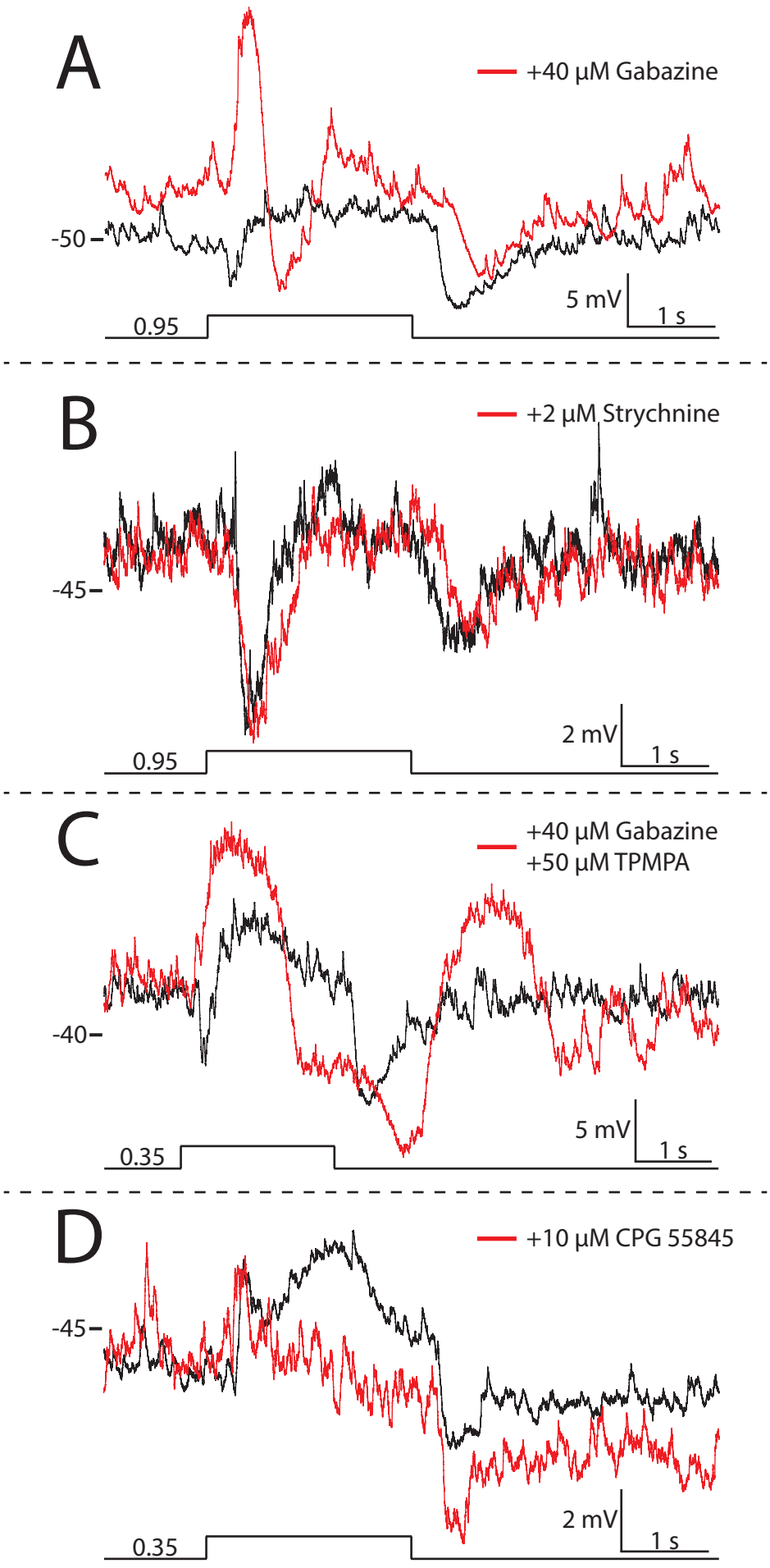
A
+40 µM Gabazine
-50
5 mV
1 s
0.95
B
+2 µM Strychnine
-45
2 mV
1 s
0.95
C
+40 µM Gabazine
+50 µM TPMPA
-40
5 mV
1 s
0.35
D
+10 µM CPG 55845
-45
2 mV
1 s
0.35

Figure 17. SBAC threshold light responses in control (black) and inhibitory blockers (red). (A) Gabazine eliminates the ON hyperpolarization while not affecting the other components of the threshold response. (B) Strychnine has no effect on the threshold response. (C) Gabazine and TPMPA do not block either the ON depolarization or OFF hyperpolarization of the SBAC threshold response. (D) CPG-55845 reduces the ON depolarization of the SBAC threshold response. Stimuli of 2 second full field steps of 440 nm light with indicated intensities (log_{10} Rh*/rod/s).

baseline membrane potential did not change in the presence of TPMPA and Gabazine compared to the depolarized membrane potential in Gabazine alone.

CGP-55845

CGP-55845 is an antagonist of metabotropic $GABA_B$ receptors. Despite the lack of direct ion conductance changes, $GABA_B$ receptors have modulatory effects on other ion conductances including other GABA receptor types and potassium channels. In the presence of CGP-55845, the ON depolarization of the SBAC was reduced compared to control conditions (Figure 17D). Both the ON hyperpolarization and the OFF hyperpolarization appeared to be unchanged. These limited number of experiments (n=2) suggest that $GABA_B$ receptors modulate ion conductances that are responsible for the ON depolarization. There was no obvious effect on the baseline membrane potential on the SBAC in the presence of CGP-55845.

Bright Light Pharmacology

For many pharmacological agents, I conducted a full intensity series to compare the light responses across various light levels in the presence of synaptic blockers. The addition of cone photoreceptor pathways to the light response increased the complexity of the response and synaptic wiring diagram.

L-APB

At 1000 Rh*/rod/s, light produced depolarizations in the presence of L-APB that lasted through the light stimulation (Figure 18A). The similarities between these depolarizations and the threshold response ON depolarization is not certain. As the light intensity was increased to

very intense light (100,000 Rh*/rod/s), the ON hyperpolarization seen in control conditions reappeared. However, at our brightest light levels, the hyperpolarization lasted through the light stimulation and was decreased in amplitude compared to control conditions suggesting that perhaps this concentration of L-APB provided an incomplete block of ON bipolar cells that normally drive inhibition through amacrine cells.

NBQX

When cone light stimuli (> 500 Rh*/rod/s) were presented to cells perfused with NBQX, the ON hyperpolarization reappeared although it was greatly reduced in amplitude compared to control conditions (Figure 18B). The initial fast depolarization following light stimulation was eliminated in NBQX and the OFF hyperpolarization was eliminated in some cells, but remained in others. These experiments along with L-APB data demonstrate that SBACs are receiving inhibitory inputs in the absence of excitatory synaptic transmission, which is difficult to comprehend in the retina due to the release of glutamate from all bipolar cell types.

AP-5

In an attempt to understand the presence of synaptic inputs in the absence of excitatory transmission, I performed experiments looking at the effects of NMDA receptors on SBAC light responses. Although I had a small sample size when perfused alone (n=1), it is apparent that the addition of AP-5 had no visible effects on the ON and OFF hyperpolarizations seen in the SBAC (Figure 18C). However, when AP-5 was added to the standard concentration of NBQX, which I previously described as retaining both ON and OFF hyperpolarizations, the combination of these two excitatory synaptic blockers eliminated all previous hyperpolarizations (Figure 18D).

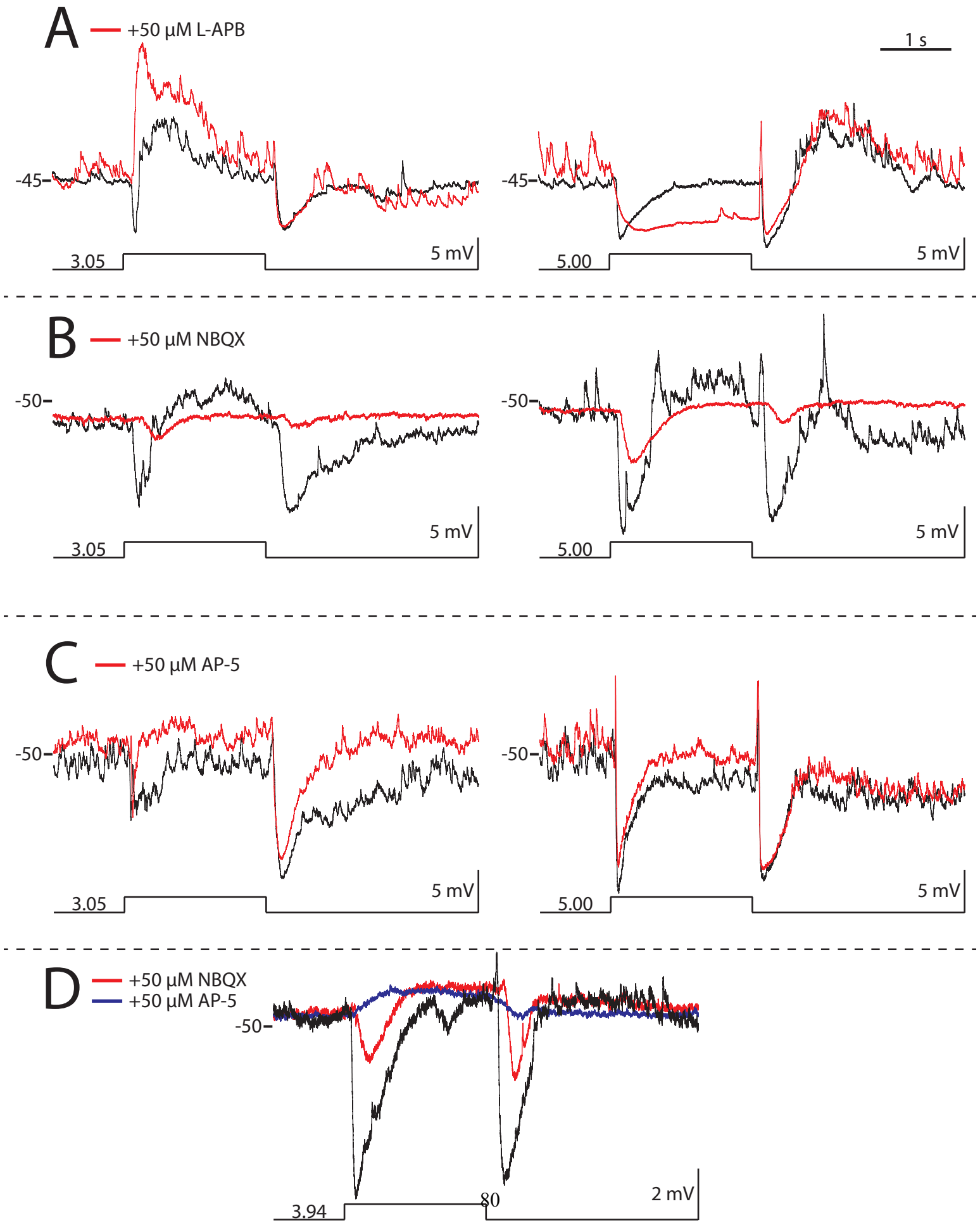
A
+50 µM L-APB
1 s
-45
3.05
5 mV
-45
5.00
5 mV
B
+50 µM NBQX
-50
3.05
5 mV
-50
5.00
5 mV
C
+50 µM AP-5
-50
3.05
5 mV
-50
5.00
5 mV
D
+50 µM NBQX
+50 µM AP-5
-50
3.94
80
2 mV

Figure 18. SBAC response to bright light in control (black) and excitatory blockers (red). (A) L-APB eliminates the ON hyperpolarization in medium light, but not in bright light. (B) The ON and OFF hyperpolarizations return in the presence of NBQX in medium and bright light stimuli. (C) AP-5 does not affect the medium and bright light intensity responses. (D) AP-5 (blue) eliminates the ON and OFF hyperpolarization present in NBQX. Stimuli of 2 second full field steps of 440 nm light with indicated intensities ($\log_{10}$ Rh*/rod/s).

Remaining after light stimulation at cone light levels (>1000 Rh*/rod/s) was a small (2-5 mV) depolarization that continued to the end of the light stimulation. The depolarization could be due to gap-junction coupling of SBACs to a cone ON-bipolar cell or incomplete block of excitatory inputs that I described at low light levels in NBQX. It was not blocked by either 10 µM UBP-310 or 100 µM GYKI-53655 (data not shown), which are antagonists for kainate and AMPA and kainate receptors, respectively.

Gabazine

Having tested the effects of excitatory synaptic blockers on SBACs, I attempted to isolate the excitatory inputs through the use of inhibitory blockers to eliminate the ON and OFF hyperpolarizations. Strychnine did not appear to have any obvious effects on the membrane potential or light evoked responses of the SBAC, but application of 40 µM Gabazine produced large changes in the light responses from control conditions. In the presence of the $GABA_A$ antagonist Gabazine, the ON and OFF hyperpolarizations produced during light stimulation were completely eliminated and replaced with a large (15-20 mV) depolarizations that returned to the baseline potential after 500 ms, occasionally becoming more negative than the resting potential and repolarizing for the duration of the light stimulus (Figure 19). At the cessation of the light stimulus, another smaller depolarization (10 mV) replaced the normal hyperpolarizing OFF response. In the presence of Gabazine, both the ON and OFF hyperpolarization were eliminated and revealed strong excitatory inputs demonstrating that both cone light levels hyperpolarizations at light ON and OFFset are from a GABA-ergic amacrine cell.

When I added 75 µM L-APB to Gabazine in an attempt to eliminate the fast depolarization at light onset, again I received surprising results. At lower light levels (<1000

Rh*/rod/s), the depolarization remained as seen in Gabazine alone. In contrast, intense light stimulations (>1000 Rh*/rod/s) strongly hyperpolarized (20 mV) SBACs during light presentation that lasted for nearly the entire duration of the stimulus (data not shown). The OFF depolarization remained as in Gabazine alone.

NBQX and Inhibitory Blocker Cocktail

Due to the complicated results from using antagonists alone and in simple combination, I attempted to entirely block inhibitory inputs to the cell to determine the nature of the excitatory responses. Our first experiment used NBQX in combination with an inhibitory blocker cocktail of gabazine and strychnine at standard concentrations. In this combination of blockers, the SBAC was completely silent at rest, as discussed previously in NBQX, but cone light level stimulation produced a small depolarization (<5 mV) that triggered a very large >30 mV depolarization (Figure 20A). Compared to NBQX, it appears that the inhibitory blockers prevent an input that returns the membrane to rest in NBQX alone, and allows the cell to become strongly depolarized. There is no secondary hyperpolarization or depolarization at light OFFset, and often the depolarization plateau extends for greater than 1 s beyond the cessation of light stimulation. Blocking NMDA receptors with D-AP5 eliminated the large triggered depolarization seen in the responses recorded in the presence of NBQX and inhibitory blockers, but a smaller depolarizing ON response remained that was ultimately eliminated by L-APB (Figure 20B).

Discussion

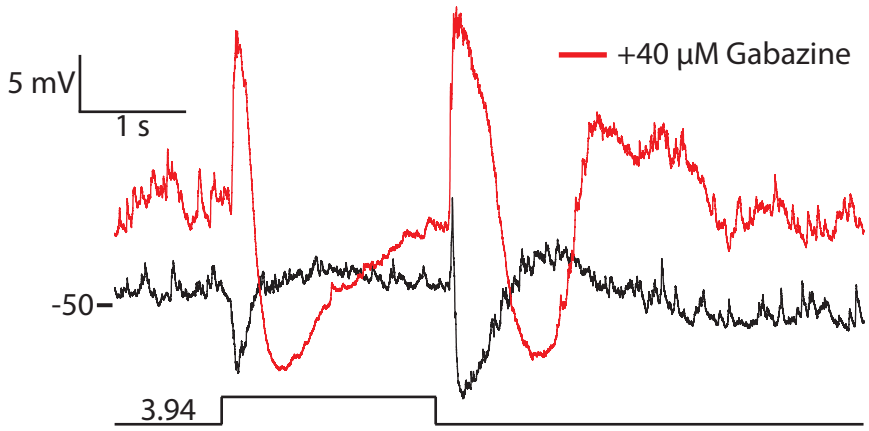

Figure 19. Gabazine eliminates both the ON and OFF hyperpolarizations at bright light intensities. The presence of 40 µM Gabazine replaces ON and OFF hyperpolarizations in control (black) to depolarizations (red) for bright light intensities. Stimuli of 2 second full field steps of 440 nm light with indicated intensities (log10 Rh*/rod/s).

Threshold Response Synaptic Wiring Diagram

The light response of the SBAC depends on light intensity. While there are cell to cell differences between SBAC recordings, the basic light intensity series is similar in all cells. The threshold SBAC light response that occurred at light levels that only stimulate rod photoreceptors (<9 Rh*/rod/s) is a combination of three distinct inputs: an ON hyperpolarization, an ON depolarization, and an OFF hyperpolarization. As the light intensity increases, SBACs maintain these aspects of their response, but additional inputs become apparent in the recordings at intensities that stimulate cone photoreceptors. At cone light levels, fast "spike-like" depolarizations occur at both on and offset. The SBAC light response consists of a summation of a number of synaptic inputs at higher light intensities. The minor cell to cell variation of the light responses may be due to the different balances of these inputs changing the waveform by the various strengths and kinetics of the underlying inputs. Based on the difficulty of interpreting the experimental data, I have attempted to design a synaptic wiring diagram that fits our pharmacology data for the threshold light response only.

The ON hyperpolarization was eliminated by three traditional synaptic blockers: L-APB, NBQX, and gabazine. These results suggest that the ON hyperpolarization originates in the rod photoreceptor that activates a metabotropic glutamate receptor on the rod bipolar cell, which in turn releases glutamate onto AMPA receptors of an unidentified amacrine cell. This unknown amacrine cell then releases GABA onto a SBAC $GABA_A$ receptor during light stimulation. Bath application of AP-5 nor any of the other inhibitory antagonists effectively blocks the ON hyperpolarization.

While I hypothesize that the rod photoreceptor passes the signal through the rod bipolar cell and onto an unknown amacrine cell to the SBAC, I cannot rule out the possibility that the

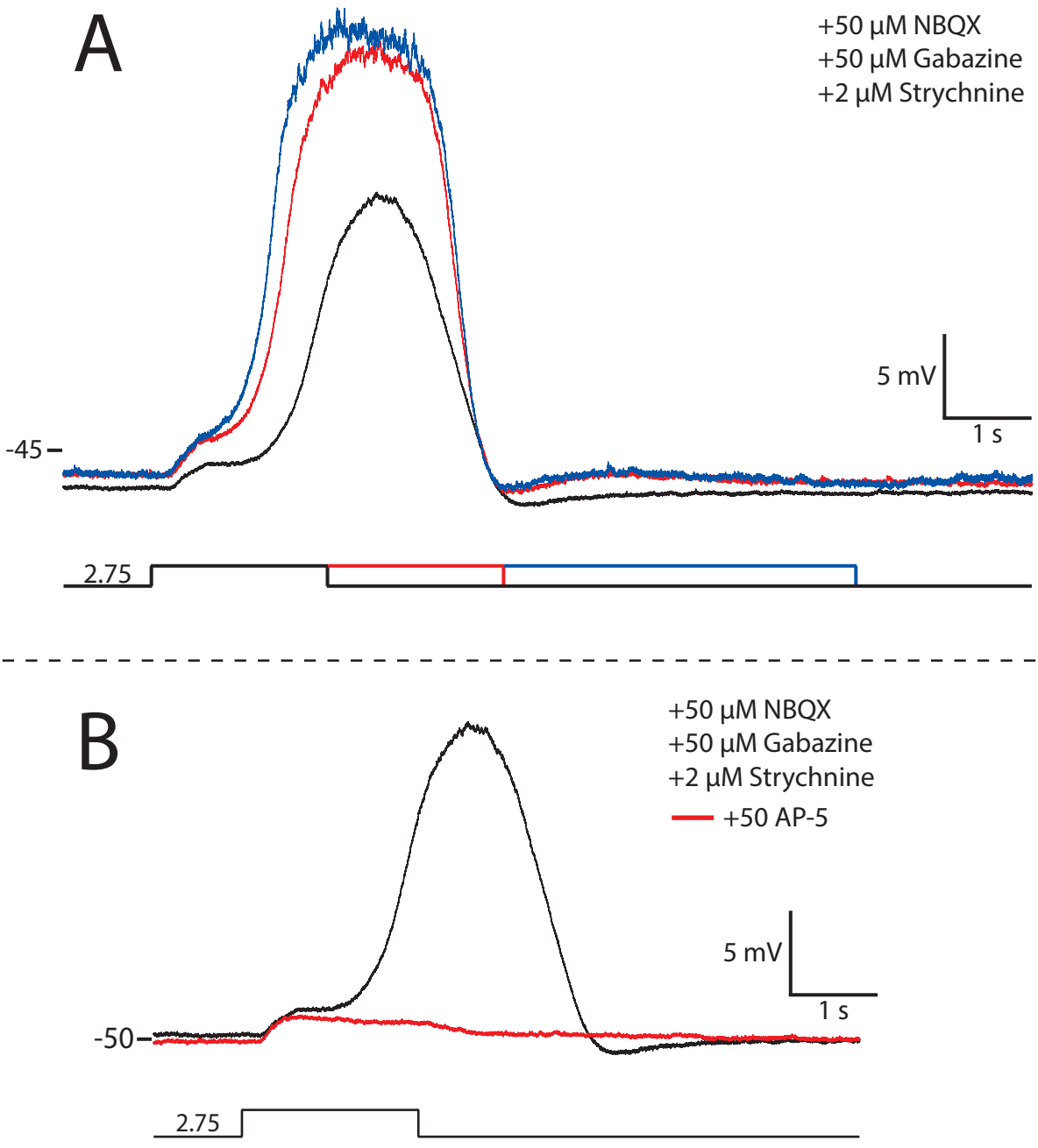

Figure 20. NMDA receptors play a role in SBAC excitation at bright intensities. (A) SBAC light evoked response for various stimuli durations in the presence of NBQX, gabazine, and Strychnine. (B) The large depolarization in the presence of NBQX, gabazine, and strychnine is reduced with AP-5. The remaining small depolarization was eliminated with L-APB (data not shown). Stimuli of 2 second full field steps of 440 nm light with indicated intensities (log10 Rh*/rod/s).

rods pass the signal onto cone photoreceptors via electrical coupling (DeVries and Baylor, 1995) and travel through an ON cone bipolar cell to the unidentified GABAergic amacrine cell. This hyperpolarization is present throughout a six degree of magnitude light intensity series. However, the amplitude of the hyperpolarization peaks after light intensities that typically begin to activate cone photoreceptors (>1,000 Rh*/rod/s) and does not increase with stronger light stimuli. This suggests that the light response is not due to electrical coupling to cone photoreceptors as increasing light would activate the electrically coupled cone and produce a larger signal that would last throughout the light stimulation.

The ON depolarization is a complicated synaptic response that I have yet to fully understand. As with all three components of the threshold response, the signal must originate in the rod photoreceptors. As with nearly all pathways in the retina, the ON depolarization was blocked with NBQX. Interestingly, the ON depolarization was present in L-APB, and was increased in amplitude with the elimination of the ON hyperpolarization. These results imply that the signal does not originate in the ON pathway and must come through an OFF cone bipolar cell. However, the signal is a depolarization and OFF bipolar cells are inhibited during light stimulation preventing the excitation of downstream cells. Therefore, the most logical explanation for the ON depolarization response is a light-evoked disinhibition of a tonically active amacrine cell. This circuit would suggest that an SBAC receives tonic inhibitory input from an amacrine cell driven by an OFF cone bipolar cell. At light onset, the inhibition is removed due to OFF bipolar cell inhibition. The membrane potential of the SBAC is liberated from the tonic inhibition and depolarizes. Unfortunately, in an inhibitory cocktail of blockers including gabazine, TPMPA, and strychnine, the depolarization fails to be eliminated. The $GABA_B$ antagonist, CGP 55845, reduced the depolarization present in control conditions.

$GABA_B$ receptors are metabotropic and are not directly associated with ion channels, but they are known to modulate other GABA receptors and ion channels. The lack of effect with other standard pharmacological blockers on the ON depolarization suggests that $GABA_B$ receptors are modulating other channels on either the SBAC or an upstream cell. Additional experiments are necessary to determine the specific effects of these channels on SBAC physiology.

The threshold light response of SBACs also demonstrates a hyperpolarization at light offset. Using standard pharmacological blockers targeting all GABA and glycine receptors, I was unable to fully block the OFF hyperpolarization of the SBACs. In our experiments, I was only able to eliminate the OFF hyperpolarization through the application of NBQX, which does not give much information about the circuitry of the cell. However, as with the ON depolarization, the OFF hyperpolarization was not blocked by L-APB, suggesting that the signal does not originate in the rod bipolar cell. However, there are no OFF rod bipolar cells. Recent evidence suggests that rod photoreceptor are able to make synapses with OFF cone bipolar cells (Soucy, et al., 2008) that could be responsible for the activation of the cell that provides OFF inhibition to the SBAC.

The information obtained from these pharmacology experiments only allows us to construct an incomplete circuit diagram to explain each component of the threshold light response (Figure 21).

Bright Light Circuitry

As the light stimulus intensity is increased to activate cone photoreceptors, additional inputs become apparent in the light responses of SBACs. Due to the difficulty describing

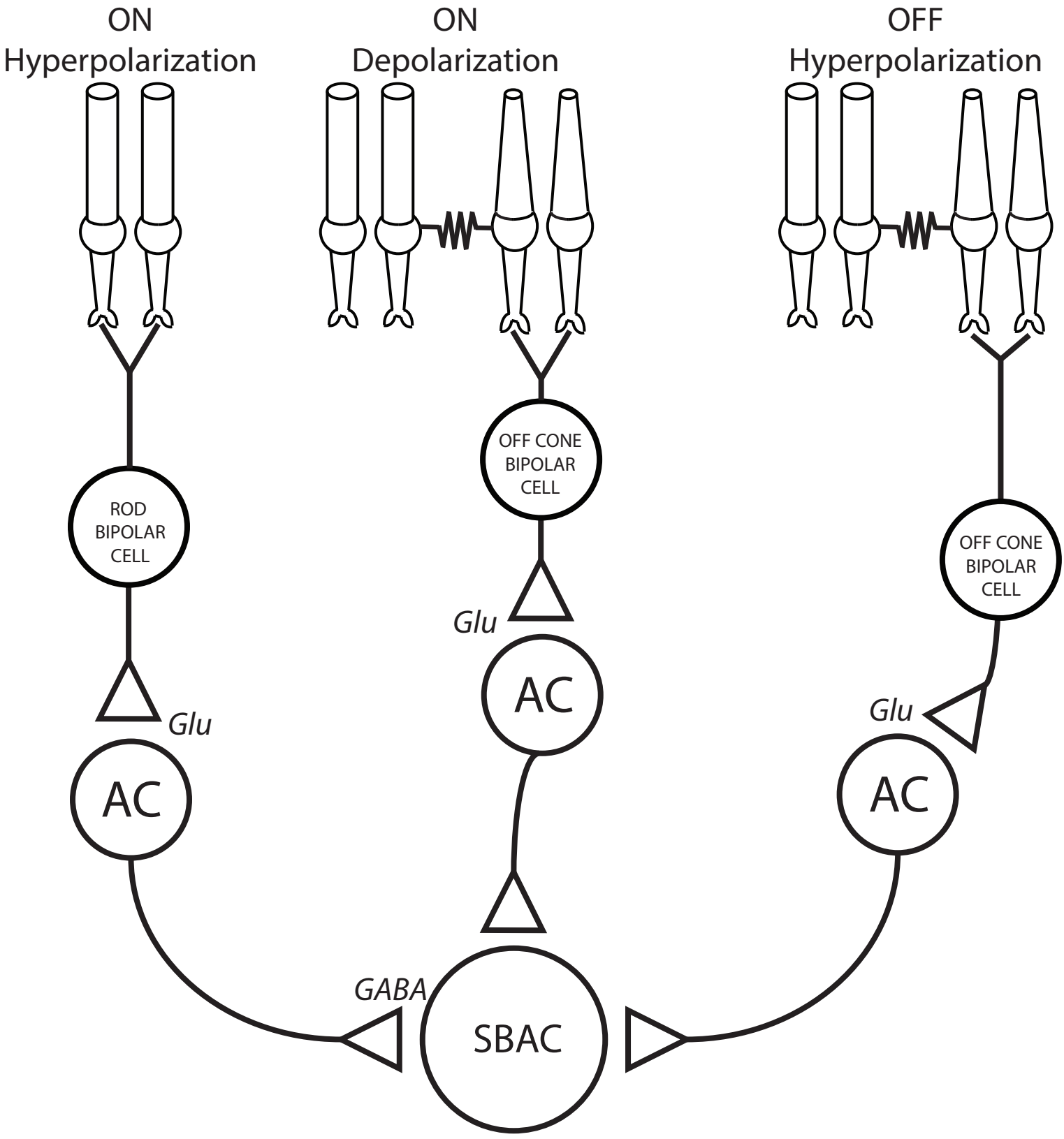

Figure 21. SBAC threshold response synaptic wiring diagram. In the incomplete proposed scheme, each component of the SBAC threshold light response is represented through an individual pathway. Only the ON hyperpolarization pathway is complete, while more data is necessary to finish the ON depolarization and OFF hyperpolarization. In each case, the response originates in the rod photoreceptors and ends through an unknown amacrine cell.

potential circuitry for the threshold light response, I abstained from speculating about specific cone inputs, but focused on observations and curiosities that emerge from these studies.

At light levels greater than 1000 Rh*/rod/s, a fast transient depolarization occurs at light offset regardless of the length of light stimulation. After the brief spike-like depolarization, the cell displays the OFF hyperpolarization of the membrane potential that occurs with all light levels. The depolarization can be augmented with the addition of gabazine, which blocks the OFF hyperpolarization and increases the duration of the light offset depolarization at cone light levels. The OFF depolarization is only activated at brighter light levels and not blocked by any inhibitory blocker, nor is it blocked by L-APB, suggesting that it originates in an OFF cone bipolar cell. The fast depolarization is eliminated in the presence of NBQX, suggesting that this portion of the light response is due to direct AMPA receptor activation of the SBAC from an OFF cone bipolar cell.

As with the threshold light response, bright light inputs are difficult to understand using standard pharmacological blockers. NBQX was able to eliminate all light-evoked potentials at the threshold light response, but increased light intensities demonstrated the return of both ON and OFF hyperpolarizations in the AMPA receptor blocker that are difficult to understand. An incomplete block of AMPA and kainite receptors seem unlikely at these concentrations of NBQX. More likely is a partnership between AMPA and NMDA type glutamate receptors that must be taking place at multiple synapses.

The involvement of NMDA type glutamate receptors becomes evident in experiments conducted with bright light stimuli in the presence of AMPA, $GABA_A$, and glycine receptor blockers. The large, slow depolarization in the presence of these receptor blockers has the largest amplitude response from any current that I have isolated. The initial depolarization and

plateau suggests that an initial depolarization is necessary to trigger the larger depolarization that is very stereotyped in appearance despite the length of the light stimulus (Figure 20). This depolarization is greatly reduced by the addition of AP-5, suggesting that NMDA input through the cone pathway is influencing the response characteristics of the SBAC. Additional studies are required to fully understand the interaction between the multiple synaptic inputs that the cell receives both during and following light stimulation.

In summary, SBACs are a narrow-field bistratified amacrine cell that responds to both light on and offset with a small hyperpolarizations over a wide range of stimulus intensities. The role of the SBAC in the mouse retina is as equally perplexing as the synaptic input that it receives. The synaptic targets of its outputs are unknown, impeding our understanding of the cell's role in the inner retina. The location of dendrites in both ON and OFF layers of the retina allow the cell to participate in crossover inhibition between the two streams of visual processing through the retina. Crossover inhibition has been implicated in correcting for nonlinearities in the visual pathway, but the mechanism involving this cell is unclear (Molnar et al., 2009). The most striking characteristic of the SBAC is the diminutive response to light over six orders of magnitude of intensity. Figure 15 shows a less than 15 mV response in either polarity to any stimulus that spans a large range of intensities. The insignificance of the light intensity for the SBAC suggests that it faithfully supplies its targets with inputs at the presentation of any light. Unlike the DAC, where hundreds of previous studies laid the ground work for understanding the function of the light responses of that cell, I aim to understand the connections of the SBAC much earlier than the cell's function in the retina. With additional studies I hope to further our

understanding of the two contrasting types of amacrine cells in the mouse retina and apply this information to help complete the library of uncharacterized cell types.

APPENDIX

EFFECTS OF D2 RECEPTOR ON DAC PHYSIOLOGY

Numerous studies suggest that the release and effects of dopamine are correlated with circadian rhythms in the retina (reviewed in Witkovsky, 2004). The concentration of dopamine in the retina is higher during the day than at night time, and has been implicated in many effects in the retina regarding the switch from rod to cone mediated vision. This includes regulating gap junctions to modify receptive fields of cells, modulating ion channels to change intrinsic properties of cells, and increasing disk shedding of photoreceptors. Dopamine is the main neuromodulator in the retina and has been implicated in many functions that are ultimately responsible for differences in ganglion cell output in rod versus cone light levels. DACs express a D2 dopamine receptor that suggests that the cells are modulated by their own dopamine release; i.e. they have autoreceptors for dopamine that work through a D2-subtype of dopamine receptor in the rat retina. (Derouiche and Asan, 1999). I sought to determine the effects of dopamine on DACs. All animals were maintained in the animal facility on a 12 hour light cycle beginning at 6AM. Previous experiments used the original protocol in which an animal that had been in its normal diurnal cycle was taken 3 hours into the light and dark-adapted for 2 hours before dissection and experimentation. For testing the results of day and night on DACs, we used animals at two different periods of their light/dark cycle and named them subjective day and subjective night. subjective day experiments were conducted by taking the animal 3 hours into his light cycle and keeping the animal light adapted for an additional 2 hours until dissection and experimentation. The dissected retina was kept in darkness to preserve photopigment and

light-responsive properties of the retina. Light dissected animals did not display any sensitivity to light stimuli, likely due to photobleaching of the photoreceptors following removal of the Retinal Pigment Epithelium. Subjective night experiments were conducted by taking the animal 3 hours into the dark cycle and continuing to dark adapt for 2 additional hours. Dissection and experimentation were also conducted in the dark and the retina was stored in the dark until used for experimentation. Dark storage of the retina did not have an effect on physiology of the recorded DACs (data not shown). The subjective day and night conditions will provide information about the differences in DAC physiology at night and day. The original protocol is a combination of both conditions where an animal in the subjective day is light adapted for two hours prior to experimentation. The original protocol will allow us to determine the cause of light adaptation on DAC behavior. The animals in these experiments express GFP on a C57/Bl6 mouse background, which is unable to produce melatonin naturally. Melatonin is necessary for mice to release dopamine in a circadian rhythm, but C57/Bl6 mice require the exposure to light for the rhythmic diurnal changes in retinal dopamine (Doyle et al., 2002). Therefore, in our mouse dopamine release is not controlled by circadian processes, so that differences in DAC physiology in different conditions are the result of light adaptation rather than circadian effects.

See Figure 22A for details on experimentation.

Results

DACs were targeted for whole-cell recording in the current clamp configuration and their resting membrane potential was recorded in all three conditions (Figure 22). In the original protocol, the average DAC resting membrane potential sat at -42.3 mV (± 7.21 standard deviation; n= 72). This is in contrast to light adapted subjective day cells where the average

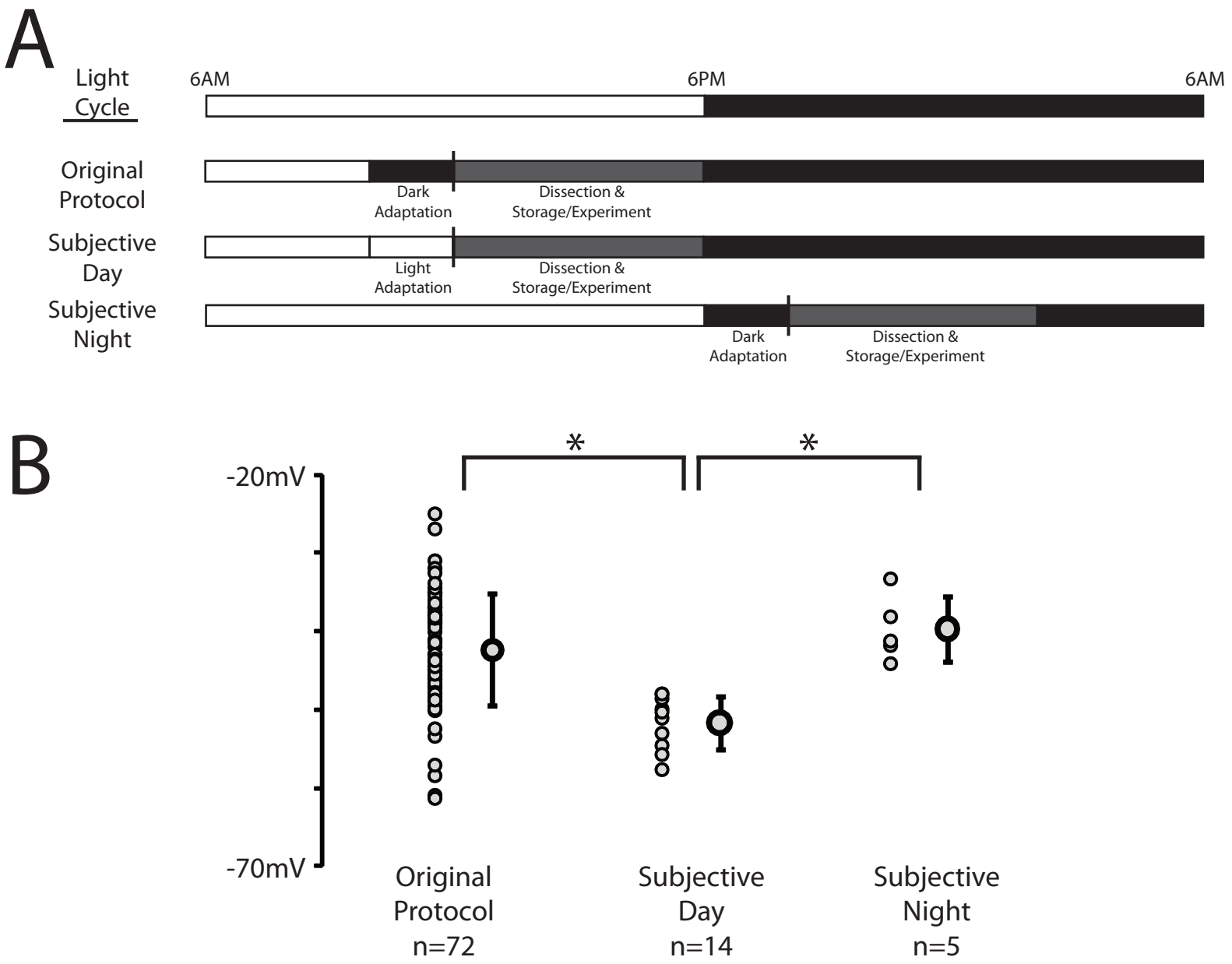

Figure 22. Light Condition Determines DAC Membrane Potential. (A) Light conditions of animals. All animals are housed in identical 12H:12H Light: Dark cycles. Animals in the original protocol were taken during light exposure, dark adapted for two hours and housed in darkness throughout dissection and experimentation. Subjective day animals were kept in light until dissection, when the dissected retinas were housed in the dark until used in experiments to prevent bleaching of the photopigment. Subjective night animals were taken at the beginning of their Dark cycle, dark adapted for two hours, and dissected and stored in the dark until used in experiments. (B) DAC resting potentials taken from whole-cell recordings at zero-current potentials for di˜erent light conditions. Recordings performed in the subjective night were more depolarized than cells in the subjective day (mean -39.6mV to -51.6mV). Membrane potentials of cells in the original proto-col were distributed a wide range of voltages (mean -42.3mV).

baseline membrane potential was more hyperpolarized at -51.6 mV (± 3.39 standard deviation; n=14) and during the animals' subjective night had average resting membrane potentials that were more depolarized at -38.5 mV (± 4.25 standard deviation; n=6). Both the subjective day and subjective night membrane potentials were statistically significant from both each other and the original protocol (Students t-test; $p<0.05$).

DACs recorded in different adaptation states also had varying action potential firing rates depending on the condition of the animal. As mentioned earlier, the majority of DACs are spontaneously active in resting conditions (>90% in Newkirk et al., 2013). Spiking cells studied in the original protocol condition were grouped into three categories that were either continuously active, steadily discharging with intermixed bursts of spikes, or periodically bursting, demonstrating that cells studied in this condition are capable of multiple modes of baseline activity. As shown in Figure 22B, during subjective night experiments DACs had a depolarized membrane potential and fired action potentials in the absence of stimulation in contrast to subjective day experiments that were hyperpolarized and nearly absent of baseline spike activity (Figure 23A). DACs recorded in the original protocol had an average firing rate of 2.1 Hz (1.55 standard deviation; n=72) that was statistically larger than subjective day spontaneous firing rates of 0.14 Hz (0.29 standard deviation; n=14; Student's t-test $p<0.05$). Subjective night DACs had an increased average spontaneous firing rate of 2.7 Hz (1.4 standard deviation; n=5). The average firing rates of subjective night and subjective day cells were statistically significant from each other (Student's t-test; $p<0.05$). As with the baseline membrane potential there were large differences in spike rate between subjective night and subjective day while original protocol cells covered the entire range of firing rate. (Figure 23B).

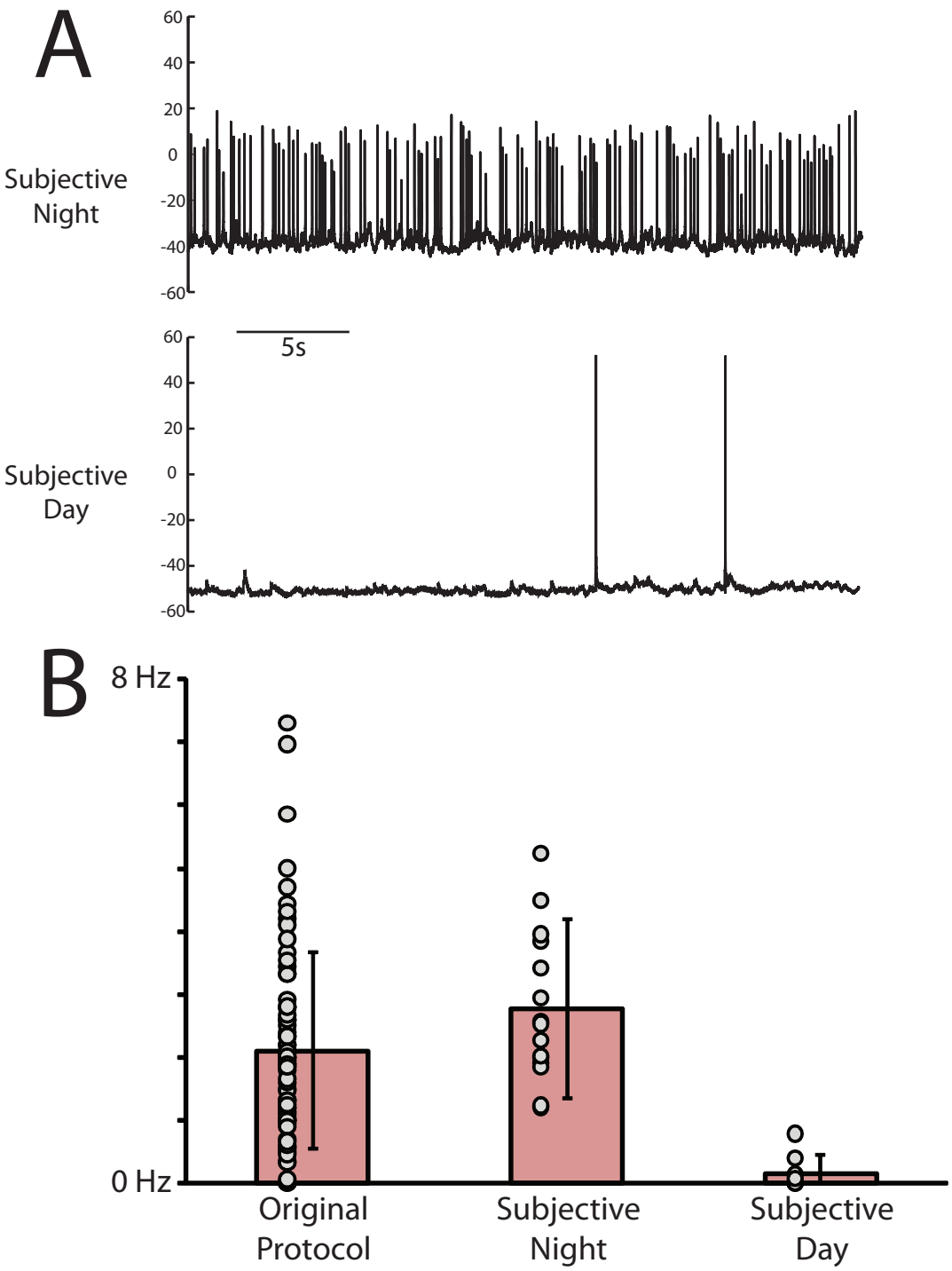

Figure 23. DACs have increased spontaneous activity in dark conditions. (A) Whole cell recording examples of DAC resting potential in Subjective Day (top) and Subjective Night (bottom) at the zero-current potential. DACs are more spontaneously active in subjective night, but have reduced spike height compared to cells recorded in subjective day. (B) Spontaneous ÿring frequency of each light condition shows that DACs ÿre more frequently in subjective night (3.2Hz) than day (0.1Hz). Error bars represent standard deviation of individual cells (spheres).

The difference in DAC resting potential and spontaneous firing rates in subjective day and night conditions suggested a difference in intrinsic properties. We gave long lasting (>20 second) hyperpolarizing current pulses to look for evidence of "sag" currents that suggest a difference in ion channel conductance between conditions. "Sag" currents for original protocol conditions were studied in Newkirk, et al., 2013. In Figure 24A, example cells for subjective night and day are shown with responses to the same series of hyperpolarizing current injections. Both conditions show a rebound burst of action potentials following the hyperpolarizing step, but during a long hyperpolarizing current injection evidence of a slow depolarization or "sag" is evident in the subjective night example compared to subjective day. The presence of "sag" current is most obvious at the beginning of the hyperpolarizing step, as the majority of this depolarization occurs in the first 5 seconds of the hyperpolarization. To quantify this "sag" current, I took the difference between the minimum membrane voltage during the hyperpolarization and the steady membrane potential at the end of the hyperpolarization. I call this number the "depolarizing drift" as it signifies the amount of depolarization that occurs during the hyperpolarizing current injection. An example of this depolarizing drift is visible in Figure 24B. The amount of depolarizing drift is plotted as a function of the minimum membrane voltage for each hyperpolarizing pulse. Figure 24C shows that for a given minimum voltage from a current injection, the amount of depolarizing drift or "sag" current for DACs is much greater in subjective night DACs compared to subjective day. The amount of depolarizing drift is greater in subjective night conditions compared to subjective day at any membrane potential measured. The cause of these differences is not clear, but it is possible that DACs in 'subjective night' have an I_H conductance driving the membrane potential back towards its baseline. The possibility of I_H mediated currents were discussed when describing the four basic types of

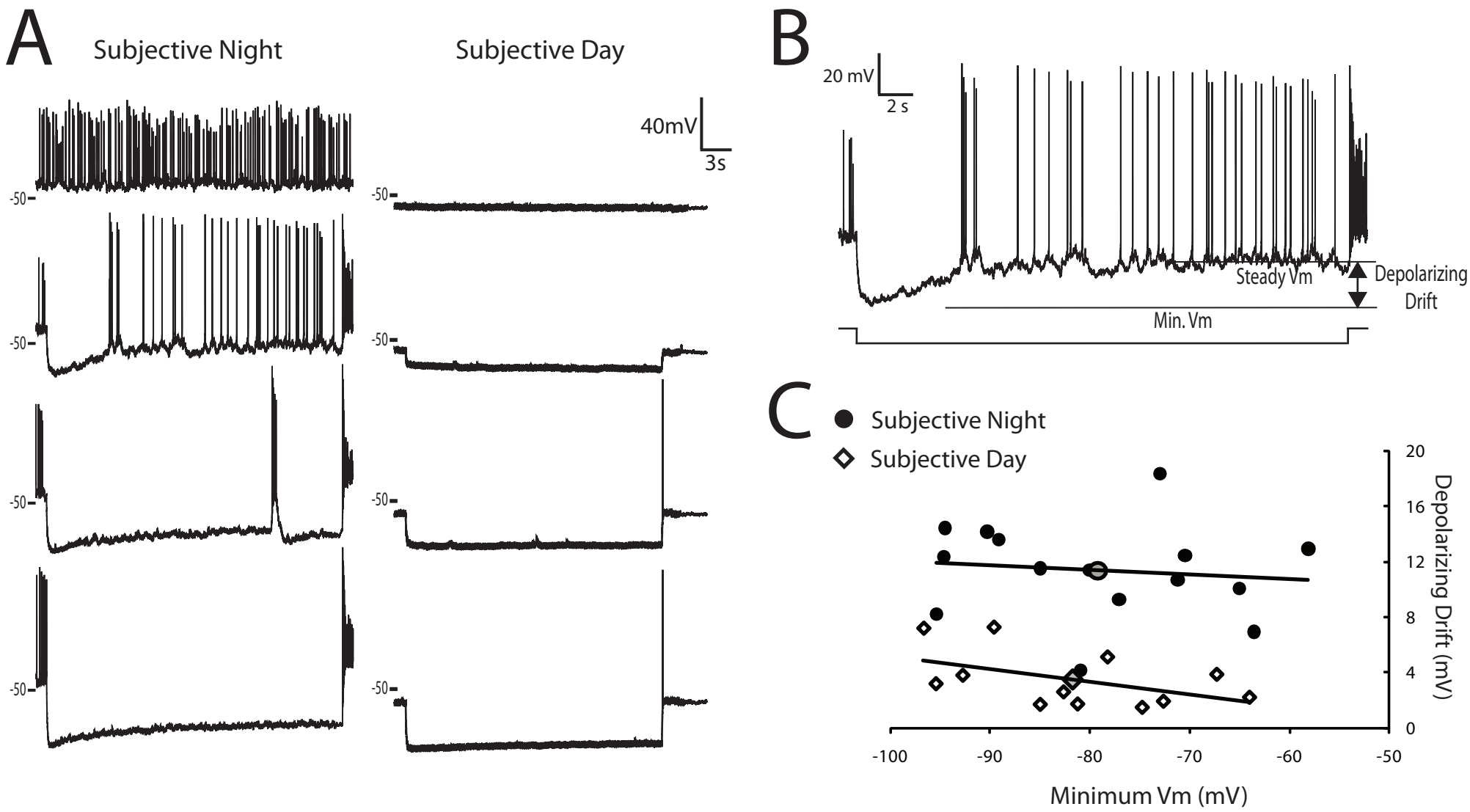

Figure 24. DAC Stability Depends on Light Condition. (A) Long Hyperpolarizing pulses were given to whole-cell DAC recordings. In subjective night recordings there was a substantial amount of depolarizing drift during the long current pulse. (B) Subjective Night recording example to demonstrate depolarizing drift calculation. The di˜erence between the smallest hyperpolarized voltage (minimum voltage) and the steady voltage (voltage calculated from the averaged last 5 seconds of pulse) gives the depolarizing drift. Di˜erent steps of current were used in both light conditions to measure the amount of depolarizing drift. Two example DACs from the subjective night and day show the di˜erence between the amounts of depolarizing drift for each light condition. (C) The amount of depolarizing drift for the minimum voltage is plotted for each light condition. The linear regression through each set of points demonstrates the increased amount of depolarizing drift for subjective night (dots) compared to subjective day (diamonds).

baseline activity seen in DACs. Differences between cells in the original protocol appear to imitate the differences in both subjective day and night. We did not attempt to demonstrate that I_H was responsible for the "sag" currents in any light condition.

Targeting of DACs for recording is possible due to their expression of D2 dopamine receptors, which are known to activate a G-protein coupled receptor signaling cascade that eventually decreases intracellular cyclic AMP for various effects on the cell. These effects are generally believed to be inhibitory towards cell excitability, including direct and indirect inhibition of calcium channels through Gβγ coupled mechanisms (Beaulieu and Gainetdinov, 2011). In the following set of experiments, we set out to determine the effects of dopamine on the DAC.

We studied DACs in subjective night conditions to mimic nighttime in the retina. We then attempted to determine the effects of activating D2 dopamine receptors on DACs, thereby mimicking day conditions for these cells. In the presence of 30 μM quinpirole, a D2 agonist that mirrors the release of dopamine for DACs, subjective night cells became hyperpolarized with decreased spontaneous firing frequencies (Figure 25). We also tested the effects of quinpirole on DACs original protocol conditions. In Figure 25B, the average resting membrane potential of DACs before quinpirole application was -40.4 mV (±5.6 standard deviation; n= 8). In every cell treated with quinpirole, the baseline membrane potential hyperpolarized to an average of -49.1 mV (±5 standard deviation; n=8). The hyperpolarization was present in both subjective night and original protocol conditions and brought the resting membrane potential close to the average potential of cells in subjective day conditions (-51.6 mV). The hyperpolarizing effects of quinpirole were statistically significant (Student's paired t-test, $p<0.005$), suggesting that quinpirole application was a very accurate model of day time vision in these retina.

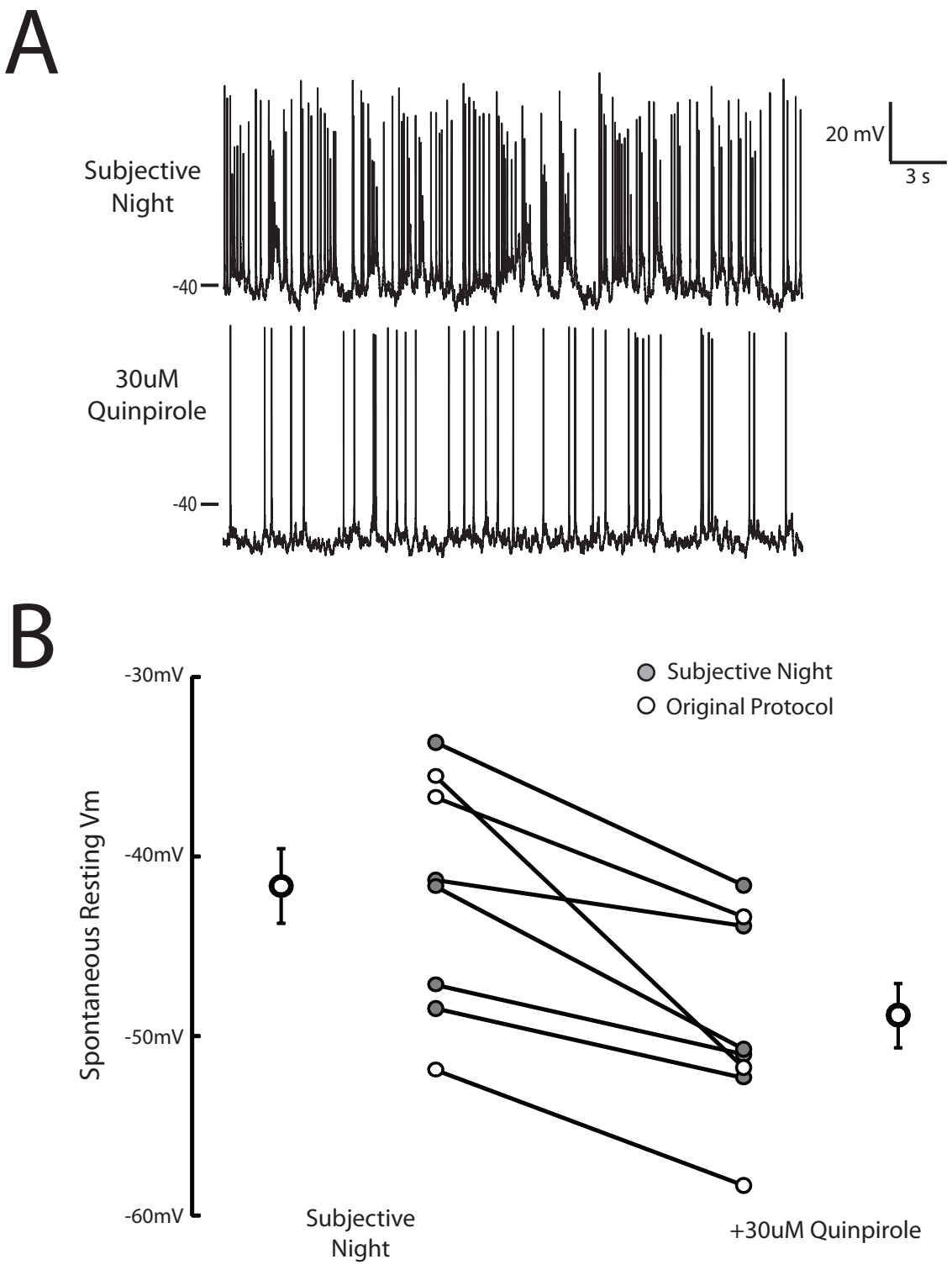

Figure 25. Quinpirole Hyperpolarizes Subjective Night DACs. (A) An example DAC whole-cell recording shows spontaneous activity before and after bath application of 30uM quinpirole. The DAC membrane potential hyperpolarizes and decreases spontaneous ÿring frequency. (B) A plot of average and individual cells' spontaneous resting potential of subjective night (gray circles) and original protocol (open circles) DACs before and after exposure to quinpirole. In every cell there was a hyperpolarization of membrane voltage. Error bars represent standard deviation.

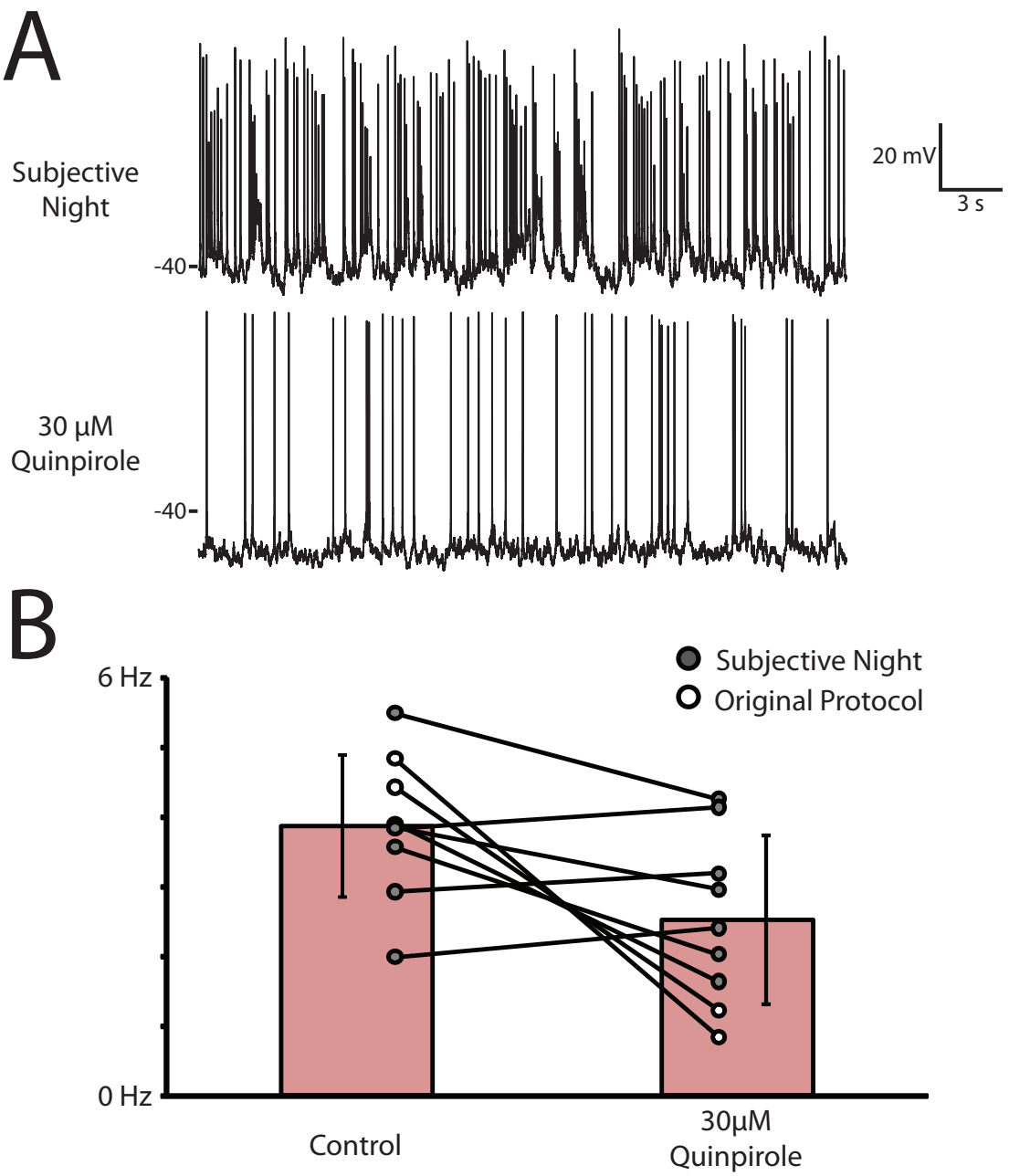

Figure 26. Quinpirole alters the spontaneous ÿring frequency of DACs. (A) An example spontaneous trace of a DAC in the subjective night recording condition before and after application of 30 µM Quin-pirole. (B) The e˜ects on spontaneous ÿring rate of eight di˜erent cells in either the subjective night (gray circles) or original protocol (open circles) recording condition. While the e˜ects in ÿring rate are not signiÿcant, this is can be partially attributed to changes in resting potential.

As with baseline membrane potential, the addition of quinpirole to DACs in subjective night conditions mimicked the behavior of DACs subjective day conditions for baseline action potential firing frequencies. Figure 26 shows spontaneously active DACs in both subjective night and original protocol conditions. The average firing frequency of control cells was 3.9 Hz (1.2 standard deviation; n=8) compared to 2.1 Hz (1.2 standard deviation; n=8) following the addition of bath applied quinpirole. Figure 26A shows the effects of individual cells before and after the addition of quinpirole. The overall spike rate decreases, but three cells show a slight increase in firing rate. These cells demonstrate a hyperpolarized membrane potential in the presence of quinpirole that was more advantageous for spontaneous action potentials (data not shown). Quinpirole effectively mimicked the conditions obtained in subjective day conditions by decreasing the baseline membrane potential and decreasing firing rate.

Long hyperpolarizing pulses were given in cells in subjective night in the absence and presence of 30 μM quinpirole. Again, we were interested in the presence of a depolarizing drift or "sag" current. In Figure 27 the average depolarizing drift is plotted for a minimum given voltage. For a minimum voltage of -80 mV, the average depolarizing drift in subjective night is 11.4 mV (±3.5 standard deviation; n=13). In the presence of quinpirole, the depolarizing drift is reduced to an average of 5.7 mV (±2.1 standard deviation; n=13) indicating that the amount of "sag" current that is reduced in the presence of quinpirole is statistically significant (Student's t-test, $p<0.005$). For comparison, DACs recorded in the subjective day condition were shown to have a 3.5 mV "sag" current (Figure 24). These experiments demonstrate that quinpirole is effective at imitating the DAC at light-adapted conditions and suggest that differences in baseline properties of DACs in the presence of light is due to activation of their D2 dopamine receptors.

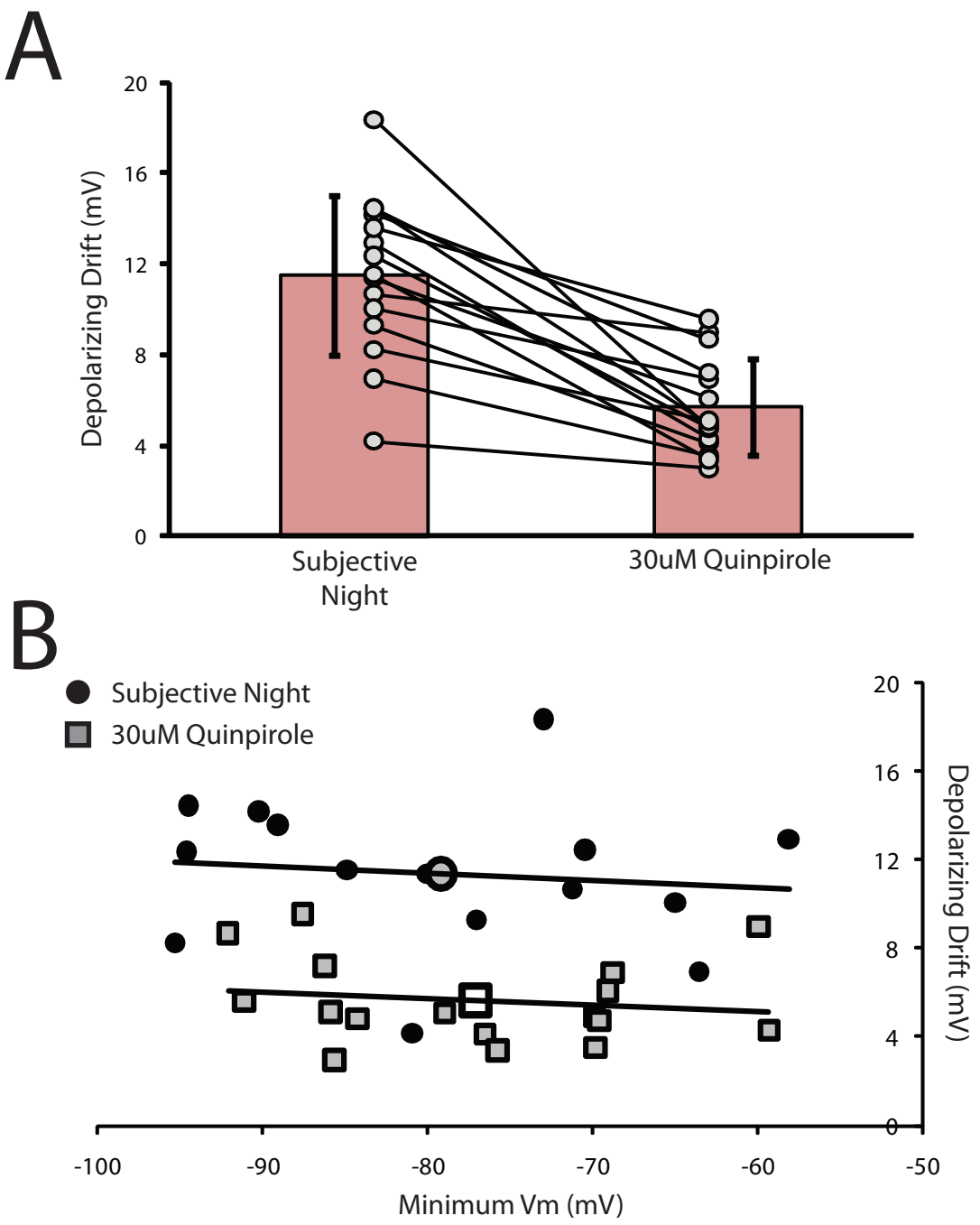

Figure 27. Quinpirole Reduces Depolarizing Drift in Subjective Night DACs. (A) The addition of 30uM quinpirole to the perfusion decreases the depolarizing drift in long hyperpolarizing pulses delivered in DAC whole cell recordings. The bar graph illustrates the average (with standard deviation error bars) for the subjective night condition before and after the addition of quinpirole to each individual cell (spheres). (B) The depolariz-ing drift is plotted against the minimum voltage of long hyperpolarizing pulses given in current-clamp conÿgu-ration of a DAC whole-cell recording. DACs in subjective night were perfused with 30uM quinpirole and plot-ted before (black circles) and after (gray squares) treatment. Linear regressions were ÿt to each population to demonstrate the decrease of depolarizing drift in the presence of quinpirole.

	Subjective Night	**+Quinpirole**	**Subjective Day**
Dopamine	Low	High (for D2 receptors)	High
Baseline Potential	-38.5	-49.1	-51.6
Spike Rate	2.7	2.1	0.14
I_H at -80 mV	11.4	5.7	3.5

Table 1. Comparing the effects of DAC baseline properties in different recording conditions

DISCUSSION

There were noticeable effects between DACs recorded at night and day conditions. Table 1 (SBAC Table 1) summarizes these effects including the effects of quinpirole. Generally, both the subjective day and addition of quinpirole to subjective night retinas decreased DAC baseline activity. Subjective day conditions and quinpirole also decreased the effects of I_H in hyperpolarizing current steps described in previous experiments obtained with the original protocol (Newkirk et al., 2013). These results suggest the D2 autoreceptor modulates the baseline activity of DACs depending on the retinal concentration of dopamine.

Dopamine receptors are G-protein coupled receptors that are separated into two distinct classes based on their effects on modulating adenylyl cyclase throughout the brain. One group, the D1-like receptors (D1 and D5) are positively coupled, while D2-like receptors (D2, D3, and D4) inhibit adenylyl cyclase through coupling with $G\alpha_{i/o}$. Modulating intracellular cyclic AMP is the main function of the receptors in cells, but they also can have other modulatory effects (reviewed in Beaulieu and Gainetdinov, 2011). D1-like receptors are found throughout the retina in nearly every major cell type. In the rodent retina, the majority of D2 receptors are present on DACs and on photoreceptor inner segments, with small localizations to other parts of the retina, suggesting that the use of D2 receptor agonists in our recordings should have fairly specific effects to our cells (Nguyen-Legros J, et al., 1999; Veruki 1997).

Quinpirole activates the D2 receptor to mimic the physiology of the DAC in subjective day conditions. The activation of D2-type receptors reduces excitability through unknown mechanisms in the DAC. We did not look at specific ion conductance differences in different conditions, but there was decreased I_H-type current in the presence of quinpirole. It is unknown if D2 receptors affect I_H conductances in DACs, but it has been demonstrated to inhibit I_H currents in *Xenopus* rod photoreceptors through Ca^{2+} activated G protein cascade (Akopian and Witkovsky, 1996). We did not attempt to identify the method of quinpirole action on D2 receptors. Therefore, additional experiments in DACs are necessary to determine the cause of baseline activity differences when DAC D2 receptors are activated either through quinpirole or light.

Our results appear to be counterintuitive to expected results given that the retinal concentration of dopamine is known to be increased during the day (Melamed et al.,1984; Wirz-Justice et al., 1984; Nir et al., 2000). Why would a DAC with a lower spike rate cause more

dopamine release? Our results suggest that DAC spike rate does not directly affect retinal dopamine concentration.

A substantial amount of work suggests that dopamine synthesis is controlled by light exposure. Early studies in rats show that light, even for as little as 15 minutes, increases activity of tyrosine hydroxlase, the rate limiting step in dopamine synthesis more than fourfold (Iuvone et al., 1978). Aromatic L-amino acid decarboxylase, the enzyme responsible for the formation of dopamine from L-DOPA, is also increased in light (Hadjiconstantinou et al., 1988). The apparent increase in dopamine production gives rise to an increase in metabolites that are able to process the increased dopamine levels, creating peaks of dopamine concentration at the onset and offset of light (Doyle et al., 2002). We have demonstrated that moderate to bright light intensity stimulates increased action potential firing in DACs. The release of dopamine from DACs has been demonstrated to be spike dependent based on amperometry experiments in cultured retina dopaminergic neurons (Puopolo et al., 2001). However, while we demonstrate higher spike rates of DACs in subjective night conditions, previous studies would suggest a decrease in dopamine release due to decreased levels of dopamine synthesis.

The original protocol places a subjective day animal into at least two hours of dark adaptation. Previous results in the original protocol describe four distinct modes of baseline activity for DACs. Subjective day or night conditions only provide a single distinct group of cells based on baseline activity. Our data suggests that DACs in the original protocol are in an intermediate transition between subjective day and subjective night modes, due to the switch from light exposure to dark adaptation. Figure 22 demonstrates the baseline membrane potential of all three conditions. Subjective day and night have defined groups, while original protocol cells appear to run the gamut of possible baseline physiology. There was no apparent

relationship between original protocol membrane potential and time spent in dark adaptation (results not shown), but this alone cannot rule out the possibility of a transitional phase in the original protocol that should be considered in future experiments.

Neurobiology of Disease

Functional Stability of Retinal Ganglion Cells after Degeneration-Induced Changes in Synaptic Input

David J. Margolis,[1] Gregory Newkirk,[1] Thomas Euler,[2] and Peter B. Detwiler[1]

[1]Department of Physiology and Biophysics and Program in Neurobiology and Behavior, University of Washington, Seattle, Washington 98195, and [2]Department of Biomedical Optics, Max Planck Institute for Medical Research, 69120 Heidelberg, Germany

Glutamate released from photoreceptors controls the activity and output of parallel pathways in the retina. When photoreceptors die because of degenerative diseases, surviving retinal networks are left without their major source of input, but little is known about how photoreceptor loss affects ongoing synaptic activity and retinal output. Here, we use patch-clamp recording and two-photon microscopy to investigate morphological and physiological properties of identified types of ON and OFF retinal ganglion cells (RGCs) in the adult (36–210 d old) retinal degeneration *rd-1/rd-1* mouse. We find that strong rhythmic synaptic input drives ongoing oscillatory spike activity in both ON and OFF RGCs at a fundamental "beating" frequency of ~10 Hz. Despite this aberrant activity, ON and OFF cells maintain their characteristic dendritic stratification, intrinsic firing properties, including rebound firing in OFF cells, balance of synaptic excitation and inhibition, and dendritic calcium signaling. Thus, RGCs are inherently stable during degeneration-induced retinal activity.

Key words: **retinal degeneration; photoreceptor; blindness; ganglion cells; dendrites; calcium**

Introduction

The vertebrate retina is an image processor. Visual information is detected by rod and cone photoreceptors, filtered through parallel synaptic pathways, encoded in action potentials by 12–15 different types of retinal ganglion cells (RGCs), and sent to the brain via the optic nerve (Masland, 2001; Wassle, 2004; Field and Chichilnisky, 2007). Synaptic output signals from photoreceptors initiate this sequence of events by controlling the activity of downstream retinal circuits. Permanent loss of photoreceptors, as occurs in many types of degenerative diseases (Phelan and Bok, 2000; Daiger et al., 2007), would be expected to have dramatic functional consequences, but alterations in the physiology of surviving retinal circuitry have not been specified.

In the retinal degeneration *rd-1/rd-1* (RD) mouse, rod and cone photoreceptors progressively die in the first weeks after birth, leading eventually to the severe changes in cellular architecture and remodeled neural circuitry that characterize retinal degeneration (Blanks et al., 1974; Carter-Dawson et al., 1978; Jimenez et al., 1996; Strettoi and Pignatelli, 2000; Marc et al., 2003; Punzo and Cepko, 2007). Little is known about the functional adaptations that accompany these morphological changes. Recent studies in the RD mouse indicate that, surprisingly, photoreceptor loss results in increased rather than decreased retinal activity (Marc et al., 2007; Stasheff, 2008). Excitation mapping of organic cations showed increased glutamate drive [postnatal day 60 (P60)–P90] (Marc et al., 2007), and multielectrode array recordings indicated that RGC spike rate has also increased (P7–P115) (Stasheff, 2008). But how the functional properties of RGCs change after photoreceptor loss, including presynaptic and postsynaptic mechanisms, is not understood. This information is critical for retina-based vision rescue strategies, which depend on functional stability of RGCs and their underlying synaptic circuits.

Previous work on three functional types of "large soma" RGCs in wild-type (WT) mouse retina [ON, OFF transient (OFF-T), and OFF sustained (OFF-S)] found distinguishing differences in their dendritic morphology, synaptic input, and intrinsic physiological properties (Pang et al., 2003; Murphy and Rieke, 2006; Margolis and Detwiler, 2007). These cells are excited by either light increments (ON cells) or decrements (OFF cells) and represent the output of two fundamental parallel pathways (Schiller, 1992). Their dendritic arbors stratify at different depths within the inner plexiform layer (IPL), and they exhibit characteristic intrinsic electrical properties, including the ability of OFF cells to fire "rebound" bursts after hyperpolarization (Margolis and Detwiler, 2007).

Here, we take advantage of these distinctive differences to identify ON and OFF type RGCs in the blind RD retina and investigate the effect of photoreceptor loss on their morphological, electrophysiological and Ca^{2+} signaling properties using a combination of patch-clamp recordings and two-photon laser-scanning fluorescence microscopy. We find that strong rhythmic synaptic input drives oscillatory spike activity in both ON and OFF RGCs at P36–P50, when virtually all photoreceptors are lost. Intrinsic properties of RGCs, however, are maintained, even into

Received Sept. 18, 2007; revised May 14, 2008; accepted May 14, 2008.

This work was supported by National Institutes of Health Grants EY02048 (P.B.D.), GM07108 (D.J.M.), and EY01730-31 (Vision Research Center), Human Frontiers Science Program Grant RGP-0067 (G.N.), and the Max Planck Society (T.E.). We thank W. Denk for design and construction of the two-photon microscope and continued support and advice, F. Dunn, I. Fine, A. Horsager, and F. Rieke for helpful discussion, D. Possin for histology, and P. Newman for technical assistance.

Correspondence should be addressed to either of the following: Peter B. Detwiler, Department of Physiology and Biophysics, University of Washington, Box 357290, Seattle, WA 98195, E-mail: detwiler@u.washington.edu; or David J. Margolis at his present address, Department of Neurophysiology, Brain Research Institute, University of Zurich, CH-8057 Zurich, Switzerland, E-mail: margolis@hifo.uzh.ch.

DOI:10.1523/JNEUROSCI.1533-08.2008

 0270-6474/08/286526-11$15.00/0

late-stage retinal degeneration (P210). These results reveal a high degree of functional stability in RGCs, despite dramatic degeneration-induced changes in synaptic activity.

Materials and Methods

Animals. Experimental procedures were similar to those in previous work (Margolis and Detwiler, 2007). All experiments were done in accordance with local and national guidelines for animal care. Unless noted otherwise adult C3HeJ mice (*rd-1/rd-1*) were used at P36–P50 (P44 ± 4, mean ± SD; $n = 12$), when their retinas were not responsive to light because of the loss of photoreceptors. Experiments were also done on RGCs from P124, P158, and P210 RD retina (one mouse at each age). These ages represent later stages in the degenerative disease and show evidence of more advanced changes in retina structures (Jones et al., 2003, 2005; Marc and Jones, 2003; Marc et al., 2003, 2007). In this, as in other studies (Pang et al., 2003; Murphy and Rieke, 2006; Sagdullaev et al., 2006; Margolis and Detwiler, 2007), information about WT (C57BL/6) RGCs was obtained from adult (P28–P56) animals and used for controls as indicated in the figures. Both WT and RD mice were obtained from The Jackson Laboratory. Animals were housed in temperature-regulated facilities on a 12 h light/dark cycle and had *ad libitum* access to food and water. Neither WT nor RD mice were dark adapted for these experiments.

Tissue preparation. Retinas from WT and RD mice were treated identically. Mice were killed by cervical dislocation. Their eyes were removed, bathed in room temperature-oxygenated (gassed with 95% O_2 and 5% CO_2) Ames medium (Sigma), hemisected, and the cornea and lens were removed. The resulting eyecup was cut into two to four pieces, and the retina was isolated by gently teasing it from the pigment epithelium. Extra pieces/eyecups were stored in oxygenated Ames until needed. The vitreous was removed from the retina with forceps before mounting it flat, photoreceptor-side down, on Anodisc filter paper (Whatman) that was mechanically fixed to the glass bottom of a recording chamber, mounted on the stage of a two-photon fluorescence microscope (see below), and superfused with warmed (30–34°C), oxygenated Ames at a rate of 4–8 ml/min.

Cell identification. The flat-mount retina was viewed on a video monitor using infrared illumination and a CCD camera. WT RGCs were identified as ON, OFF transient, or OFF sustained based on physiological and morphological criteria, as in previous work (Margolis and Detwiler, 2007). Light responses from WT cells could often be used for cell identification even under light adapted conditions. In the presence of synaptic blockers for WT, and in all cases for RD retinas, cell types were identified based on their morphology using differences in the retinal location of their dendritic arbors. The depth of dendritic stratification in the IPL was measured as described in a previous study (Margolis and Detwiler, 2007). Briefly, at the end of patch recording, green fluorescence from an RGC filled with a Ca^{2+} indicator (see below) was measured using *Z*-series image stacks and compared with red fluorescence acquired simultaneously from bath-applied sulforhodamine-101 (SR-101). In an SR-101-stained *Z*-series image stack, the inner and outer boarders of the IPL borders were defined (starting at the ganglion cell layer) as the first and last image to contain no somata, respectively. Dendritic stratification was expressed as the location of the peak dendritic fluorescence within the IPL borders.

Histology. For gross morphological comparison, WT and RD retinas were fixed in PIPES-buffered 2.5% glutaraldehyde/1.6% paraformaldehyde, dehydrated, plastic-embedded, and stained with 10% Richardson's stain. Cross sections (5 μm) from midperipheral retina were photographed using a 40× 1.3 numerical aperture (NA) oil objective and standard light microscopy. Shrinkage caused by fixation/dehydration was not corrected for.

Electrical recordings. Cells in the ganglion cell layer with large diameter (18–25 μm) somas were targeted for patch-clamp recordings in the flat-mount retina. Electrode access to a selected cell was obtained by using an empty patch pipette to microdissect the internal limiting membrane above it (Taylor et al., 2000; Murphy and Rieke, 2006; Margolis and Detwiler, 2007). Patch-clamp recordings were made using 3–7 MΩ electrodes, and signals were amplified using either Axopatch 200B or Axoclamp 2B amplifiers. For whole-cell recordings, unless noted otherwise, the standard internal solution contained (in mM) 120 K-gluconate, 5 NaCl, 5 KCl, 5 HEPES, 1 $MgCl_2$, 1 adenosine 5′-triphosphate, and 0.1 guanosine 5′-triphosphate, adjusted to pH 7.4 with KOH, plus 125–140 μM Oregon Green BAPTA-1 (OGB-1) or 250 μM Fluo-5F for Ca^{2+} imaging (Invitrogen). In experiments involving ratiometric fluorescence measurements, the internal solution also included 100 μM Alexa-594, a Ca^{2+} insensitive dye. In experiments to isolate inhibitory and excitatory currents the voltage-clamp internal solution contained (in mM) 105 Cs-$MeSO_4$, 10 tetraethylammonium Cl, 20 HEPES, lidocaine *N*-ethyl bromide, 5 ATP-Mg, and 0.5 GTP-Tris, plus 125–140 μM OGB-1 or 250 μM Fluo-5F. Corrections for a 10 mV liquid junction potential were done off-line. To isolate cells from synaptic inputs, we used a mixture of bath-applied synaptic antagonists (in μM): 20 CNQX, 50 APV, 1 strychnine, 50 picrotoxin, and 50 L-APB [a metabotropic glutamate receptor 6 (mGluR6) agonist]. Current and voltage stimuli were generated and data acquired through an ITC-16 interface (Instratech) using software written in Igor Pro (Wavemetrics) by Fred Rieke (University of Washington, Seattle, WA). All chemicals were purchased from Sigma or Tocris.

Optical recordings. Fluorescence measurements were made using a custom built two-photon laser-scanning microscope (Denk et al., 1990; Euler et al., 2002; Margolis and Detwiler, 2007), designed around Sutter micromanipulators (Sutter Instrument) and controlled by CfNT software (written by Ray Stepnoski, Bell Laboratories, Murray Hill, NJ; and Michael Muller, Max-Planck-Institute for Medical Research, Heidelberg, Germany). Fluorescence excitation was provided by a pumped infrared laser (Mira; Coherent) at 905–930 nm, and collected by a 60× 1.0 NA water-immersion objective (Nikon). Custom bandpass (BP) filters (Chroma Technology) directed green (535 BP 50 nm) and red (622 BP 36 nm) fluorescence to two independent photomultiplier tubes (Hamamatsu). The green channel was used for Ca^{2+} indicator fluorescence, and the red channel was used for either bath-applied SR-101 or intracellularly applied Alexa-594.

Data analysis. Electrophysiological data were analyzed in Igor Pro, which was also used to analyze optical data along with ImageJ (http://rsb.info.nih.gov/ij/). To measure the frequency characteristics of electrical activity, power spectral density functions (PSDs) were computed from long (>15 s) current or voltage sweeps using built-in routines in Igor that measured power in 1.22 Hz bins. The fundamental "beating" frequency was measured as the peak power in the range 3–20 Hz, determined by Gaussian fit to PSDs. Fits were used to obtain a more accurate estimation than allowed by the 1.22 Hz binning. PSDs were computed from either cell-attached spiking, whole-cell current-clamp recordings of subthreshold and superthreshold voltage, or whole-cell voltage-clamp recordings of synaptic currents. Clear peaks were evident from all of these types of recordings and rhythmicity could be confirmed in raw traces by visual inspection. Beating frequencies as measured from current- and voltage-clamp recordings were combined for group averages (see Table 1) because they were not different when measured using either type of recording. Correlation (see Figs. 4, 5) was measured with the Pearson test.

To relate properties of calcium signaling and evoked spike firing (see Fig. 7), we chose a simple index of $\Delta F/F$ per spike, expressed as the percentage Ca^{2+} change (after background subtraction) per action potential. For responses to depolarizing stimuli, $\Delta F/F$ per spike was measured from responses in the middle (linear) range of a cell's spike frequency–current intensity relationship. For rebound firing, $\Delta F/F$ per spike was calculated from strong responses usually comprised of two to four spikes.

Results

Identification of ganglion cell types in RD retina

In the RD mouse, the vast majority of photoreceptors die within 2–3 weeks of age and outer retina morphology is severely altered (Blanks et al., 1974; Carter-Dawson et al., 1978; Farber et al., 1994; Jimenez et al., 1996; Punzo and Cepko, 2007). By P40, photoreceptor outer segments as well as the outer nuclear layer

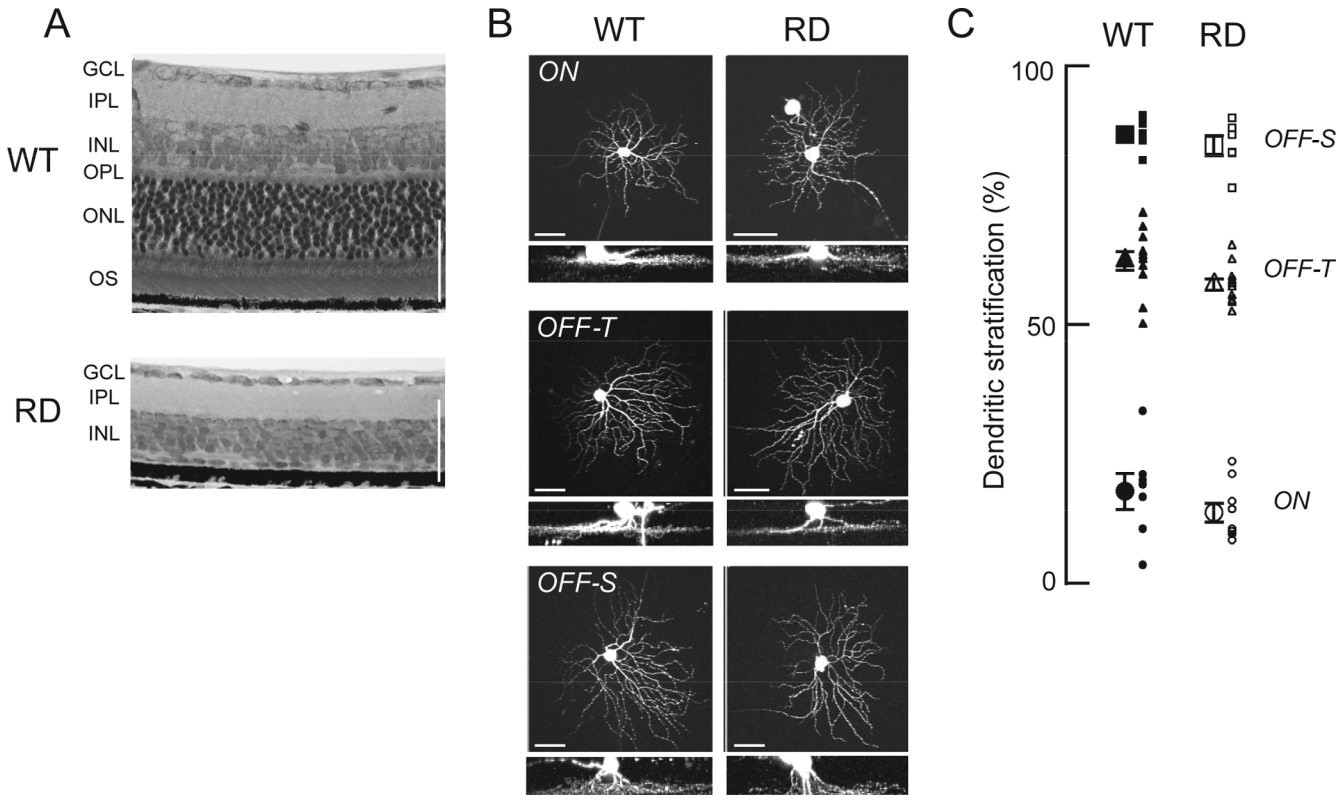

Figure 1. Identification of three RGC types in adult RD retina (mean age ± SD, P44 ± 4). ***A***, Cross sections of fixed tissue show gross structural differences of WT and RD retinas. Note the lack of outer plexiform layer (OPL), outer nuclear layer (ONL), and photoreceptor outer segments (OS) in RD retina. GCL, Ganglion cell layer; INL, inner nuclear layer. ***B***, Two-photon *z*-projections (larger top images) and side projections (below) of three identified types of WT (left) and RD (right) RGCs. Cells were filled with 125 μM OGB-1 during patch-clamp recordings. ***C***, Dendritic stratification within the IPL for populations of ON ($n = 7$ WT, 9 RD), OFF-T ($n = 12$ WT, 12 RD), and OFF-S ($n = 5$ WT, 6 RD) RGCs from WT (filled symbols) and RD (open symbols) retina. See Results for statistical comparisons. The WT data in ***C*** is from Margolis and Detwiler (2007). Scale bars, 50 μm. Error bars indicate SEM.

and outer plexiform layer have been mostly eliminated (Fig. 1*A*). In contrast, inner retina structures appear intact, including the inner nuclear layer, IPL, and ganglion cell layer at this age and older (P196 and P226) (supplemental Fig. 3, available at www.jneurosci.org as supplemental material). This is consistent with descriptions in numerous previous studies (Strettoi and Pignatelli, 2000; Strettoi et al., 2002; Jones et al., 2003; Marc and Jones, 2003; Marc et al., 2003) and shows that RGCs survive after photoreceptor loss and subsequent degenerative changes in the retina (Jones and Marc, 2005; Daiger et al., 2007).

In adult WT mouse retina, three types of ON and OFF ganglion cells (ON, OFF transient and OFF sustained) have been identified and can be reproducibly targeted for recording based on their large-diameter (18–25 μm) cell bodies (Pang et al., 2003; Murphy and Rieke, 2006; Margolis and Detwiler, 2007). These cells are typically classified based on their functional responses to visual stimuli, e.g., ON (excited at light onset) or OFF (excited at light offset), but this is not possible in adult RD retina because photoreceptors have degenerated and light responses are abolished by ~P25 (Stasheff, 2008). However, ON and OFF RGCs also have known differences in dendritic structure, notably their stratification depth within the IPL (Nelson et al., 1978). In WT retina, ON, OFF-transient, and OFF-sustained cells can be identified based on this criteria (Margolis and Detwiler, 2007). We hypothesized that dendritic stratification depth might still enable identification of these cell types in the blind RD retina.

In a flat-mount preparation of RD retina, cells in the ganglion cell layer with the largest soma diameters (18–25 μm) were targeted for whole-cell recording, filled with fluorescent Ca^{2+} indicator (OGB-1 or Fluo-5F), and imaged using two-photon fluorescence microscopy (Fig. 1*B*). The branching pattern and size of dendritic arbors of these cells appeared similar to WT cells. Measurement of dendritic stratification showed three clusters at different depths in the IPL (Fig. 1*C*). Data from 27 identified ON, OFF-T, and OFF-S RGCs in RD retina are compared with WT in Figure 1*C*. As in WT retina, RD cells stratified in three distinct levels of the IPL (ON, 13.7 ± 1.8%; OFF-T, 57.7 ± 1.0%; OFF-S, 84.6 ± 1.9%; $p \ll 0.001$ for ON–OFF-T and OFF-T–OFF-S). Stratification depths were not statistically different from WT [data are from the study by Margolis and Detwiler (2007)] in any of the three groups (ON: $p = 0.33$; RD, $n = 9$; WT, $n = 7$; OFF-T: $p = 0.06$; RD, $n = 12$; WT, $n = 12$; OFF-S: $p = 0.41$; RD, $n = 6$; WT, $n = 5$).

Because the differences in the stratification depth of the dendrites of RGCs in the RD retina corresponded to the differences in the dendritic depths of ON, OFF-S and OFF-T RGCs in the light-sensitive WT retina, they were used to identify these cell types in the light-insensitive RD retina. Experiments described in later sections further validate this classification scheme by demonstrating that the different morphological classes of RD cells exhibit the same distinguishing intrinsic electrical and dendritic Ca^{2+} signaling properties as the three functional cell types in the WT retina. Based on these criteria, RGCs in the RD retina will be referred to henceforth as either ON, OFF-S, or OFF-T.

RGCs in retinas from adult RD mice ranging in age from P36–P210 were studied using a combination of electrical and optical recording. The retinas from older animals (>P50) were thin and fragile making it difficult to isolate an acceptably intact

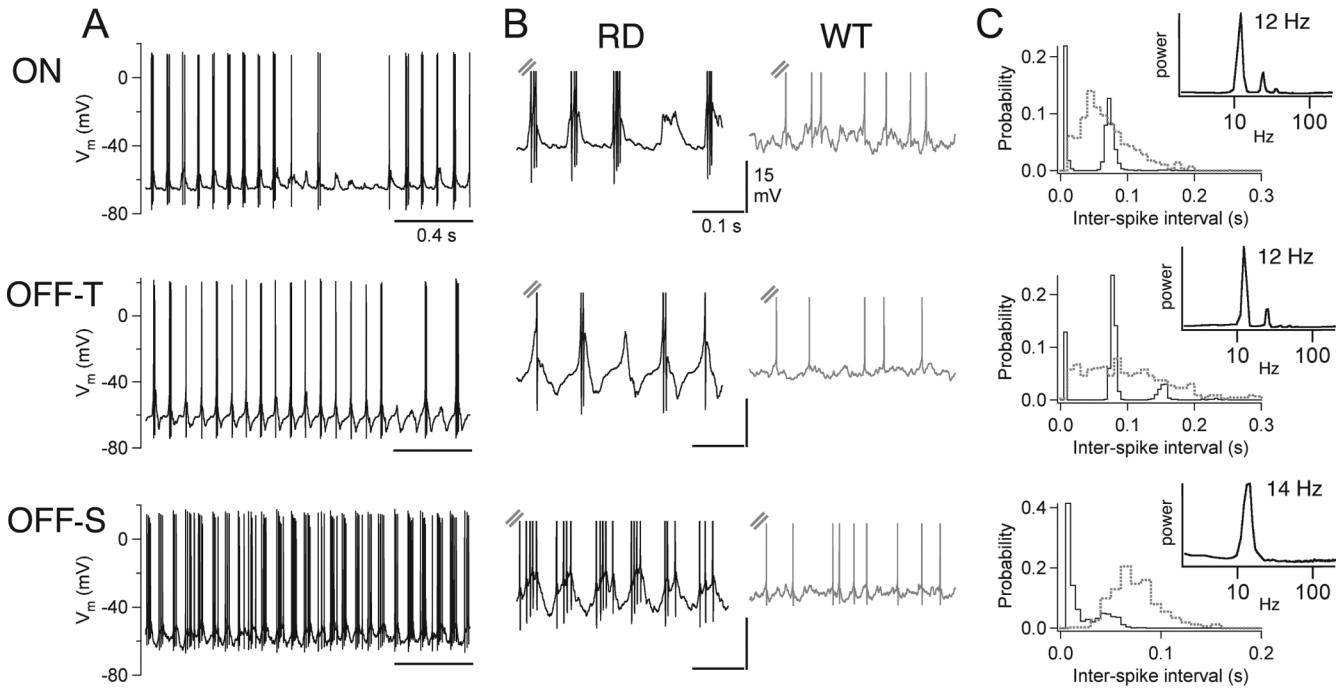

Figure 2. Rhythmic resting spike activity in identified RD RGCs. ***A***, Whole-cell current-clamp recordings from ON, OFF-T, and OFF-S RGCs in RD retina. ***B***, Activity on an expanded time scale. Note the underlying oscillatory membrane depolarizations present in RD (left, black) but not WT (right, gray) cells. ***C***, Interspike interval histograms from cells in ***B***. Solid line, RD; dotted line, WT. Insets show the power spectra for RD RGCs (same cells as in ***B***). Note the clear presence of peak frequencies at 12–14 Hz in these cells.

Table 1. Properties of resting spiking and synaptic currents in identified ganglion cell types in RD retina

	Spike rate (Hz)	CV of ISI	Fund. freq. (Hz)	Peak EPSC (pA)
ON	22.0 ± 4.6 (11)	1.2 ± 0.1 (11)	9.2 ± 0.7 (13)	−294 ± 53 (11)
OFF-T	25.1 ± 6.6 (10)	1.1 ± 0.2 (10)	8.9 ± 0.8 (15)	−189 ± 42 (10)
OFF-S	32.7 ± 7.0 (4)	1.1 ± 0.1 (4)	8.5 ± 1.0 (7)	−137 ± 34 (5)

Data are shown as mean ± SEM. The number of cells (*n*) is shown in parentheses. ISI, Interspike interval; Fund. freq., fundamental frequency. $V_{hold} = -70$ mV.

retina for whole mount recordings. Thus the majority of studies were done on P36–P50 animals, with experiments to evaluate the physiological properties of RGCs on small numbers older RD animals.

Rhythmic resting spike activity in RD RGCs

In normal (WT) RGCs, the resting spike activity in the absence of light is irregular with little underlying temporal structure (Pang et al., 2003; Murphy and Rieke, 2006; Sagdullaev et al., 2006; Margolis and Detwiler, 2007). In contrast, in RD mice, ON, OFF-T, and OFF-S RGCs displayed striking and consistent patterns of rhythmic resting spike activity (Fig. 2). All three cell types showed continuous rhythmic bursts of spikes with an interburst beating frequency of ~10 Hz (Fig. 2*A*). Examination of subthreshold membrane potential revealed oscillatory depolarizations at the same frequency, each crested by 0–5 spikes (Fig. 2*B*, left). Such activity patterns were not observed in any recordings from WT cells of the same type (Fig. 2*B*, right). Histograms of interspike interval showed groups corresponding to the fundamental beating frequencies (~12 Hz/0.08 s interval in these example cells), as well as the higher-frequency spike bursts (Fig. 2*C*). Spectral analysis revealed clear peaks in power corresponding to the beating frequencies (Fig. 2*C*, insets). The mean beating frequency in all recorded cells (P36–P50) was 9.0 ± 0.4 Hz (n = 35 total; 13 ON, 15 OFF-T, 7 OFF-S; range, 3–14 Hz). There were no differences in beating frequencies between ON and OFF cell types ($p > 0.2$) (Table 1). The beating frequency of any given cell was the same as measured in either current or voltage clamp (see Fig. 4); therefore, data from both types of recording was pooled for calculation of group means. The overall resting mean spike rate (including spikes that occur in bursts during rhythmic firing) was 24.9 ± 3.5 Hz (n = 25 total; 11 ON, 10 OFF-T, 4 OFF-S; range, 5–80 Hz). This is, on average, about twice the mean spike rate of WT cells (Margolis and Detwiler, 2007; Stasheff, 2008). It is also ~2.5-fold higher than the beating frequency, which reflects the fact that rhythmic synaptic input typically generated more than a single spike (see Fig. 4). The high (>1) coefficients of variation (CV = SD/mean) are another consequence of the rhythmic nature of firing. These measures are summarized in Table 1. Persistent rhythmic spike activity was present in every recording from identified ON, OFF-T, and OFF-S RGCs in the P36–P50 age group as well as in cells from animals as old as P210, albeit at a slower rate. In older animals both the fundamental beating frequency and mean spike rate were reduced twofold to threefold (supplemental Fig. 3, available at www.jneurosci.org as supplemental material). Maintained rhythmic spike activity is a characteristic feature of RGCs in RD retina that is not seen in WT RGCs. It was present in whole-cell and cell-attached (loose patch) extracellular recordings regardless of the time of day or length of the experiment. These results indicate that the retina continues to generate output signals in both the early and later stages of degeneration-induced loss of photoreceptors.

Oscillatory synaptic input underlies altered resting activity

The aberrant activity that gives rise to rhythmic spiking in RD RGCs could be generated either intrinsically, by voltage-dependent conductances that give rise to pacemaker currents, or

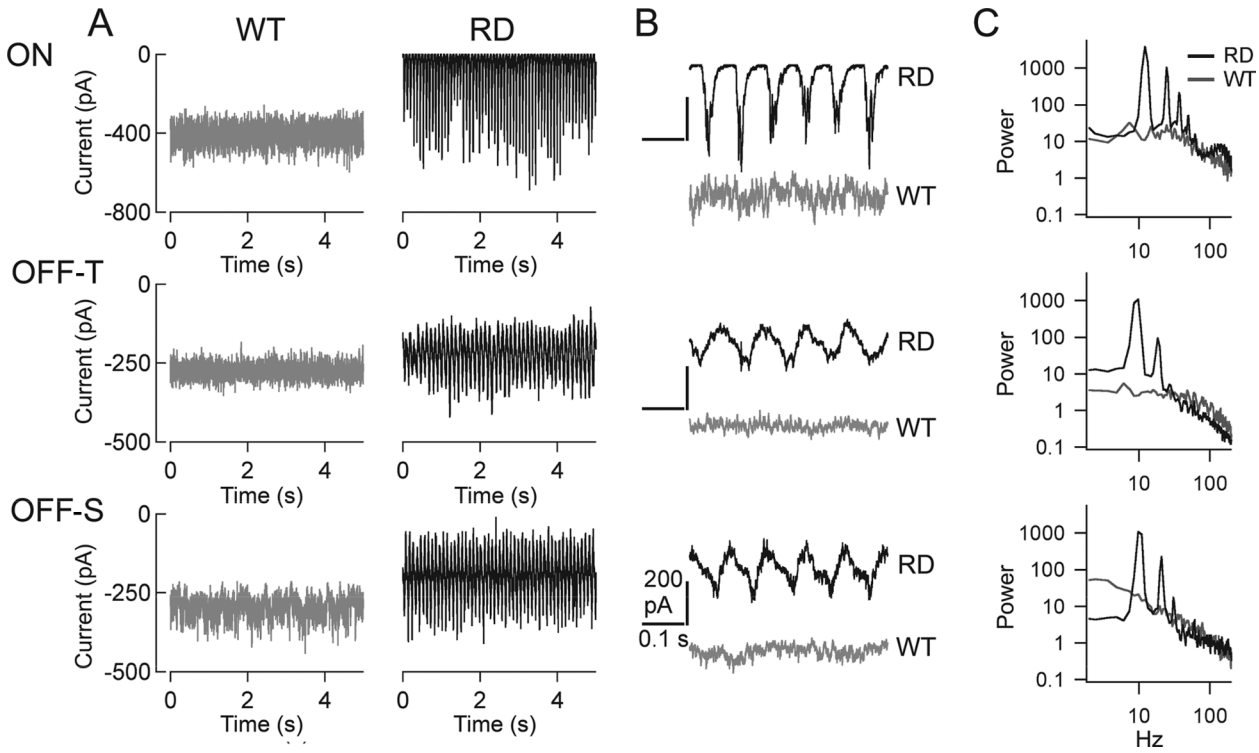

Figure 3. Rhythmic resting synaptic currents in identified RD RGCs. ***A***, Whole-cell voltage-clamp recordings of resting synaptic currents in ON, OFF-T, and OFF-S RGCs from WT (left, gray) and RD (right, black) retinas ($V_{hold} = -70$ mV). ***B***, Currents on an expanded time scale. Note the strong periodicity in RD currents from all three cell types and different dynamics of currents in ON and OFF cells. ***C***, Power spectra of RD (black) and WT (gray) currents (the same cells as in ***B***). The multiple peaks in RD spectra reflect harmonics of the fundamental beating frequency of ~10 Hz.

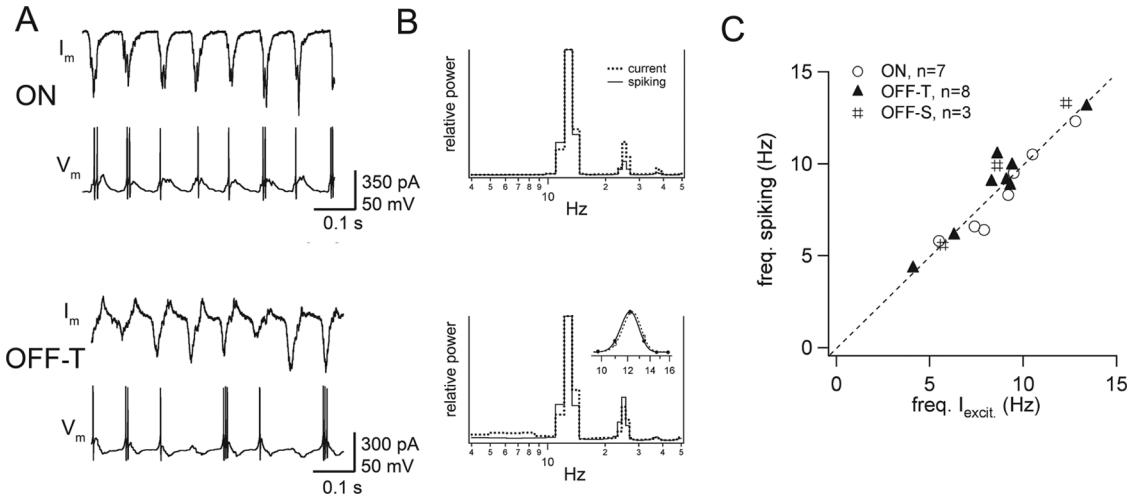

Figure 4. Correlation between spiking and synaptic currents in individual RD RGCs. ***A***, Whole-cell voltage-clamp (top; $V_{hold} = -70$ mV) and current-clamp (bottom) recordings from individual ON (above) and OFF-T (below) cells. ***B***, Power spectra of current (dotted line) and voltage (solid line) from the cells in ***A***. The inset shows Gaussian fits to spectra in the range of 3–20 Hz. ***C***, Correlation of peak frequencies of spiking and synaptic currents in individual cells ($n = 18$), as measured from power spectra.

extrinsically, by reverberant synaptic input. To test the possibility that synaptic mechanisms are the source of rhythmic activity, RGC membrane potential was held at −70 mV in whole-cell voltage clamp and resting input currents were measured. Under these conditions, the recorded current showed ongoing clear-cut amplitude fluctuations in ON, OFF-T, and OFF-S cells (Fig. 3) at about the same frequency as rhythmic spiking activity (Fig. 2). Baseline currents of this nature were only seen in RGCs from RD retina: membrane current recorded under the same conditions from WT cells was dominated by low-amplitude baseline synaptic noise with few resolvable discreet events (Fig. 3*B*). Power spectra of RD current recordings revealed peaks at ~10 Hz that were not present in WT recordings (Fig. 3*C*) and generally matched the frequency of spike activity in current-clamp recordings from RD RGCs (Fig. 2). The correspondence between rhythmic variation in current and voltage (spiking) was examined explicitly by comparing sequential voltage- and current-clamp recordings from the same cells. The traces in Figure 4*A* illustrate the temporal coincidence between peak inward currents and peak depolarizations that evoked spike bursts in an ON and OFF RD RGC. Spectral analysis of these records reinforces this point by showing that power peaks at the same frequency in voltage and current

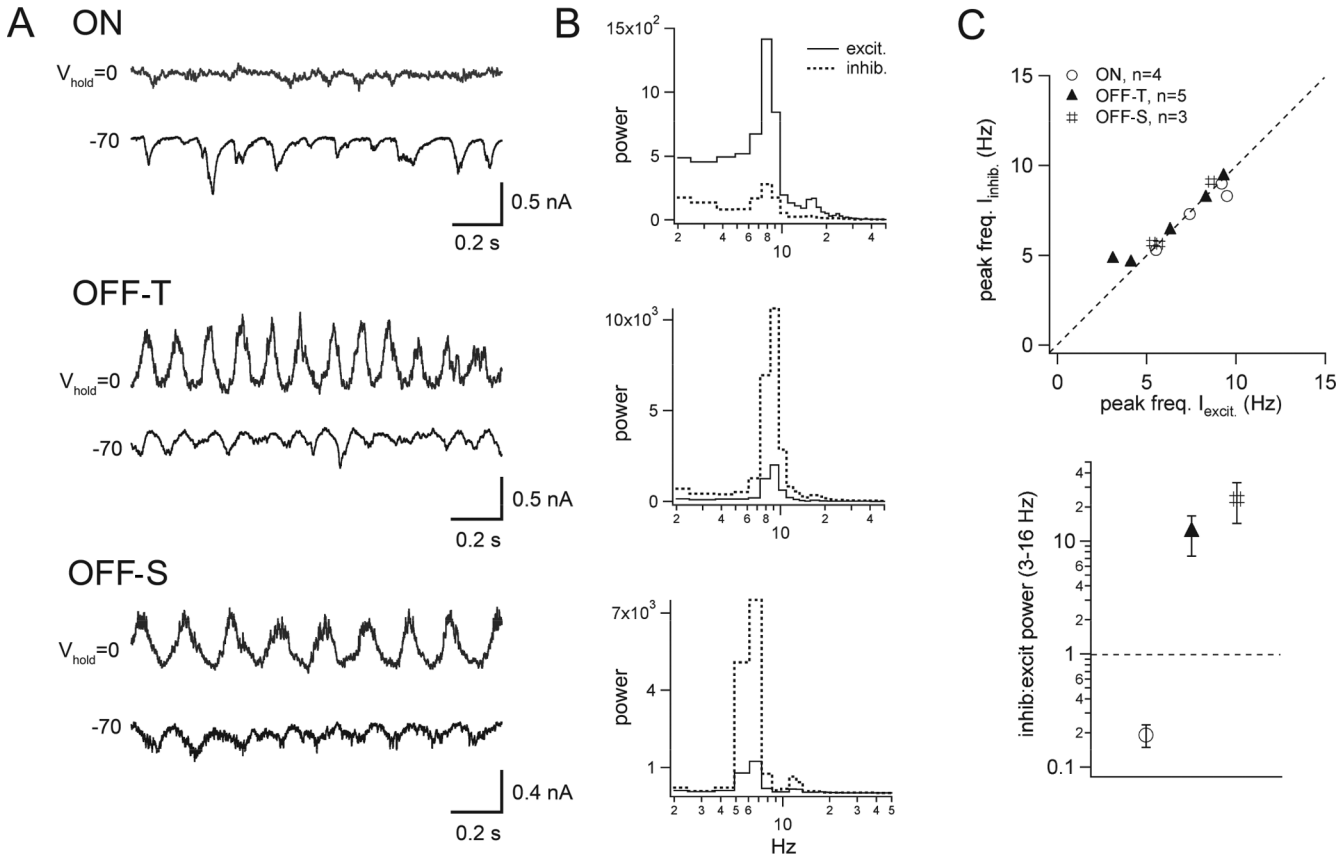

Figure 5. Distinct balance of excitatory and inhibitory synaptic currents in ON and OFF RD RGCs. ***A***, Comparison of excitatory ($V_{hold} = -70$ mV; black, bottom traces) and inhibitory ($V_{hold} = 0$ mV; gray, top traces) synaptic currents from individual cells. ***B***, Power spectra of excitatory (solid line) and inhibitory (dotted line) currents from the cells in ***A***. ***C***, Top, Correlation between frequency of inhibitory and excitatory currents from individual ON, OFF-T, and OFF-S cells ($n = 12$). Frequency measured from power spectra as in Figure 4. Bottom, Ratio of inhibitory to excitatory power for ON, OFF-T, and OFF-S cells. Note that the ratio is low for ON cells and high for OFF cells, reflecting a distinct balance of excitatory and inhibitory synaptic currents. Recordings were made with $CsMeSO_4$ internal solution (see Materials and Methods). Error bars indicate SEM.

recordings in both cell types (Fig. 4*B*). The strong correlation ($r = 0.95$; $p < 0.001$) between the peak frequency of spiking and the peak frequency of currents from all individual cells where both were recorded ($n = 18$ total; 7 ON, 8 OFF-T, 3 OFF-S) is apparent in the plot of Figure 4*C*.

The fluctuating current recorded from voltage-clamped RGCs in RD retina were reduced by >90% by exposure to a mixture of synaptic antagonists (in μM) 50 L-APB, 20 CNQX, 50 APV, 1 strychnine, and 50 picrotoxin (supplemental Fig. 1, available at www.jneurosci.org as supplemental material). This is additional evidence that the rhythmic currents are generated extrinsically by spontaneous variation in synaptic inputs. The baseline fluctuations in current were still present, however, in the presence of L-APB alone, an mGluR6 agonist, indicating that the source of the persistent synaptic activity that gives rise to the oscillatory activity is downstream of the photoreceptor-to-ON bipolar synapse (supplemental Fig. 1, available at www.jneurosci.org as supplemental material).

Balance of excitation and inhibition in RD RGCs

Thus far, the experiments have shown that rhythmic synaptic input drives firing in both ON and OFF RGCs in the RD retina. Differences in the amplitude and dynamics of synaptic inputs to ON and OFF cells are also apparent: at rest ($V_{hold} = -70$ mV), there are monophasic inward currents in ON cells and biphasic currents in OFF-T and OFF-S cells. This could reflect a different balance of excitatory (inward) and inhibitory (outward) synaptic currents in these cell types, consistent with the different allotment of excitatory and inhibitory synaptic input to ON and OFF cells in WT RGCs (Pang et al., 2003; Murphy and Rieke, 2006) (supplemental Fig. 2, available at www.jneurosci.org as supplemental material). To examine more closely the effect of photoreceptor degeneration on the balance of synaptic inputs to RD RGCs, membrane currents were recorded in voltage clamp from RGCs held at membrane potentials that were close to the reversal potential for excitatory (0 mV) and inhibitory (−70 mV) synaptic currents (Taylor et al., 2000; Pang et al., 2003; Murphy and Rieke, 2006). Recordings of resting currents in ON and OFF RD RGCs at −70 and 0 mV are shown in Figure 5*A*. In ON cells, large-amplitude rhythmic excitatory currents ($V_{hold} = -70$ mV) were reduced by changing the holding potential to 0 mV. In OFF cells, the small-amplitude rhythmic inward currents recorded at −70 mV were replaced by large-amplitude outward currents at $V_{hold} = 0$ mV (Fig. 5*A*). The difference in the recorded currents at these two holding potentials in these three cell types was quantitated using spectral analysis. It is apparent in the power spectra plotted in Figure 5*B* that the peak power at the cells beat frequency was largest in currents recorded at −70 mV in the ON cell and at 0 mV in the OFF cells. Data pooled from a collection of 12 RGCs in RD retina (4 ON, 5 OFF-T, 3 OFF-S) showed that there is a strong correlation ($r = 0.96$; $p < 0.001$) between the frequency of peak power of the currents recorded at −70 and 0 mV (Fig. 5*C*, top). These results indicate that

excitatory and inhibitory inputs are active at the same fundamental frequency in ON and OFF type RD RGCs. The ratio of inhibitory-to-excitatory power in the ON and OFF cell types is very different, however, with OFF cells receiving >10-fold stronger inhibition than ON cells (Fig. 5*C*, bottom). This is consistent with previous measurements of the relative weights of inhibitory and excitatory conductances in ON and OFF RGCs in the WT retina (Pang et al., 2003; Murphy and Rieke, 2006) and supports the conclusion that the balance of excitatory and inhibitory inputs to ON and OFF RGCs is mostly conserved in RD retina.

Similarity of intrinsic firing properties in WT and RD RGCs

Because the continuous generation of rhythmic synaptic input and spike activity might be expected to provoke compensatory changes in cellular physiology (Gorter et al., 2002; Frick and Johnston, 2005), spike generation and firing properties of WT (Margolis and Detwiler, 2007) and RD RGCs were compared. In the presence of synaptic blockers the intrinsic characteristics of electrically evoked spike activity in ON, OFF-T, and OFF-S RGCs were indistinguishable in RD and WT retinas (Fig. 6). Both ON and OFF cells in RD retina showed similar changes in firing frequency with increasing amplitude current injection, as well as similar spike-frequency adaptation and capacity for sustained firing (Fig. 6*A*). The maximum stimulated firing frequencies were ~300–400 Hz and not different in RD compared with WT in any cell type (Fig. 6*C*) (ON: WT, 317 ± 45 Hz, $n = 6$; RD, 341 ± 46 Hz, $n = 3$; $p = 0.7$; OFF-T: WT, 315 ± 52 Hz, $n = 5$; RD, 362 ± 39 Hz, $n = 4$; $p = 0.7$). Action potential durations were submillisecond in all recordings (WT, $n = 12$; RD, $n = 14$).

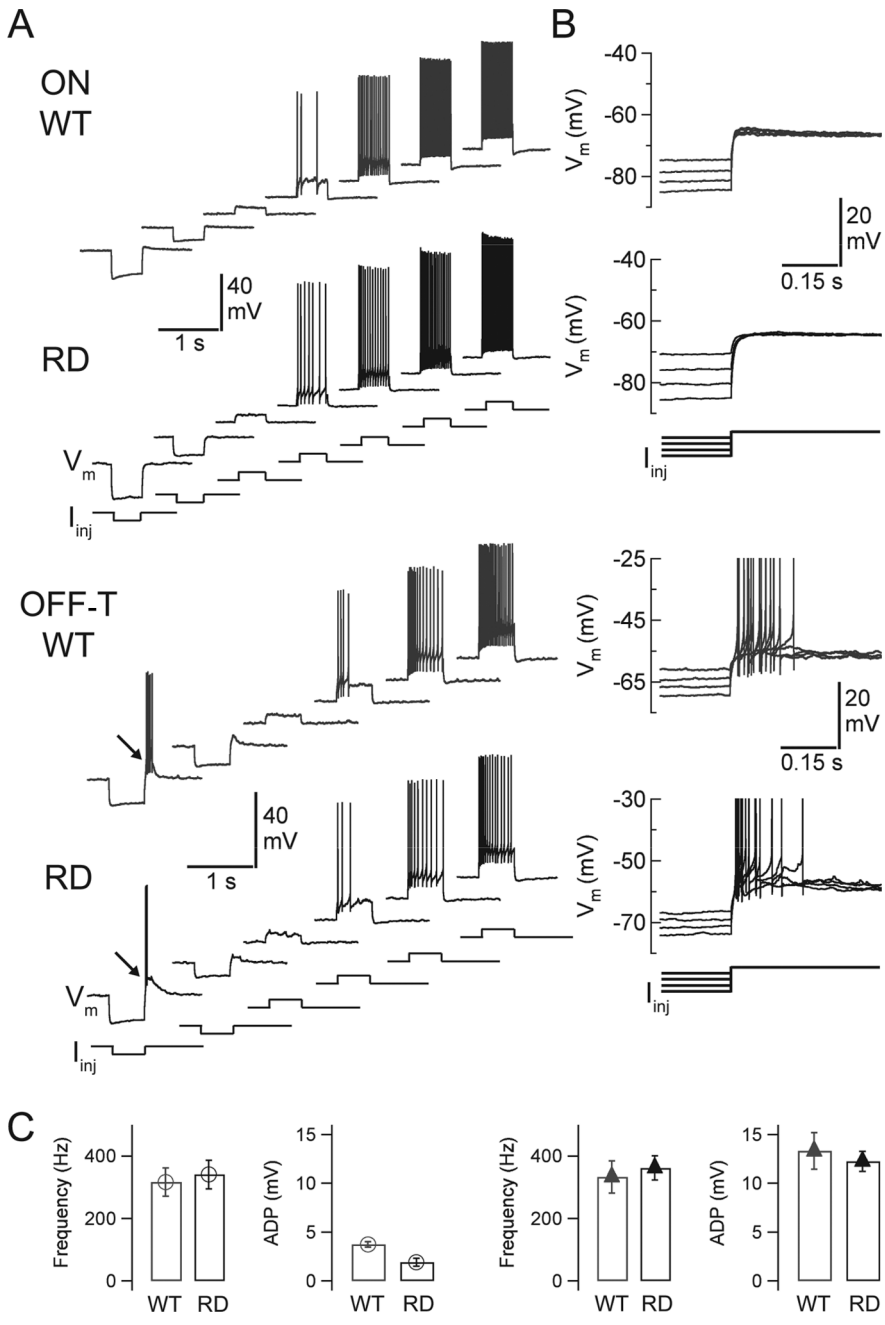

Figure 6. Similarity of intrinsic electrical properties in WT and RD RGCs. ***A***, Voltage (V_m) responses to injected current (Iinj) for ON (top) and OFF-T (bottom) cells recorded in whole-cell current-clamp mode in the presence of synaptic blockers (in μM: 50 L-APB, 20 CNQX, 50 APV, 1 strychnine, and 50 picrotoxin). Arrows indicate presence of rebound firing in both WT and RD OFF-T cells. ***B***, Four superimposed responses to negative current injection. The strength of the responses is proportional to the level of hyperpolarization. ***C***, Average maximum firing frequency and ADP strength for ON (left; $n = 6$ and 3) and OFF-T cells (right; $n = 5$ and 4, respectively).

Like in WT retina, RD ON RGCs lacked the ability for rebound firing (Fig. 6*B*), even when driven to very negative voltages (<−100 mV). Consistent with this, afterdepolarization (ADP) amplitude was approximately twofold to fourfold smaller in ON (<5 mV) than OFF cells (>10 mV). In three RD ON cells, ADP amplitude was smaller than in WT ON cells (WT, 3.7 ± 0.3 mV, $n = 6$; RD, 1.9 ± 0.4 mV, $n = 3$; $p < 0.05$).

OFF cells in RD retina showed characteristic WT-like responses to negative current injection. Importantly, they continued to exhibit rebound excitation after a hyperpolarizing potential change (Fig. 6*A*, arrows, *B*). This is a distinguishing difference between ON and OFF RGCs in WT retina (Margolis and Detwiler, 2007) (D. J. Margolis, A. J. Gartland, T. Euler, W. Denk, and P. B. Detwiler, unpublished observation). ADP amplitudes in RD OFF-T cells were large and not different from WT (WT, 13.3 ± 1.9 mV, $n = 5$; RD, 12.3 ± 1.0 mV, $n = 4$; $p = 0.7$) (Fig. 6*C*). Rebound duration and the relationship to the strength of negative current injection were also essentially the same in RD and WT RGCs (Fig. 6*B*). Three of three RD OFF-S cells also showed WT-like intrinsic properties, including rebound firing (data not shown).

Together, these results indicate that the distinct differences in intrinsic electrophysiological properties of ON and OFF RGCs are still present in RD retina. RGC intrinsic firing properties are stable despite altered ongoing synaptic input.

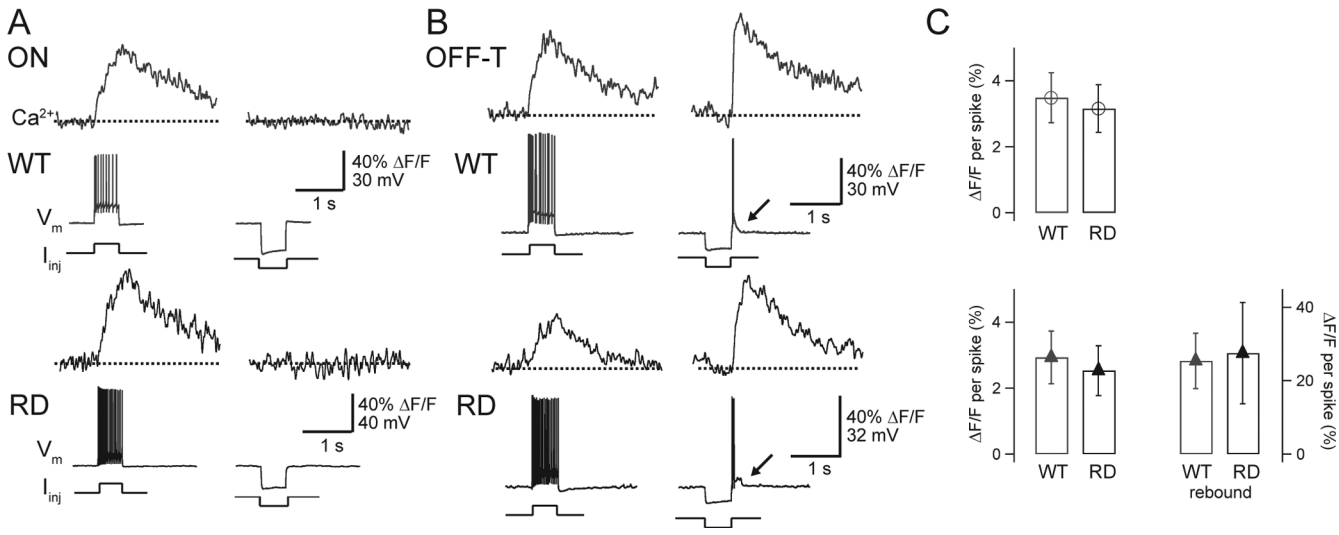

Figure 7. Similarity of spike- and rebound-evoked Ca^{2+} signals in WT and RD RGCs. ***A***, Ca^{2+} signals (Ca^{2+}) recorded from proximal dendrites during voltage responses (V_m) to injected current (Iinj) in ON WT (top) and RD (bottom) RGCs. ***B***, Same as ***A*** for OFF-T RGCs. Recordings were made in whole-cell current clamp in the presence of synaptic blockers (in μM: 50 L-APB, 20 CNQX, 50 APV, 1 strychnine, and 50 picrotoxin). Arrows indicate the presence of rebound firing. ***C***, Mean Ca^{2+} signal amplitude per spike ($\Delta F/F$ per spike) for ON (top; WT, $n = 4$; RD, $n = 3$) and OFF-T (bottom; WT, $n = 4$[5]; RD, $n = 3$) RGCs. Note that WT and RD cells display similar Ca^{2+} signaling profiles for both spiking and rebound firing. Error bars indicate SEM.

Similarity of dendritic Ca^{2+} signals in WT and RD RGCs

To test further for changes in the intrinsic properties of RGCs we compared the functional expression of voltage-gated Ca^{2+} channels in the dendrites of RGCs from WT and RD retina. Changes in Ca^{2+}-dependent fluorescence were measured from line scans across RGC proximal dendrites using two-photon fluorescence microscopy. In both ON and OFF cells, depolarizing current injection generated spikes and increased intracellular Ca^{2+} (Fig. 7*A*,*B*), resulting from activation of high-voltage-activated Ca^{2+} channels. Figure 7 also shows that OFF, but not ON, cells have the additional capacity for rebound spike excitation at the termination of a hyperpolarizing voltage step. As shown previously (Margolis and Detwiler, 2007), rebound excitation in OFF cells results from deinactivation of low-voltage-activated (LVA) Ca^{2+} channels, making them available for activation when the voltage is stepped in the depolarized direction back to the resting potential. The experiments illustrated in Figure 7, *A* and *B*, were repeated on a number of ON and OFF cells and the results quantified by measuring the relative fluorescence change per spike ($\Delta F/F$ per spike) (see Materials and Methods). The bar graphs in Figure 7*C* show that there were no significant differences in the fluorescence change per spike in WT versus RD ON and OFF RGCs. In ON cells from WT and RD retina, $\Delta F/F$s per spike were 3.5 ± 0.8 and $3.2 \pm 0.7\%$, respectively ($n = 4$ and 3, respectively; $p = 0.8$) and in OFF cells it was 2.9 ± 0.8 and $2.5 \pm 0.8\%$, respectively ($n = 4$ and 3, respectively; $p = 0.7$). For spikes evoked by rebound firing, $\Delta F/F$ per spike was 25.3 ± 7.6 and $27.5 \pm 13.8\%$ ($n = 5$ and 3; $p = 0.9$) in OFF cells from WT and RD retina, respectively (Fig. 7*C*). The results of these experiments support the conclusion that photoreceptor degeneration and the associated subsequent changes in retinal physiology do not affect the expression and basic properties of voltage-evoked dendritic Ca^{2+} signals in either ON or OFF RGCs.

Ca^{2+} homeostasis during rhythmic activity in RD RGCs

The resting level of baseline Ca^{2+} is a trigger of apoptosis and thus plays a well-established role in cell survival. To evaluate the potential influence of baseline Ca^{2+} on the survival of ganglion cells in retinal degeneration, Ca^{2+} was measured during resting activity in selected dendrites of RGCs from RD retina. Figure 8*A* shows two-photon fluorescence images of an ON and OFF RGCs from RD retina. The red boxes mark the proximal dendritic location of line scans (500 Hz sampling rate) used to measure the Ca^{2+}-dependent fluorescence signals that are traced in red along with the simultaneously recorded spike activity from each cell. Slow fluctuations in Ca^{2+} were evident during resting activity in both ON and OFF cells. Calcium appeared to rise and fall with changes in spike rate on a time scale of ~1 s. Power spectral analysis showed that resting Ca^{2+} changes were dominated by low-frequency components ($n = 6$ cells) (data not shown) with insignificant power in the frequency range of the rhythmic spontaneous spike activity (5–15 Hz). Although obvious Ca^{2+} changes were not seen with individual bursts of spikes, a correspondence between spiking and Ca^{2+} was apparent when spike activity was collected over broader bin widths (150 ms) to monitor slower changes in spike rate (Fig. 8*B*). Changing the spike rate by hyperpolarizing current injection caused a marked reduction in the baseline Ca^{2+} level in ON but not in OFF cells. This illustrated in the Figure 8*B* (middle and bottom). In the ON cell, there was a decrease in resting Ca^{2+} at the onset of the negative current pulse, with the presence of slow, low amplitude Ca^{2+} fluctuations during the period of increased membrane potential that approximately matched the changes in spike rate. At the termination of the hyperpolarizing step, Ca^{2+} rapidly retuned to the resting Ca^{2+} level. Resting Ca^{2+} signals in OFF cells also tracked changes in spike rate (Fig. 8*B*, right, top), but hyperpolarizing current injection caused a less obvious reduction on the baseline Ca^{2+} level. Hyperpolarizing the OFF cell did, however, give rise to discrete large amplitude fluctuations in Ca^{2+} (Fig. 8*B*, right, middle, bottom). These increases in Ca^{2+} were often, but not always, associated with increases in spike activity. When displayed on a faster time base (Fig. 8*C*, right), it was apparent that individual Ca^{2+} signals were coincident with single spikes as well as with regenerative-like voltage events that were subthreshold for generating full-blown action potentials (Fig. 8*C*, right, arrows).

OFF RGCs are also capable of rebound excitation during resting spike activity, as shown before in the presence of synaptic blockers (Fig. 7). The termination of hyperpolarizing current pulse in OFF, but not ON cells from the RD retina triggered a burst of spikes and a large increase in Ca^{2+} under resting condi-

tions (Fig. 8*C*, bottom right). This result and the finding that negative current injection reveals large amplitude discrete Ca^{2+} fluctuations is consistent with the deinactivation of LVA Ca^{2+} channels by hyperpolarization, making them accessible for activation by depolarizing voltage changes, as in WT OFF RGCs. The differences in Ca^{2+} signaling in ON and OFF cells suggest that these cell types use distinct mechanisms to regulate Ca^{2+} at rest. The overall observation that dendritic Ca^{2+} signals in RD RGCs are similar to WT, in both ON and OFF cell types, supports the conclusion that expression of voltage-gated Ca^{2+} channels is stable after photoreceptor degeneration.

Discussion

Our experiments show that there is ongoing rhythmic spike activity in three identified types of RGCs in the adult RD retina, the classic mouse model of retinal degeneration. Spiking was driven by oscillatory synaptic input from presynaptic circuitry, rather than changes in the intrinsic electrical or Ca^{2+} signaling properties of RGCs. These findings represent the first detailed electrophysiological measurements from identified types of RGCs in the RD retina, and highlight the functional stability of RGCs during retinal disease. The results have important implications for vision rescue strategies.

Altered firing resulting from aberrant synaptic input

To evaluate the effect of the absence of photoreceptors on the physiology of selected ganglion cells, the properties ON, OFF-T, and OFF-S RGCs in the WT and RD mouse retinas were compared. The distinctive rhythmic voltage fluctuations and spike activity present in the RD retina is not present in these cell types in WT retina (Pang et al., 2003; Murphy and Rieke, 2006; Sagdullaev et al., 2006; Margolis and Detwiler, 2007). Nor has this activity been reported under physiological conditions in any other type of adult mammalian RGC. Thus, the periodic spike activity at a characteristic frequency of ~10 Hz represents a specific form of aberrant activity present during the early stages of retinal degeneration. Two recent reports showing increased glutamate signaling (Marc et al., 2007) and overall spiking activity (Stasheff, 2008) in RD retina are consistent with this view. We found rhythmic activity in older mice (up to P210), but at a reduced rate. Thus, rhythmic retinal output may be a general feature of retinal degeneration throughout progression of the disease.

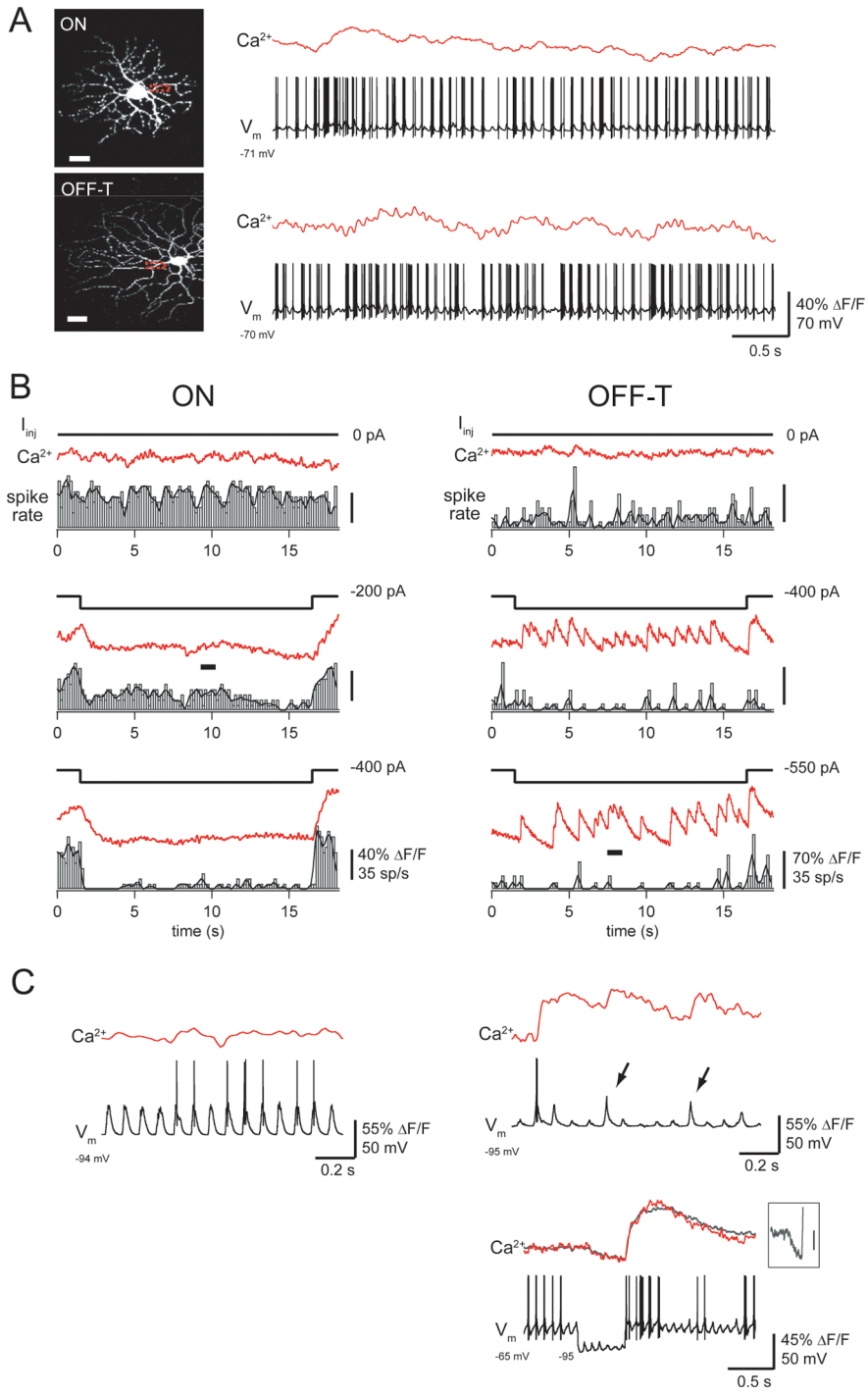

Figure 8. Calcium dynamics during resting activity in RD RGCs. ***A***, Simultaneously recorded calcium indicator fluorescence (Ca^{2+}, red) and membrane potential (V_m, black) from cells show at left. Red boxes on proximal dendrites indicate scanned regions. ***B***, Ca^{2+} signals (red) and spike rate (black; bin width, 150 ms) during resting activity [injected current (Iinj) = 0] from two different cells than in ***A***. Note the longer time scale. In the ON cell (left), Iinj reduced spike rate and resting Ca^{2+}. Baseline membrane potentials for the ON cell at rest (during pulse) were −71, −70 (−94), and −70 (−108) mV for top, middle, and bottom panels, respectively. Baseline membrane potentials for the OFF-T cell at rest during pulse were −70, −70 (−87), −70 (−95) mV for top, middle, and bottom panels, respectively. ***C***, Blow-ups of regions corresponding to bars in ***B*** (middle, ~t = 9 s for ON cell; bottom, ~t = 7 s for OFF-T cell). Note that both spikes and subthreshold regenerative-like events are associated with Ca^{2+} signals during hyperpolarization in OFF-T cell (arrows). The bottom right plot shows rebound-evoked Ca^{2+} signal during resting activity (Iinj = −400 pA for 0.5 s). The superimposed gray trace is the mean of three responses to −550, −400, and −300 pA. The hyperpolarizing portion of the mean response is shown in the inset on the right to emphasize Ca^{2+} decrease. Scale bars: ***A***, 25 μm; ***C***, inset, 10% Δ*F*/*F*.

The results showed that the rhythmic spike activity was caused by oscillatory synaptic input in both ON, OFF-T, and OFF-S RGCs. This indicates that the loss of photoreceptor input to the retina and/or the synaptic alterations that occur during retinal degeneration result in recurrent episodic release of neurotransmitter across parallel ON and OFF retinal pathways. Available evidence argues against the possibility that the activity occurs in phase across the full mosaic of RGCs. Electroretinogram recordings from RD mice (Strettoi et al., 2002) and humans (Francis et al., 2005) with retinal dystrophy show no signs of oscillatory potentials, which would be expected to be seen if the entire retina were "beating" synchronously. There is also no sign of synchronous activity in multielectrode recordings from RD mouse retina (Stasheff, 2008), consistent with the rhythmic retinal activity being asynchronous at least on a spatial scale of >200 μm, the spacing of the multielectrode array.

It is unclear what effect ongoing RGC spike activity may have on postsynaptic visual targets in the brain, but it is known that the RD retina retains functional synaptic connections with higher visual centers (Bi et al., 2006; Chen et al., 2006). Thus, it is possible that the persistent retinal activity we have observed in the blind retina is the source of photopsia in patients with retinitis pigmentosa who describe the sensation of seeing random flashes or shimmering lights in the absence of visual stimulation (Lepore, 1990; Amos, 1999; Murtha and Stasheff, 2003).

Maintenance of dendritic structure, firing properties and Ca^{2+} signaling

Despite the cellular changes that occur during retinal degeneration (Marc et al., 2003; Jones and Marc, 2005), the dendrites of three identified RGC types retain their characteristic branching and stratification patterns. That morphological changes are known to occur in horizontal and bipolar cells of RD retina (Strettoi and Pignatelli, 2000) and generally in response to altered synaptic input in other cell types (Deitch and Rubel, 1984; Kossut and Juliano, 1999), suggests that RGCs have a remarkable degree of morphological stability. These cells, the output cells of the retina, are also functionally stable. This is supported by the fact that the characteristic differences in the intrinsic electrical properties and dendritic Ca^{2+} signals between ON and OFF RGCs are the same in WT and RD retinas. Although there is little evidence of plasticity in the adult retina (Xia et al., 2007), it is nevertheless surprising that the irreversible and long term disruption of normal retinal architecture and function has no effect on the fundamental properties of ON and OFF output cells. The inherent stability of RGCs may be designed to ensure the maintenance of normal retina circuitry during prolonged changes in illumination that occur diurnally. Light, for example, by suppressing transmitter release from photoreceptors deprives the retina of photoreceptor output, which is also a consequence of photoreceptor loss in retinal degeneration.

The function of rhythmic activity: a link between cell survival and Ca^{2+} homeostasis?

What is the function of RGC activity after photoreceptor loss? One possibility is that RGCs must be active to survive. Neuronal survival depends on maintaining appropriate intracellular Ca^{2+} concentration. Because reducing spike activity by direct hyperpolarization changes Ca^{2+} dynamics in both ON and OFF cells (Fig. 8), it is likely that persistent spike activity plays a role keeping Ca^{2+} at a level that is compatible with cell survival. It has been proposed that a self-excitatory process plays a role in cell survival during retinal degeneration (Jones and Marc, 2005). The presence of persistent synaptic input at a fixed "resonant" frequency across both ON and OFF retinal pathways, and the majority of randomly sampled RGCs (Stasheff, 2008), is consistent with this proposal. Oscillatory activity may therefore represent an intrinsic retinal mechanism necessary for cell survival, and may be a general strategy for keeping neurons alive in the absence of normal synaptic transmission. This hypothesis could be tested by comparing the survival of RGCs in RD retina in the presence and absence of long-term synaptic blockade using intraocular injection of slow release antagonists.

Strategies for selective stimulation of visual pathways

Our results have important implications for developing new strategies for restoring vision in blindness caused by retinal degeneration. Several promising approaches involving cell transplantation (MacLaren et al., 2006) as well as direct electrical (Zrenner, 2002; Hetling and Baig-Silva, 2004; Weiland et al., 2005; Fried et al., 2006; Sekirnjak et al., 2006) and optical (Bi et al., 2006; Farah et al., 2007) stimulation of surviving RGCs are currently being pursued. A major impasse is the inability to stimulate different retinal pathways selectively, which is a necessary step for the recovery of normal vision.

OFF, but not ON, cells are capable of rebound excitation, a burst of action potentials at the termination of a hyperpolarizing voltage step (Margolis and Detwiler, 2007). This distinguishing feature between OFF and ON cells is retained in the RD mouse (Figs. 6–8) and may offer a potential target for selective control of ON and OFF retinal outputs. Rebound excitation stimulates OFF but not ON RGCs directly, without engaging the synaptic circuitry. However, rebound requires ~50–500 ms of hyperpolarization (Lee et al., 2003; Margolis and Detwiler, 2007), which is difficult to achieve via extracellular electrical stimulation (such as that used in epi-retinal prosthetic devices). A combination of new molecular-genetic and optical methods could potentially be used to accomplish this. The bidirectional control of neural activity with different wavelengths of light has been reported recently using the expression of light sensitive ion channels and pumps (Zhang et al., 2007). In these studies, blue light was used to activate channelrhodopsin-2 (ChR2), leading to net cation influx and depolarization, whereas yellow light was used to activate halorhodopsin (NpHR), causing chloride influx and hyperpolarization. Bi et al. (2006) expressed ChR2 in retinas of RD mice, and showed that in the presence of synaptic blockers RGC firing patterns could be controlled with light in precise spatiotemporal patterns. However, ChR2 expression was not confined to particular types of RGCs, effectively changing all RGCs to ON cells; furthermore, expression of NpHR was not attempted. One possibility is that NpHR expression could be used to drive rebound firing in OFF RGCs. This approach could provide a way to selectively control different retinal pathways, and would represent a significant step toward development of a prosthetic device that mimics natural vision.

References

Amos JF (1999) Differential diagnosis of common etiologies of photopsia. J Am Optom Assoc 70:485–504.

Bi A, Cui J, Ma YP, Olshevskaya E, Pu M, Dizhoor AM, Pan ZH (2006) Ectopic expression of a microbial-type rhodopsin restores visual responses in mice with photoreceptor degeneration. Neuron 50:23–33.

Blanks JC, Adinolfi AM, Lolley RN (1974) Photoreceptor degeneration and synaptogenesis in retinal-degenerative (rd) mice. J Comp Neurol 156:95–106.

Carter-Dawson LD, LaVail MM, Sidman RL (1978) Differential effect of the rd mutation on rods and cones in the mouse retina. Invest Ophthalmol Vis Sci 17:489–498.

Chen SJ, Mahadevappa M, Roizenblatt R, Weiland J, Humayun M (2006) Neural responses elicited by electrical stimulation of the retina. Trans Am Ophthalmol Soc 104:252–259.

Daiger SP, Bowne SJ, Sullivan LS (2007) Perspective on genes and mutations causing retinitis pigmentosa. Arch Ophthalmol 125:151–158.

Deitch JS, Rubel EW (1984) Afferent influences on brain stem auditory nuclei of the chicken: time course and specificity of dendritic atrophy following deafferentation. J Comp Neurol 229:66–79.

Denk W, Strickler JH, Webb WW (1990) Two-photon laser scanning fluorescence microscopy. Science 248:73–76.

Euler T, Detwiler PB, Denk W (2002) Directionally selective calcium signals in dendrites of starburst amacrine cells. Nature 418:845–852.

Farah N, Reutsky I, Shoham S (2007) Patterned optical activation of retinal ganglion cells. Conf Proc IEEE Eng Med Biol Soc 1:6368–6370.

Farber DB, Flannery JG, Bowes-Rickman C (1994) The rd mouse story: seventy years of research on an animal model of inherited retinal degeneration. Prog Retin Eye Res 13:13–64.

Field GD, Chichilnisky EJ (2007) Information processing in the primate retina: circuitry and coding. Annu Rev Neurosci 30:1–30.

Francis PJ, Marinescu A, Fitzke FW, Bird AC, Holder GE (2005) Acute zonal occult outer retinopathy: towards a set of diagnostic criteria. Br J Ophthalmol 89:70–73.

Frick A, Johnston D (2005) Plasticity of dendritic excitability. J Neurobiol 64:100–115.

Fried SI, Hsueh HA, Werblin FS (2006) A method for generating precise temporal patterns of retinal spiking using prosthetic stimulation. J Neurophysiol 95:970–978.

Gorter JA, Borgdorff AJ, van Vliet EA, Lopes da Silva FH, Wadman WJ (2002) Differential and long-lasting alterations of high-voltage activated calcium currents in CA1 and dentate granule neurons after status epilepticus. Eur J Neurosci 16:701–712.

Hetling JR, Baig-Silva MS (2004) Neural prostheses for vision: designing a functional interface with retinal neurons. Neurol Res 26:21–34.

Jimenez AJ, Garcia-Fernandez JM, Gonzalez B, Foster RG (1996) The spatio-temporal pattern of photoreceptor degeneration in the aged rd/rd mouse retina. Cell Tissue Res 284:193–202.

Jones BW, Marc RE (2005) Retinal remodeling during retinal degeneration. Exp Eye Res 81:123–137.

Jones BW, Watt CB, Frederick JM, Baehr W, Chen CK, Levine EM, Milam AH, Lavail MM, Marc RE (2003) Retinal remodeling triggered by photoreceptor degenerations. J Comp Neurol 464:1–16.

Jones BW, Watt CB, Marc RE (2005) Retinal remodelling. Clin Exp Optom 88:282–291.

Kossut M, Juliano SL (1999) Anatomical correlates of representational map reorganization induced by partial vibrissectomy in the barrel cortex of adult mice. Neuroscience 92:807–817.

Lee SC, Hayashida Y, Ishida AT (2003) Availability of low-threshold Ca^{2+} current in retinal ganglion cells. J Neurophysiol 90:3888–3901.

Lepore FE (1990) Spontaneous visual phenomena with visual loss: 104 patients with lesions of retinal and neural afferent pathways. Neurology 40:444–447.

MacLaren RE, Pearson RA, MacNeil A, Douglas RH, Salt TE, Akimoto M, Swaroop A, Sowden JC, Ali RR (2006) Retinal repair by transplantation of photoreceptor precursors. Nature 444:203–207.

Marc RE, Jones BW (2003) Retinal remodeling in inherited photoreceptor degenerations. Mol Neurobiol 28:139–147.

Marc RE, Jones BW, Watt CB, Strettoi E (2003) Neural remodeling in retinal degeneration. Prog Retin Eye Res 22:607–655.

Marc RE, Jones BW, Anderson JR, Kinard K, Marshak DW, Wilson JH, Wensel T, Lucas RJ (2007) Neural reprogramming in retinal degeneration. Invest Ophthalmol Vis Sci 48:3364–3371.

Margolis DJ, Detwiler PB (2007) Different mechanisms generate maintained activity in ON and OFF retinal ganglion cells. J Neurosci 27:5994–6005.

Masland RH (2001) The fundamental plan of the retina. Nat Neurosci 4:877–886.

Murphy GJ, Rieke F (2006) Network variability limits stimulus-evoked spike timing precision in retinal ganglion cells. Neuron 52:511–524.

Murtha T, Stasheff SF (2003) Visual dysfunction in retinal and optic nerve disease. Neurol Clin 21:445–481.

Nelson R, Famiglietti Jr EV, Kolb H (1978) Intracellular staining reveals different levels of stratification for on- and off-center ganglion cells in cat retina. J Neurophysiol 41:472–483.

Pang JJ, Gao F, Wu SM (2003) Light-evoked excitatory and inhibitory synaptic inputs to ON and OFF alpha ganglion cells in the mouse retina. J Neurosci 23:6063–6073.

Phelan JK, Bok D (2000) A brief review of retinitis pigmentosa and the identified retinitis pigmentosa genes. Mol Vis 6:116–124.

Punzo C, Cepko C (2007) Cellular responses to photoreceptor death in the rd1 mouse model of retinal degeneration. Invest Ophthalmol Vis Sci 48:849–857.

Sagdullaev BT, McCall MA, Lukasiewicz PD (2006) Presynaptic inhibition modulates spillover, creating distinct dynamic response ranges of sensory output. Neuron 50:923–935.

Schiller PH (1992) The ON and OFF channels of the visual system. Trends Neurosci 15:86–92.

Sekirnjak C, Hottowy P, Sher A, Dabrowski W, Litke AM, Chichilnisky EJ (2006) Electrical stimulation of mammalian retinal ganglion cells with multielectrode arrays. J Neurophysiol 95:3311–3327.

Stasheff SF (2008) Emergence of sustained spontaneous hyperactivity and temporary preservation of OFF responses in ganglion cells of the retinal degeneration (rd1) mouse. J Neurophysiol 99:1408–1421.

Strettoi E, Pignatelli V (2000) Modifications of retinal neurons in a mouse model of retinitis pigmentosa. Proc Natl Acad Sci USA 97:11020–11025.

Strettoi E, Porciatti V, Falsini B, Pignatelli V, Rossi C (2002) Morphological and functional abnormalities in the inner retina of the rd/rd mouse. J Neurosci 22:5492–5504.

Taylor WR, He S, Levick WR, Vaney DI (2000) Dendritic computation of direction selectivity by retinal ganglion cells. Science 289:2347–2350.

Wassle H (2004) Parallel processing in the mammalian retina. Nat Rev Neurosci 5:747–757.

Weiland JD, Liu W, Humayun MS (2005) Retinal prosthesis. Annu Rev Biomed Eng 7:361–401.

Xia Y, Nawy S, Carroll RC (2007) Activity-dependent synaptic plasticity in retinal ganglion cells. J Neurosci 27:12221–12229.

Zhang F, Wang LP, Brauner M, Liewald JF, Kay K, Watzke N, Wood PG, Bamberg E, Nagel G, Gottschalk A, Deisseroth K (2007) Multimodal fast optical interrogation of neural circuitry. Nature 446:633–639.

Zrenner E (2002) Will retinal implants restore vision? Science 295:1022–1025.

J Neurophysiol 98: 1042–1047, 2007.
First published May 23, 2007; doi:10.1152/jn.01294.2006.

Facilitation of Somatic Calcium Channels Can Evoke Prolonged Tail Currents in Rat Hypoglossal Motoneurons

Anna T. Moritz, Gregory Newkirk, Randall K. Powers, and Marc D. Binder
Department of Physiology and Biophysics, School of Medicine, University of Washington, Seattle, Washington

Submitted 11 December 2006; accepted in final form 17 May 2007

Moritz AT, Newkirk G, Powers RK, Binder MD. Facilitation of somatic calcium channels can evoke prolonged tail currents in rat hypoglossal motoneurons. *J Neurophysiol* 98: 1042–1047, 2007; doi:10.1152/jn.01294.2006. Voltage-dependent persistent inward currents (PICs) make an important contribution to the input-output properties of alpha motoneurons. PICs are thought to be mediated by membrane channels located primarily on the dendrites as evidenced by prolonged tail currents following the termination of a voltage step and by a clockwise hysteresis in the whole cell inward currents recorded in response to depolarizing then repolarizing voltage ramp commands. We report here, however, that voltage-clamp currents with these same features can be generated in isolated somatic membrane patches from rat hypoglossal motoneurons. Long-lasting (200–800 ms) tail currents after 1-s voltage-clamp pulses were observed in nucleated patches from 16 of 23 cells. Further, these somatic PICs display "facilitation" in response to conditioning depolarization as previously observed in whole cell recordings from intact neurons. Pharmacological tests suggest that the PICs were primarily mediated by Cav1 channels. Our results show that many of the features of persistent calcium currents recorded from intact motoneurons do not necessarily reflect a remote dendritic origin but can also be ascribed to the intrinsic properties of their Cav1 channels.

INTRODUCTION

Voltage-dependent persistent inward currents (PICs) make an important contribution to the input-output properties of alpha motoneurons, influencing both the transfer of synaptic current to the soma and the effects of that current on repetitive discharge (reviewed in Powers and Binder 2001). PICs appear to be mediated by membrane channels located primarily on the dendrites as evidenced by a clockwise hysteresis in the whole cell inward currents recorded in response to depolarizing then repolarizing voltage ramp commands, i.e., the deactivation of the inward current on the repolarizing ramp occurs at a lower somatic voltage than activation on the depolarizing ramp (Carlin et al. 2000; Lee and Heckman 1998; Powers and Binder 2003; Svirskis and Hounsgaard 1997). This phenomenon is thought to arise from the fact that the voltage-dependent channels carrying the inward current are electrically distant from the soma and not under voltage-clamp control. As a result, the distal channels are activated at relatively high somatic voltages during the depolarizing voltage ramp command but then continue to supply current to the soma during the repolarizing ramp command (cf. Booth et al. 1997; Carlin et al. 2000; Lee and Heckman 1998). Other signs that distal dendritic channels may make a significant contribution to inward voltage-clamp currents are a delayed current onset in response to a depolarizing voltage-clamp step (Booth et al. 1997; Carlin et al. 2000; Muller and Lux 1993; Powers and Binder 2003) and a prolonged decay following the termination of the step (Carlin et al. 2000; Powers and Binder 2003).

It is also possible that many of the features of PICs might result from a depolarization-induced facilitation of Cav1 channels that is independent of their location as reported in hippocampal neurons (Kavalali and Plummer 1994), hippocampal pyramidal neurons (Cloues et al. 1997), embryonic spinal motoneurons (Hivert et al. 1999), and cerebellar granule cells (Koschak et al. 2007). The "anomalous gating" of the Cav1 channels, consisting of prolonged channel reopenings during repolarizations after strong depolarizations, has been well characterized (Forti and Pietrobon 1993; Hivert et al. 1999), but the molecular mechanisms remain unresolved (see Koschak et al. 2007; Perrier et al. 2002 for discussion).

The goal of this study was to determine the extent to which the kinetics of calcium channels in isolated somata might account for some of the characteristics of the PICs observed in rat hypoglossal motoneurons (Powers and Binder 2003). To do so, we used the "nucleated patch" technique (Martina and Jonas 1997) to isolate a sphere (~20 μm) of somatic membrane from the rest of the cell. Our novel finding was that, contrary to the "remote dendritic hypothesis," nucleated patch recordings can also display a clockwise hysteresis in the whole cell calcium currents recorded in response to voltage ramp commands as well as delayed onsets and prolonged tail currents after voltage-clamp steps. Further, these somatic PICs display "facilitation" in response to conditioning depolarization as previously observed in whole cell recording from intact neurons (Svirskis and Hounsgaard 1997). These results suggest that many of the characteristics of PICs recorded in rat hypoglossal motoneurons may be mediated by the intrinsic properties of the Cav1 channels in these cells and may not be dependent on their spatial distribution.

METHODS

Slice preparation

The general experimental and surgical procedures used here have been detailed in recent publications from our laboratory (Powers and Binder 2003; Zeng et al. 2005). Experiments were carried out in accordance with the animal-welfare guidelines at the University of Washington. Sprague-Dawley rats (15–18 days old) of either sex were anesthetized by injection of 1.8 ml/kg im of a 5:1.6:6.6 solution of

Address for reprint requests and other correspondence: M. D. Binder, Dept. of Physiology and Biophysics, University of Washington School of Medicine, Box 357290, Seattle, WA 98195-7290 WA (E-mail: mdbinder@u.washington.edu).

The costs of publication of this article were defrayed in part by the payment of page charges. The article must therefore be hereby marked "*advertisement*" in accordance with 18 U.S.C. Section 1734 solely to indicate this fact.

ketamine:xylazine:saline. When fully anesthetized, the animals were decapitated. To study hypoglossal motoneurons, a section of brain stem was removed and glued to a Plexiglas tray filled with cooled, modified artificial cerebrospinal fluid (ACSF). A series of transverse slices 250 μm thick were cut throughout the length of the hypoglossal nucleus, transferred to a holding chamber and incubated at room temperature (19–21°C) for 30 min in the modified ACSF followed by incubation in standard ACSF.

Solutions and chemicals

The modified ACSF solution contained (in mM) 220 sucrose, 3 KCl, 1.25 NaH_2PO_4, 26 $NaHCO_3$, 2 $MgCl_2$, 2 $CaCl_2$, and 10 D-glucose. Kynurenic acid (1 mM) and sodium lactate (4 mM) are added to improve cell viability. The standard ASCF is identical to that of the modified ACSF except that 120 mM NaCl is substituted for sucrose, and kynurenic acid is omitted.

Various channel blockers or agonists were added to the standard ACSF. In all experiments, potassium channel blockers (4 mM 4-AP; 10 mM TEACl) were used. The following were applied from stock solution aliquots: FPL 64176 (10 μM prepared in DMSO; Sigma), nifedipine (10 μM prepared in absolute ethanol; Sigma), TTX (1 μM prepared in P*i*-free recording ACSF; Molecular Probes), ω-agatoxin IVA (480 nM; Alomone Labs), and ω-conotoxin GIVA (4 μM; Bachem). These toxin concentrations are saturating in this preparation (Umemiya and Berger 1994). To study isolated inward currents, the pipette solution was composed of (in mM) 100 CsCl, 20 TEACl, 5 $MgCl_2$, 2 bis-(*o*-aminophenoxy)-*N,N,N′,N′* tetraacetic acid (BAPTA), 10 HEPES, 5 Na_2ATP, 0.5 Na_3GTP, and CsOH/HCl for pH 7.3.

Measurement and recording techniques

Whole cell and nucleated patch recordings were obtained from the somata of rat hypoglossal motoneurons using a Zeiss Axioskop equipped with Nomarski optics for differential interference contrast and infrared video recording. Motoneuron identity was based on anatomical location and the similarity of intrinsic properties to our previous samples (Powers and Binder 2003; Sawczuk et al. 1997; Zeng et al. 2005). The patch electrodes were glass pipettes with tip diameters of 1–2 μM and resistances of 3–6 MΩ positioned with a Sutter MP-285 micromanipulator. Electrical recordings were made with an Axon Instruments Multiclamp 700A amplifier, digitized at 10 kHz using an Instrutech A/D board connected to a Macintosh PowerPC. Data acquisition and voltage-clamp commands were controlled by custom software routines running in Igor (WaveMetrics).

After the establishment of whole cell recording, the membrane potential was clamped at –70 mV. Whole cell currents were measured in response to triangular voltage-clamp commands (28 mV/s) from –70 to 0 mV and back and to a series of 1-s voltage-clamp steps delivered at 4-s intervals, each increasing in amplitude by 10 mV beginning at –70 mV.

After the whole cell measurements had been made, the transition to nucleated patch was attempted. To do so, a light negative pressure was applied to the recording pipette, and simultaneously the pipette was retracted slowly (~20 μ/s) from the soma at an angle of 37°. Once the pipette and attached somatic membrane neared the surface of the slice, the pipette was retracted vertically (100 μ/s) out of the plane of the slice. Success was assessed visually by the appearance of a sphere of membrane on the end of the pipette, which could be moved freely above the slice. Isolation was confirmed electrophysiologically by a dramatic decrease in input conductance. Once the nucleated patch recording configuration was established, another set of voltage-clamp triangular ramps and a family of 1-s voltage steps were obtained as in whole cell mode. As the nucleated patches were typically 10–20 μ in diameter and the series resistances of the patch electrodes ranged from 4.4 to 10.6 MΩ, the voltage-clamp control was excellent, with discrepancies between the command and the actual applied voltages of <5 mV.

After these basic measurements had been made, various other tests were performed. In some instances, a set of steps with a prepulse to –50 mV were performed to inactivate Cav3 channels (Umemiya and

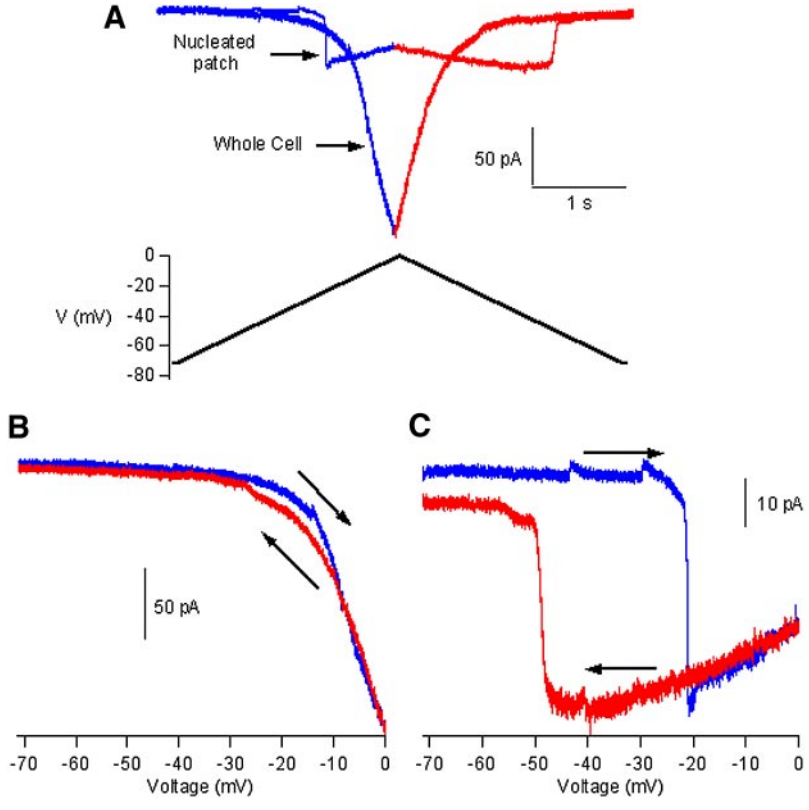

FIG. 1. *A*: calcium currents recorded in a rat hypoglossal motoneuron and in a "nucleated patch"' extracted from its soma during triangular voltage-clamp ramps. The current evoked by the depolarizing portion of the ramp is indicated in blue and that by the repolarizing portion in red. The amplitude of the inward current was reduced following nucleation. *B*: plot of current versus voltage for the whole cell recording shown in *A*. *C*: plot of current vs. voltage for the nucleated patch recording in *A* exhibiting the characteristic clockwise hysteresis associated with persistent inward currents (PICs).

Berger 1994). Tests for facilitation were performed by varying the amplitude and duration of the prepulses, with 10- to 15-s intervals between trials.

All records were leak-subtracted off-line based on scaling the responses to voltage changes within 10 mV of holding potential. The liquid junction potential was calculated using the Henderson liquid junction potential equation and mobilities (Barry and Lynch 1991) to be ~3.2 mV, so that a command potential of –70 mV, for example, would have actually been –73.2 mV. The reported values are the potentials used during experiments and do not reflect the correction for the junction potential. Mean values for tail currents are reported for trials in which a response occurred. The durations of the tail currents were quantified by first filtering the records using a fourth order Butterworth filter with a cutoff frequency of 50 Hz, then finding the times at which the derivatives of the smoothed signals exceeded a threshold value of 40 pA/s. In the recordings that did not have step-like tails, we set the threshold at the point when the current relaxed to 63% of its maximum value following the voltage step. Data were analyzed using Matlab (The Mathworks, Natick MA).

RESULTS

The data reported here were recorded from nucleated patches extracted from the somata of 23 rat hypoglossal motoneurons. Our success rate in extracting a nucleated patch after completing a series of whole cell recordings was <20%. Potassium and sodium channels were blocked in all of the experiments as described in METHODS. Inward currents were first measured in whole cell mode using triangular voltage-clamp ramps. An example of the large inward currents observed during this protocol is shown in Fig. 1. The average peak inward current in whole cell mode was 690.3 ± 741.8 (SD) pA. After establishment of a nucleated patch, the voltage-clamp triangular ramp was repeated. There was a reduction of peak inward current (168.2 ± 178.7 pA), as well as a change in the dynamics of the inward current during the biramp, as illustrated in Fig. 1, *C* versus *B*. In the nucleated patches, there was often a rapid onset and rapid cessation of the inward current, a reduction of inward current at higher voltages, and a hysteresis (Svirskis and Hounsgaard 1997) in the amplitude and time course of the inward current.

Tail currents

During the application of 1-s voltage-clamp steps, both the whole cell and nucleated patch recordings displayed sustained inward calcium currents as previously described (Powers and Binder 2003). In many instances, at the end of the voltage step, there was a prolonged tail current in both whole cell and nucleated patch recordings that gradually dissipated. Moreover, in eight of the nucleated patches, after the voltage step was completed and the holding potential had returned to –70 mV, there was a pronounced step-like tail current that remained relatively stable for a prolonged duration followed by an abrupt cessation (Fig. 2*B*). The threshold for activation of these tail currents varied by cell, with the average being –27.1 mV, ranging from −50 to –20 mV. The duration of the tail currents often increased with the amplitude of the step, although the largest amplitudes of step currents often occurred near threshold for activation. The area of the inward current during the step was associated positively with the mean amplitude of the tail currents ($r = 0.73$; $P < 0.02$).

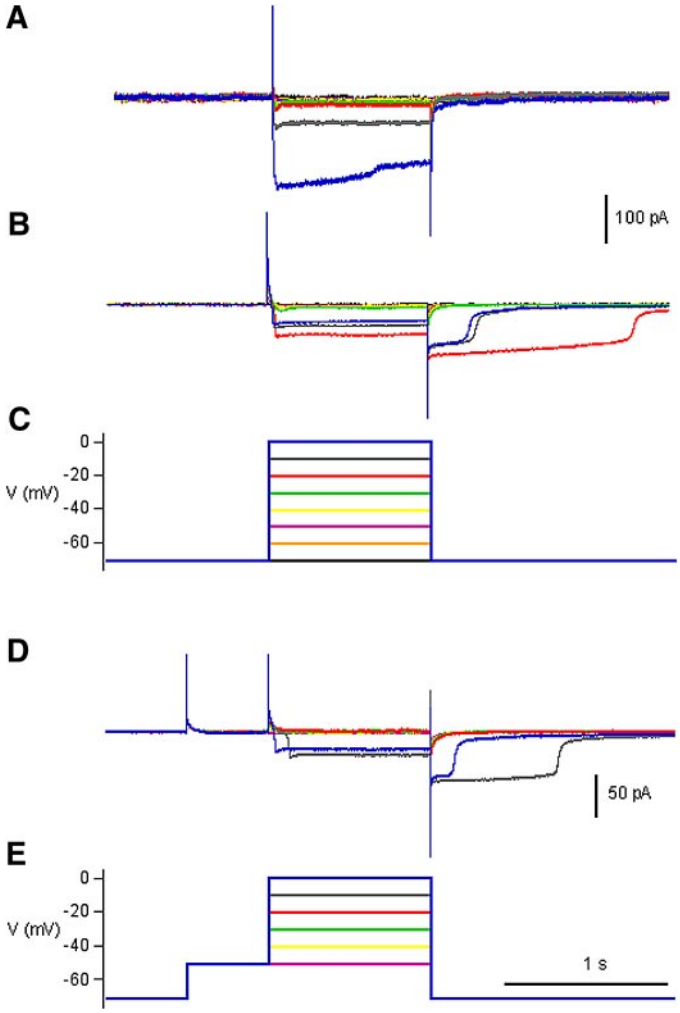

FIG. 2. Currents recorded during 1-s voltage steps in an example cell. *A*: calcium currents recorded in whole cell mode did not display prominent tail currents. *B*: immediately after extraction of a nucleated patch, the amplitude of the currents was reduced and the cell displayed prominent "step-like" tail currents with a threshold of –30 mV in this cell. *C*: voltage commands used to evoke the currents shown in *A* and *B*. *D*: preceding a voltage step with a prepulse to −50 mV to inactivate Cav3 channels had no significant effect on the tail currents but induced a delayed onset of the inward current during the step. (The currents shown in *D* were obtained after recovery from agatoxin and conotoxin. Although they are smaller than those shown in *B*, they exhibit the same qualitative features.) *E*: voltage commands used to evoke the currents shown in *D*.

In seven cells, we compared the kinetics of the inward current for voltage steps beginning at –70 mV and those preceded by at step to –50 mV to inactivate any potential contribution from Cav3 channels (Umemiya and Berger 1994). The −50-mV prepulses had no significant effect on the time course of the tail currents although in this example the delayed current onset in response to the test pulse was somewhat more pronounced (Fig. 2, *D* vs. *B*). However, delayed current onsets were also seen in the absence of a conditioning prepulse (e.g., upper black trace in Fig. 3*A*).

Role of different calcium channel subtypes

In several experiments, we obtained data in the presence of various calcium channel agonists and antagonists. We made

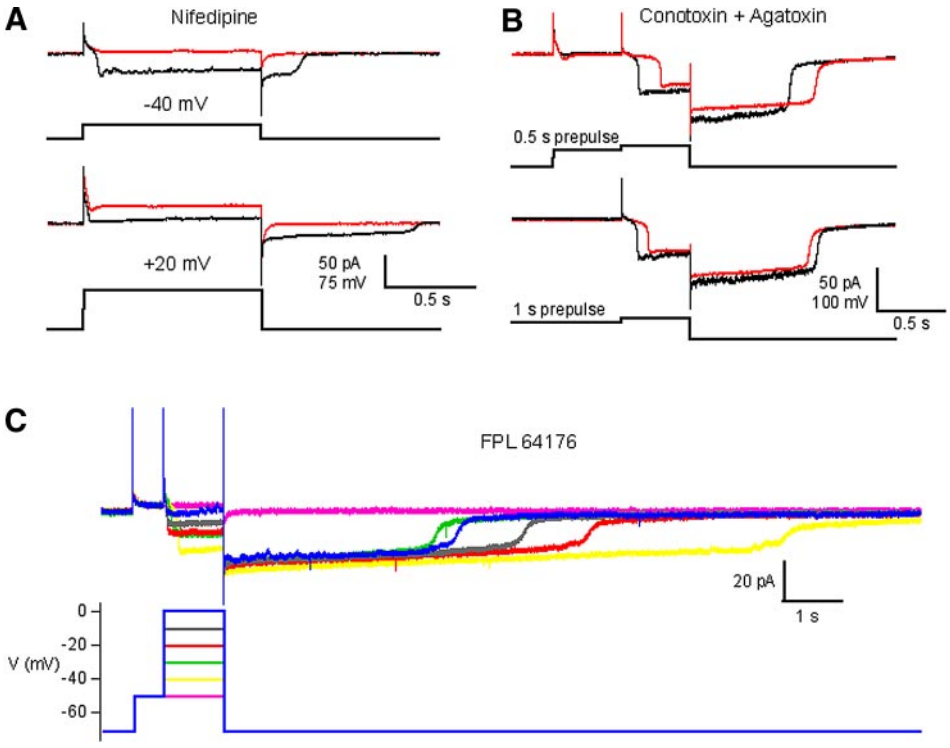

FIG. 3. Evidence for involvement of Cav1 channels. *A*: calcium currents recorded in response to voltage-clamps steps to −40 mV (*top*) and +20 mV (*bottom*) before (black traces) and after (red traces) the addition of nifedipine to block Cav1 channels. *B*: addition Cav2.1 (agatoxin) and 2.2 (conotoxin) channel blockers did not reduce the facilitation produced by 0.5- or 1-s conditioning prepulses to –30 mV. *C*: addition of the Cav1 channel agonist FPL 64176 increased the duration of the tail currents over 10-fold: note the large time scale. PreFPL recordings for the same nucleated patch shown in Fig. 2*B*. In *C*, the voltage-clamp steps were preceded by a prepulse to −50 mV to inactivate any contribution of Cav3 channels.

four nucleated patch recordings during the application of the Cav1 channel antagonist nifedipine. We also recorded the calcium currents in four cases before and after the addition of ω-conotoxin and ω-agatoxin to block Cav2.2 and Cav2.1 calcium channels, respectively. In five experiments, we examined the effects of adding the Cav1 channel agonist FPL 64176 to the bath. The results, as shown in Fig. 3, suggest that the prominent inward currents and prolonged tail currents observed in nucleated patches are carried primarily by somatic Cav1 channels. In all cases, the tail currents and the clockwise hysteresis evident in triangular voltage-clamp ramps (e.g., Fig. 1*C*) were obliterated or significantly reduced after addition of nifedipine (Fig. 3*A*, red: nifedipine, black: control). In the presence of FPL 64176, voltage steps that failed to evoke tail currents under control conditions (data not shown) evoked tail currents lasting ≤9 s (Fig. 3*C*; cf. Fig. 2*B*, recorded the same nucleated patch before the addition of FPL) and the hysteresis was enhanced. The addition of Cav2.1 and Cav2.2 channel blockers produced a minor reduction in net inward current but did not eliminate the tail currents (Fig. 4*B*, red: conotoxin + agatoxin, black: control) or the hysteresis.

Prepulse facilitation

We studied the facilitation of calcium tail currents after prepulses of varying durations and amplitudes in three of the nucleated patch experiments (cf. Cloues et al. 1997; Hivert et al. 1999; Koschak et al. 2007). We define facilitation here as the presence of a tail current after a step to a voltage that did not exhibit tail currents in the absence of a conditioning prepulse. Variations in the amplitude of short (200 ms) prepulses to +10, 0, −10, or –20 mV altered the response during a test pulse to –30 mV for 500 ms. The test pulses after the prepulses to +10, 0, and –10 mV were all followed by tail currents, whereas the prepulse to –20 mV did not evoke a tail current (Fig. 4*A*, black trace). The prepulse to +10 mV evoked the largest amplitude tail current, but the duration was longest for the prepulse to 0 mV (Fig. 4*A*, blue and red, respectively). To examine the effects of prepulse duration, a conditioning voltage step to –30 mV for 1 s, 500 ms, or 200 ms was followed by a subsequent step to –20 mV for 500 ms (Fig. 4*B*). After the 1-s and 500-ms steps (red and blue traces) there was an appreciable inward current during the step to –20 mV, which was not the case following the 200-ms prepulse (black trace). The inward current during the test step to –20 mV was similar for the 1-s and 500-ms conditioning pulses. Interestingly, the tail currents after the 1-s prepulse test were longer than after the 500-ms prepulse.

DISCUSSION

The results reported in this study provide evidence that persistent inward calcium currents with delayed onsets and prolonged tails can be generated in rat hypoglossal motoneurons by somatic Cav1 channels and thus do not necessarily reflect delayed deactivation of dendritic channels that are remote from the site of the voltage clamp. Dendritic channels have been thought to be the primary source of PICs in motoneurons on the basis of several observations. First, it was assumed that the channels mediating the PICs were voltage dependent in a conventional sense, and thus the current would be generated only when the membrane was displaced above the threshold for activation of these channels (e.g., Gutman 1991). Thus it was assumed that PICs with prolonged tails could not be generated by somatic channels under voltage-clamp because these proximal channels would be held below threshold for activation on repolarization. Instead PICs were assumed to be generated by current flow through dendritic channels that are too far from the electrode to be under perfect voltage-clamp control. Second, the slow onset of the inward current suggested

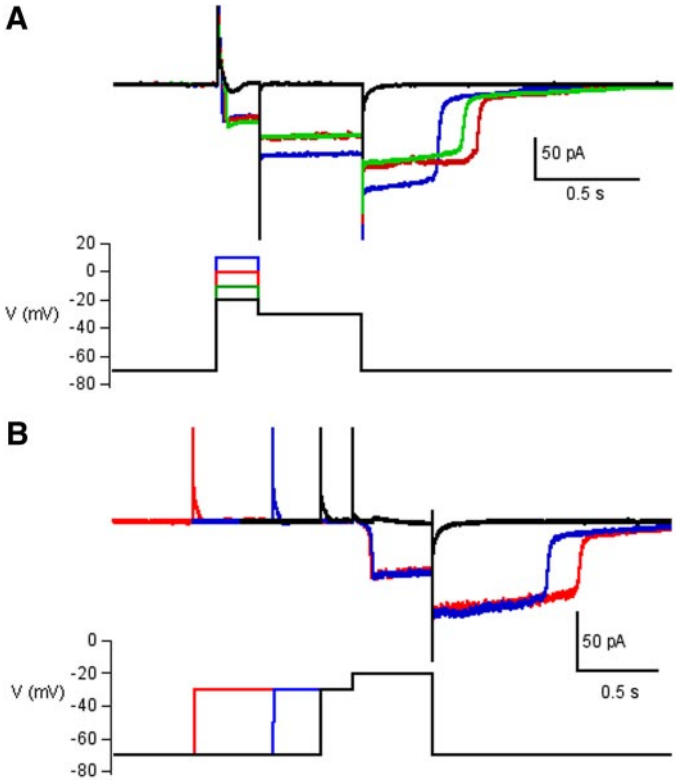

FIG. 4. Facilitation of the tail currents in nucleated patches was both time and voltage dependent. *A*: tail currents could be evoked by a test pulse that would not normally show tails if the test pulse were preceded by a short (200 ms) conditioning pulse of sufficient magnitude (> -20 mV in this cell). *B*: furthermore in the same nucleated patch, a lower amplitude conditioning pulse could evoke tail currents when the duration was long enough (>500 ms).

that time was required for voltage to spread to the site of the channels (dendrites) before they were activated (cf. Carlin et al. 2000). Third, model motoneurons can be made to exhibit inward currents during voltage clamp by placing "hot spots" of calcium channels ~400 μ from the soma (Bui et al. 2006; Elbasiouny et al. 2005; Taylor and Enoka 2004).

The results reported here suggest the possibility that many of the features of PICs in rat hypoglossal motoneurons (Powers and Binder 2003) might result from a depolarization-induced facilitation of voltage-gated calcium channels that is independent of their location as reported in other types of neurons (Cloues et al. 1997; Hivert et al. 1999; Kavalali and Plummer 1994; Koschak et al. 2007). The anomalous gating of the Cav1 channels, consisting of prolonged channel reopenings during repolarizations after strong depolarizations has been well characterized (Forti and Pietrobon 1993; Hivert et al. 1999) and could account for both the hysteresis and long tail currents. However, the tail currents and facilitation we observed in our nucleated patches could be induced with depolarizing pulses of significantly lower amplitude than those reported previously (vide supra).

The identity of the calcium channels responsible for the observed currents was also of interest to us. Our lab previously found that the calcium current in rat hypoglossal motoneurons seems to be carried predominately by Cav2.1 and 2.2 channels, with a smaller contribution from Cav1 channels (Powers and Binder 2003). Yet the present data suggest that the tail currents we observed were primarily carried by Cav1 calcium channels. The tail currents were nearly completely blocked by nifedipine and greatly enhanced by FPL, and the addition of Cav2.1 and 2.2 channel blockers did not have a significant effect on the tail currents. Furthermore we have immunohistochemical evidence for the presence of both Cav1.2 and 1.3 channels on the somata of rat hypoglossal motoneurons (Westenbroek et al. 2005). One explanation for the difference may be that in whole cell mode, when the current being measured is influenced by both somatic channels and dendritic channels, a larger proportion of dendritic Cav2.2 and 2.2 calcium channels such as we observed previously would mask the influence of somatic Cav1 channels. If this was true, only in isolated patches of somatic membrane could we observe the activity of Cav1 channels as reported here. The fact that we did not observe the step-like tails in four cells suggests that not all hypoglossal motoneurons have the same distribution of somatic Cav1 channels, consistent with our preliminary immunocyctochemical data (Westenbroek et al. 2005).

Although our data clearly show that PICs can be generated at the channel level and do not require a dendritic source, dendritic calcium channels are clearly important nonetheless. By virtue of their sheer number, dendritic calcium channels must be the primary source of PICs in motoneurons. The most parsimonious assumption would be that dendritic calcium channels exhibit the same properties observed here for the somatic channels. Thus we would speculate that the increased efficacy of synaptic input over injected somatic current in activating PICs (Bennett et al. 1998; Lee and Heckman 2000) reflects the greater surface area of the dendrites and the associated larger number of dendritic calcium channels and excitatory synaptic inputs (Cushing et al. 2005; Powers and Binder 2001).

ACKNOWLEDGMENTS

We deeply appreciate the technical assistance provided by P. Newman.

GRANTS

This work was supported by a National Institutes of Health Ruth L. Kirschstein Postdoctoral NRSA awarded to A. T. Moritz and NIH Grant NS-26840 awarded to M. D. Binder. G. Newkirk was supported in part by Human Frontiers Science Program Grant RGP0067.

REFERENCES

Barry PH, Lynch JW. Liquid junction potentials and small cell effects in patch-clamp analysis. *J Membr Biol* 121: 101–117, 1991.

Bennett DJ, Hultborn H, Fedirchuk B, Gorassini M. Synaptic acyivation of plateaus in hindlimb motoneurons of the decerebrate cat. *J Neurophysiol* 80: 2023–2037, 1998.

Booth V, Rinzel J, Kiehn O. Compartmental model of vertebrate motoneurons for Ca^{2+}-dependent spiking and plateau potentials under pharmacological treatment. *J Neurophysiol* 78: 3371–3385, 1997.

Bui TV, Ter-Mikaelian M, Bedrossian D, Rose PK. Computational estimation of the distribution of L-type Ca(2+) channels in motoneurons based on variable threshold of activation of persistent inward currents. *J Neurophysiol* 95: 225–241, 2006.

Carlin KP, Jones KE, Jiang Z, Jordan LM, Brownstone RM. Dendritic L-type calcium currents in mouse spinal motoneurons: implications for bistability. *Eur J Neurosci* 12: 1635–1646, 2000.

Cloues RK, Tavakin SJ, Marrion NV. Beta-adrenergic stimulation selectively inhibits long-lasting L-type calcium channel facilitation in hippocampal pyramidal neurons. *J Neurosci* 17: 6493–6503, 1997.

Cushing S, Bui T, Rose PK. Effect of nonlinear summation of synaptic currents on the input-output properties of spinal motoneurons. *J Neurophysiol* 94: 3465–3478, 2005.

Elbasiouny SM, Bennett DJ, Mushahwar VK. Simulation of dendritic CaV1.3 channels in cat lumbar motoneurons: spatial distribution. *J Neurophysiol* 94: 3961–3974, 2005.

Forti L, Pietrobon D. Functional diversity of L-type calcium channles in rat cerebellar neurons. *Neuron* 10: 437–450, 1993.

Gutman AM. Bistability of dendrites. *Int J Neural Syst* 1: 291–304, 1991.

Hivert B, Luvisetto S, Navangione A, Tottene A, Pietrobon D. Anomalous L-type calcium channels of rat spinal motoneurons. *J Gen Physiol* 113: 679–693, 1999.

Kavalali ET, Plummer MR. Selective potentiation of a novel calcium channel in rat hippocampal neurones. *J Physol* 480: 475–784, 1994.

Koschak A, Obermair GJ, Pivotto F, Sinnegger-Brauns MJ, Striessnig J, Pietrobon D. Molecular nature of anomalous L-type calcium channels in mouse cerebellar granule cells. *J Neurosci* 27: 3855–3863, 2007.

Lee RH, Heckman CJ. Bistability in spinal motoneurons in vivo: systematic variations in persistent inward currents. *J Neurophysiol* 80: 583–593, 1998.

Lee RH, Heckman CJ. Adjustable amplification of synaptic input in the dendrites of spinal motoneuron in vivo. *J Neurosci* 20: 6734–6740, 2000.

Martina M, Jonas P. Functional differences in Na^+ channel gating between fast-spiking interneurons and principal neurons of rat hippocampus. *J Physiol* 505: 593–603, 1997.

Muller W, Lux HD. Analysis of voltage-dependent membrane currents in spatially extended neurons from point-clamp data. *J Neurophysiol* 69: 241–247, 1993.

Perrier JF, Alaburda A, Hounsgaard J. Spinal plasticity mediated by postsynaptic L-type Ca^{2+} channels. *Brain Res Brain Res Rev* 40: 223–229, 2002.

Powers RK, Binder MD. Input-output functions of mammalian motoneurons. *Rev Physiol Biochem Pharmacol* 143: 137–263, 2001.

Powers RK, Binder MD. Persistent sodium and calcium currents in rat hypoglossal motoneurons. *J Neurophysiol* 89: 615–624, 2003.

Sawczuk A, Powers RK, Binder MD. Contribution of outward currents to spike-frequency adaptation in hypoglossal motoneurons of the rat. *J Neurophysiol* 78: 2246–2253, 1997.

Soong TW, DeMaria CD, Alvania RS, Zweifel LS, Liang MC, Mittman S, Agnew WS, Yue DT. Systematic identification of splice variants in human P/Q-type channel alpha1(2.1) subunits: implications for current density and Ca^{2+}-dependent inactivation. *J Neurosci* 22: 10142–10152, 2002.

Svirskis G, Hounsgaard J. Depolarization-induced facilitation of a plateau-generating current in ventral horn neurons in the turtle spinal cord. *J Neurophysiol* 78: 1740–1742, 1997.

Taylor AM, Enoka RM. Quantification of the factors that influence discharge correlation in model motor neurons. *J Neurophysiol* 91: 796–814, 2004.

Umemiya M, Berger AJ. Properties and function of low- and high-voltage-activated Ca^{2+} channels in hypoglossal motoneurons. *J Neurosci* 14: 5652–5660, 1994.

Westenbroek RE, Newkirk GS, Powers RK, Binder MD. Distribution of Cav1.2, Cav1.3, Cav2.1, and Cav2.2 channels on the somata and dendrites of rat hypoglossal motoneurons. *Soc Neurosci Abstr* 31: 750.11, 2005.

Zeng J, Powers RK, Newkirk G, Yonkers M, Binder MD. Contribution of persistent sodium currents to spike-frequency adaptation in rat hypoglossal motoneurons. *J Neurophysiol* 93: 1035–1041, 2005.

References

Akopian A, Witkovsky P (1996) D2 dopamine receptor-mediated inhibition of a hyperpolarization-activated current in rod photoreceptors. Journal of Neurophysiology 76(3): 1828-1835.

Alonso A, Llinas RR (1989) Subthreshold Na+-dependent theta-like rhythmicity in stellate cells of entorhinal cortex layer II. Nature 342:175-177.

Armstrong CM, Gilly WF (1992) Access resistance and space clamp problems associated with whole-cell patch clamping. Methods in enzymology 207:100-122.

Baylor DA, Hodgkin AL (1973) Detection and resolution of visual stimuli by turtle photoreceptors. The Journal of physiology 234:163-198.

Beaulieu JM, Gainetdinov RR (2011) The physiology, signaling, and pharmacology of dopamine receptors. Pharmacology Reviews 63(1): 182-217.

Bjelke B, Goldstein M, Tinner B, Andersson C, Sesack SR, Steinbusch HW, Lew JY, He X, Watson S, Tengroth B, Fuxe K (1996) Dopaminergic Transmission in the rat retina: evidence for volume transmission. Journal of Chemical Neuroanatomy 12(1): 37-50.

Bloomfield SA, Völgyi B (2009) The diverse functional roles and regulation of neuronal gap junctions in the retina. Nature Reviews Neuroscience 10(7): 495-506.

Bloomfield SA, Dacheux RF (2001) Rod vision: pathways and processing in the mammalian retina. Prog Retin Eye Res 20:351-384.

Bunney BS, Grace AA (1978) Acute and chronic haloperidol treatment: comparison of effects on nigral dopaminergic cell activity. Life Sci 23:1715-1727.

Cheng Z, ZHong YM, Yang XL (2006) Expression of the dopamine transporter in rat and bullfrog retinas. Neuroreport 17(8): 773-777.

Contini M, Lin B, Kobayashi K, Okano H, Masland RH, Raviola E (2010) Synaptic input of ON-bipolar cells onto the dopaminergic neurons of the mouse retina. The Journal of comparative neurology 518:2035-2050.

Contini M, Raviola E (2003) GABAergic synapses made by a retinal dopaminergic neuron. PNAS 100(3): 1358-1363.

Critz SD, Marc RE (1992) Glutamate antagonists that block hyperpolarizing bipolar cells increase the release of dopamine from turtle retina. Visual neuroscience 9:271-278.

Dacey DM (1990) The dopaminergic amacrine cell. The Journal of comparative neurology 301:461-489.

Davenport CM, Detwiler PB, Dacey DM (2007) Functional polarity of dendrites and axons of primate A1 amacrine cells. Visual Neuroscience 24(4): 449-457.

Denk W, Detwiler PB (1999) Optical recording of light-evoked calcium signals in the functionally intact retina. Proc Natl Acad Sci U S A 96:7035-7040.

Denk W, Strickler JH, Webb WW (1990) Two-photon laser scanning fluorescence microscopy. Science 248:73-76.

Derouoiche A, Asan E (1999) The dopamine D2 receptor subfamily in rat retina: ultrastructural immunogold and in situ hybridization studies. European Journal of Neuroscience 11(4): 1391-1402.

DeVries SH, Baylor DA (1995) An alternative pathway for signal flow from rod photoreceptors to ganglion cells in mammalian retina. PNAS 92(23): 10658-10662.

Dorenbos R, Contini M, Hirasawa H, Gustincich S, Raviola E (2007) Expression of circadian clock genes in retinal dopaminergic cells. Visual neuroscience 24:573-580.

Dowling JE, Watling KJ (1981) Dopaminergic mechanisms in the teleost retina. II. Factors affecting the accumulation of cyclic AMP in pieces of intact carp retina. Journal of neurochemistry 36:569-579.

Doyle SE, Grace MS, McIvor W, Menaker M (2002) Circadian rhythms of dopamine in mouse retina: the role of melatonin. Visual Neuroscience 19(5): 593-601.

Dreyer JK, Herrik KF, Berg RW, Hounsgaard JD (2010) Influence of phasic and tonic dopamine release on receptor activation. The Journal of neuroscience : the official journal of the Society for Neuroscience 30:14273-14283.

Dumitrescu ON, Pucci FG, Wong KY, Berson DM (2009) Ectopic retinal ON bipolar cell synapses in the OFF inner plexiform layer: contacts with dopaminergic amacrine cells and melanopsin ganglion cells. Journal of Comparative Neurology 517(2): 226-244.

Dunn FA, Lankheet MJ, Rieke F (2007) Light adaptation in cone vision involves switching between receptor and post-receptor sites. Nature 449(7162): 603-606.

Dutton A, Dyball RE (1979) Phasic firing enhances vasopressin release from the rat neurohypophysis. The Journal of physiology 290:433-440.

Euler T, Hausselt SE, Margolis DJ, Breuninger T, Castell X, Detwiler PB, Denk W (2009) Eyecup scope--optical recordings of light stimulus-evoked fluorescence signals in the retina. Pflugers Arch 457:1393-1414.

Feigenspan A, Gustincich S, Raviola E (2000) Pharmacology of GABA(A) receptors of retinal dopaminergic neurons. Journal of neurophysiology 84:1697-1707.

Feigenspan A, Gustincich S, Bean BP, Raviola E (1998) Spontaneous activity of solitary dopaminergic cells of the retina. The Journal of neuroscience : the official journal of the Society for Neuroscience 18:6776-6789.

Feng G, Meilor RH, Bernstein M, Keller-Peck C, Nguyen QT, Wallace M, Nerbonne JM, Lichtman JW, Sanes JR (2000) Neuron 28(1): 41-51.

Fioravante D, Regehr WG (2011) Short-term forms of presynaptic plasticity. Current Opinion in Neurobiology 21:269-274.

Floresco SB, West AR, Ash B, Moore H, Grace AA (2003) Afferent modulation of dopamine neuron firing differentially regulates tonic and phasic dopamine transmission. Nature Neuroscience 6:968-973.

Gingrich KJ, Roberts WA, Kass RS (1995) Dependence of the GABAA receptor gating kinetics on the alpha-subunit isoform: implications for structure-function relations and synaptic transmission. The Journal of physiology 489 (Pt 2):529-543.

Godley BF, Wurtman RJ (1988) Release of endogenous dopamine from the superfused rabbit retina in vitro: effect of light stimulation. Brain research 452:393-395.

Gonon FG (1988) Nonlinear relationship between impulse flow and dopamine released by rat midbrain dopaminergic neurons as studied by *in vivo* electrochemistry. Neuroscience 24:19-28.
Grace AA, Bunney BS (1984a) The control of firing pattern in nigral dopamine neurons: burst firing. The Journal of neuroscience : the official journal of the Society for Neuroscience 4:2877-2890.

Grace AA, Bunney BS (1984b) The control of firing pattern in nigral dopamine neurons: single spike firing. The Journal of neuroscience : the official journal of the Society for Neuroscience 4:2866-2876.

Grace AA, Bunney BS (1986) Induction of depolarization block in midbrain dopamine neurons by repeated administration of haloperidol: analysis using *in vivo* intracellular recording. The Journal of pharmacology and experimental therapeutics 238:1092-1100.

Gustincich S, Feigenspan A, Sieghart W, Raviola E (1999) Composition of the GABA(A) receptors of retinal dopaminergic neurons. The Journal of neuroscience : the official journal of the Society for Neuroscience 19:7812-7822.

Gustincich S, Feigenspan A, Wu DK, Koopman LJ, Raviola E (1997) Control of dopamine release in the retina: a transgenic approach to neural networks. Neuron 18:723-736.

Hadjiconstantinou M, Rossetti Z, Silvia C, Krajnc D, Neff NH (1988) Aromatic L-amino acid decarboxylase activity of the rat retina is modulated in vivo by environmental light. Journal of Neurochemistry 51(5): 1560-1564.

Hoshi H, Liu WL, Massey SC, Mills SL (2009) ON inputs to the OFF layer: bipolar cells that break the stratification rules of the retina. Journal of Neuroscience 29(28): 8875-8883.

Ishita S, Negishi K, Teranishi T, Shimada Y, Kato S (1988) GABAergic inhibition on dopamine cells of the fish retina: a [3H]dopamine release study with isolated fractions. Journal of neurochemistry 50:1-6.

Iuvone PM, Galli CL, Garrison-Gund CK, Neff NH (1978) Light stimulates tyrosine hydroxylase activity and dopamine synthesis in retinal amacrine neurons. Science 202:901-902.

Jeon CJ, Strettoi E, Masland RH (1998) The major cell populations of the mouse retina. Journal of Neuroscience 18(21): 8936-8946.

Jusuf PR, Haverkamp S, Grunert U (2005) Localization of glycine receptor alpha subunits on bipolar and amacrine cells in primate retina. The Journal of comparative neurology 488:113-128.

Kamp CW, Morgan WW (1981) GABA antagonists enhance dopamine turnover in the rat retina *in vivo*. European journal of pharmacology 69:273-279.

Kirsch M, Wagner HJ (1989) Release pattern of endogenous dopamine in teleost retinae during light adaptation and pharmacological stimulation. Vision research 29:147-154.

Kolb H, Cuenca N, Dekorver L (1991) Postembedding immunocytochemistry for GABA and glycine reveals the synaptic relationships of the dopaminergic amacrine cell of the cat retina. The Journal of comparative neurology 310:267-284.

Kolbinger W, Weiler R (1993) Modulation of endogenous dopamine release in the turtle retina: effects of light, calcium, and neurotransmitters. Visual neuroscience 10:1035-1041.

Kong JH, Fish DR, Rockhill RL, Masland RH (2005) Diversity of ganglion cells in the mouse retinaL unsupervised morphological classification and its limits. Journal of Comparative Neurology 489(3): 293-310.

Koulen P, Sassoe-Pognetto M, Grunert U, Wassle H (1996) Selective clustering of GABA(A) and glycine receptors in the mammalian retina. J Neurosci 16:2127-2140.

Kramer SG (1971) Dopamine: A retinal neurotransmitter. I. Retinal uptake, storage, and light-stimulated release of H3-dopamine *in vivo*. Invest Ophthalmol 10:438-452.

Lacey MG, Mercuri NB, North RA (1987) Dopamine acts on D2 receptors to increase potassium conductance in neurones of the rat substantia nigra zona compacta. The Journal of physiology 392:397-416.

Lyubarsky AL, Daniele LL, Pugh EN, Jr. (2004) From candelas to photoisomerizations in the mouse eye by rhodopsin bleaching *in situ* and the light-rearing dependence of the major components of the mouse ERG. Vision research 44:3235-3251.

MacNeil MA, Masland RH (1998) Extreme diversity among amacrine cells: implications for function. Neuron 20(5): 971-982.

Mangel SC, Dowling JE (1987) The interplexiform-horizontal cell system of the fish retina: effects of dopamine, light stimulation and time in the dark. Proceedings of the Royal Society of London Series B, Containing papers of a Biological character Royal Society 231:91-121.

Margolis DJ, Detwiler PB (2007) Different mechanisms generate maintained activity in ON and OFF retinal ganglion cells. The Journal of Neuroscience 27(22): 5994-6005.

Marshak DW (2001) Synaptic inputs to dopaminergic neurons in mammalian retinas. Progress in Brain Research 131: 83-91.

Masland RH (2012) The neuronal organization of the retina. Neuron 76(2): 266-280.
Masland RH (1998). Amacrine cells. Trends in Neuroscience 11(9): 405-410.

McCormick DA, Pape HC (1990a) Properties of a hyperpolarization-activated cation current and its role in rhythmic oscillation in thalamic relay neurones. The Journal of physiology 431:291-318.

McCormick DA, Pape HC (1990b) Noradrenergic and serotonergic modulation of a hyperpolarization-activated cation current in thalamic relay neurones. The Journal of physiology 431:319-342.

Melamed E, Frucht Y, Lemor M, Uzzan A, Rosenthal Y (1984) Dopamine turnover in rat retina: a 24-hour light-dependent rhythm. Brain Research 305(1): 148-151.

Menger N, Pow DV, Wassle H (1998) Glycinergic amacrine cells of the rat retina. Journal of Comparative Neurology 401(1): 34-46.

Mercuri NB, Bonci A, Calabresi P, Stefani A, Bernardi G (1995) Properties of the hyperpolarization-activated cation current Ih in rat midbrain dopaminergic neurons. The European journal of neuroscience 7:462-469.

Morgan WW, Kamp CW (1980) A GABAergic influence on the light-induced increase in dopamine turnover in the dark-adapted rat retina *in vivo*. Journal of neurochemistry 34:1082-1086.

Naarendorp F, Esdaille TM, Banden SM, Andrews-Labenski J, Gross OP, Pugh EN jr. (2010) Dark light, rod saturation, and the absoluteand incremental sensitivity of mouse cone vision. Journal of Neuroscience 30(37): 12495-12507.

Neher E (1992) Correction for liquid junction potentials in patch clamp experiments. Methods in enzymology 207:123-131.

Newkirk GS, Hoon M, Wong RO, Detwiler PB (2013) Inhibitory inputs tune the light response properties of dopaminergic amacrine cells in mouse retina. Journal of Neurophysiology (Epub ahead of print).

Nguyen-Legros J, Versaux-Botteri C, Vernier P (1999) Dopamine receptor localization in the mammalian retina. Molecular Neurobiology 19(3): 181-204.

Nichols CW, Jacobowitz D, Hottenstein M (1967) The influence of light and dark on the catecholamine content of the retina and choroid. Invest Ophthalmol 6:642-646.

O'Connor PM, Zucker CL, Dowling JE (1987) Regulation of dopamine release from interplexiform cell processes in the outer plexiform layer of the carp retina. Journal of neurochemistry 49:916-920.

Pang JJ, Abd-El-Barr MM, Gao F, Bramblett DE, Paul DL, Wu SM (2007) Relative contributions of rod and cone bipolar cell inputs to AII amacrine cell light responses in the mouse retina. J Physiol 580:397-410.

Pape HC, McCormick DA (1989) Noradrenaline and serotonin selectively modulate thalamic burst firing by enhancing a hyperpolarization-activated cation current. Nature 340:715-718.

Peichl L, González-Soriano J (1994) Morphological types of horizontal cell in rodent retinae: a comparison of rat, mouse, gerbil, and guinea pig. Visual Neuroscience 11(3): 501-517.

Puopolo M, Hochstetler SE, Gustincich S, Wightman RM, Raviola E (2001) Extrasynaptic release of dopamine in a retinal neuron: activity dependence and transmitter modulation. Neuron 30:211-225.

Ribelayga C, Wang Y, Mangel SC (2004) A circadian clock in the fish retina regulates dopamine release via activation of melatonin receptors. The Journal of physiology 554:467-482.

Robinson RB, Siegelbaum SA (2003) Hyperpolarization-activated cation currents: from molecules to physiological function. Annual Review of Physiology 65: 453-480.

Sagne C, El Mestikawy S, Isambert MF, Hamon M, Henry JP, Giros B, Gasnier B (1997) Cloning of a functional vesicular GABA and glycine transporter by screening of genome databases. FEBS letters 417:177-183.

Schmitz F, Konigstorfer A, Sudhof TC (2000) RIBEYE, a component of synaptic ribbons: a protein's journey through evolution provides insight into synaptic ribbon function. Neuron 28:857-872.

Soto F, Bleckert A, Lewis R, Kang Y, Kerschensteiner D, Craig AM, Wong RO (2011) Coordinated increase in inhibitory and excitatory synapses onto retinal ganglion cells during development. Neural development 6:31.

Soucy E, Wang Y, Nirenburg S, Nathans J, Meister M (1998) A novel signaling pathway from rod photoreceptors to ganglion cells in mammalian retina. Neuron 21(3):481-493.

Stefani A, Pisani A, Bernardi G, Bonci A, Mercuri NB, Stratta F, Calabresi P (1995) The modulation of dopamine receptors in rat striatum. J Neural Transm Suppl 45:61-66.

Steffen MA, Seay CA, Amini B, Cai Y, Feigenspan A, Baxter DA, Marshak DW (2003) Spontaneous activity of dopaminergic retinal neurons. Biophys J 85:2158-2169.

Storch KF, Paz C, Signorovitch J, Raviola E, Pawlyk B, Li T, Weitz CJ (2007) Intrinsic circadian clock of the mammalian retina: importance for retinal processing of visual information. Cell 130:730-741.

Strettoi E, Masland RH (1996) The number of unidentified amacrine cells in the mammalian retina. PNAS 94(25): 14906-14911.

Tsai HC, Zhang F, Adamantidis A, Stuber GD, Bonci A, de Lecea L, Deisseroth K (2009) Phasic firing in dopaminergic neurons is sufficient for behavioral conditioning. Science 324:1080-1084.

Versaux-Botteri C, Nguyen-Legros J, Vigny A, Raoux N (1984) Morphology, density and distribution of tyrosine hydroxylase-like immunoreactive cells in the retina of mice. Brain research 301:192-197.

Veruki ML, Hartveit E (2002) Electrical synapses mediate signal transmission in the rod pathway of the mammalian retina. J Neurosci 22:10558-10566.

Veruki ML (1997) Dopaminergic neurons in the rat retina express dopamine D2/3 receptors. European Journal of Neuroscience 9(5): 1096-1100.

Völgyi B, Chheda S, Bloomfield SA (2009) Tracer coupling patterns of the ganglion cell subtypes in the mouse retina. Journal of Comparative Neurology 512(5): 664-687.

Wassle H, Boycott BB (1991) Functional architecture of the mammalian retina. Physiological Reviews 71(2): 447-480.

Wassle H, Koulen P, Brandstatter JH, Fletcher EL, Becker CM (1998) Glycine and GABA receptors in the mammalian retina. Vision Res 38:1411-1430.

Wassle H, Heinze L, Ivanova E, Majumdar S, Weiss J, Harvey RJ, Haverkamp S (2009) Glycinergic transmission in the Mammalian retina. Front Mol Neurosci 2:6.

Weiler R, Baldridge WH, Mangel SC, Dowling JE (1997) Modulation of endogenous dopamine release in the fish retina by light and prolonged darkness. Visual neuroscience 14:351-356.

Williams SR, Mitchell SJ (2008) Direct measurement of somatic voltage clamp errors in central neurons. Nature Neuroscience 11:790-798.

Wirz-Justice A, Da Prada M, Remé C (1984) Circadian rhythm in rat retinal dopamine. Neuroscience Letters 45(1): 21-25.

Witkovsky P (2004) Dopamine and retinal function. Documenta ophthalmologica Advances in ophthalmology 108:17-40.

Xiao J, Cai Y, Yen J, Steffen M, Baxter DA, Feigenspan A, Marshak D (2004) Voltage-clamp analysis and computational model of dopaminergic neurons from mouse retina. Visual neuroscience 21:835-849.

Xin D, Bloomfield SA (1999) Comparison of the responses of AII amacrine cells in the dark- and light-adapted rabbit retina. Visual neuroscience 16:653-665.

Yung WH, Hausser MA, Jack JJ (1991) Electrophysiology of dopaminergic and non-dopaminergic neurones of the guinea-pig substantia nigra pars compacta in vitro. The Journal of physiology 436:643-667.

Zhang DQ, Zhou TR, McMahon DG (2007) Functional heterogeneity of retinal dopaminergic neurons underlying their multiple roles in vision. The Journal of neuroscience : the official journal of the Society for Neuroscience 27:692-699.

Zhang DQ, Stone JF, Zhou T, Ohta H, McMahon DG (2004) Characterization of genetically labeled catecholamine neurons in the mouse retina. Neuroreport 15:1761-1765.

Zhang DQ, Wong KY, Sollars PJ, Berson DM, Pickard GE, McMahon DG (2008) Intraretinal signaling by ganglion cell photoreceptors to dopaminergic amacrine neurons. P Natl Acad Sci USA 105:14181-14186.

Zweifel LS, Argilli E, Bonci A, Palmiter RD (2008) Role of NMDA receptors in dopamine neurons for plasticity and addictive behaviors. Neuron 59:486-496.